Particle tracking and identification with single-layer Timepix-series detectors

Benedikt Bergmann

Institute of Experimental and Applied Physics, Czech Technical University in Prague

Benedikt.bergmann@utef.cvut.cz

Preface

Outline the capabilities of Timepix-type detectors enabled by **high spatial granularity, nanosecond-scale** timestamping and **continuous measurement**.

Show examples of data analysis in different mixed radiation fields profiting from the single-layer **temporal and spatial coincidence analysis**, **particle identification** & precise **trajectory reconstruction**

Focus on possible use cases in **fundamental science.**

Radiation imaging detector

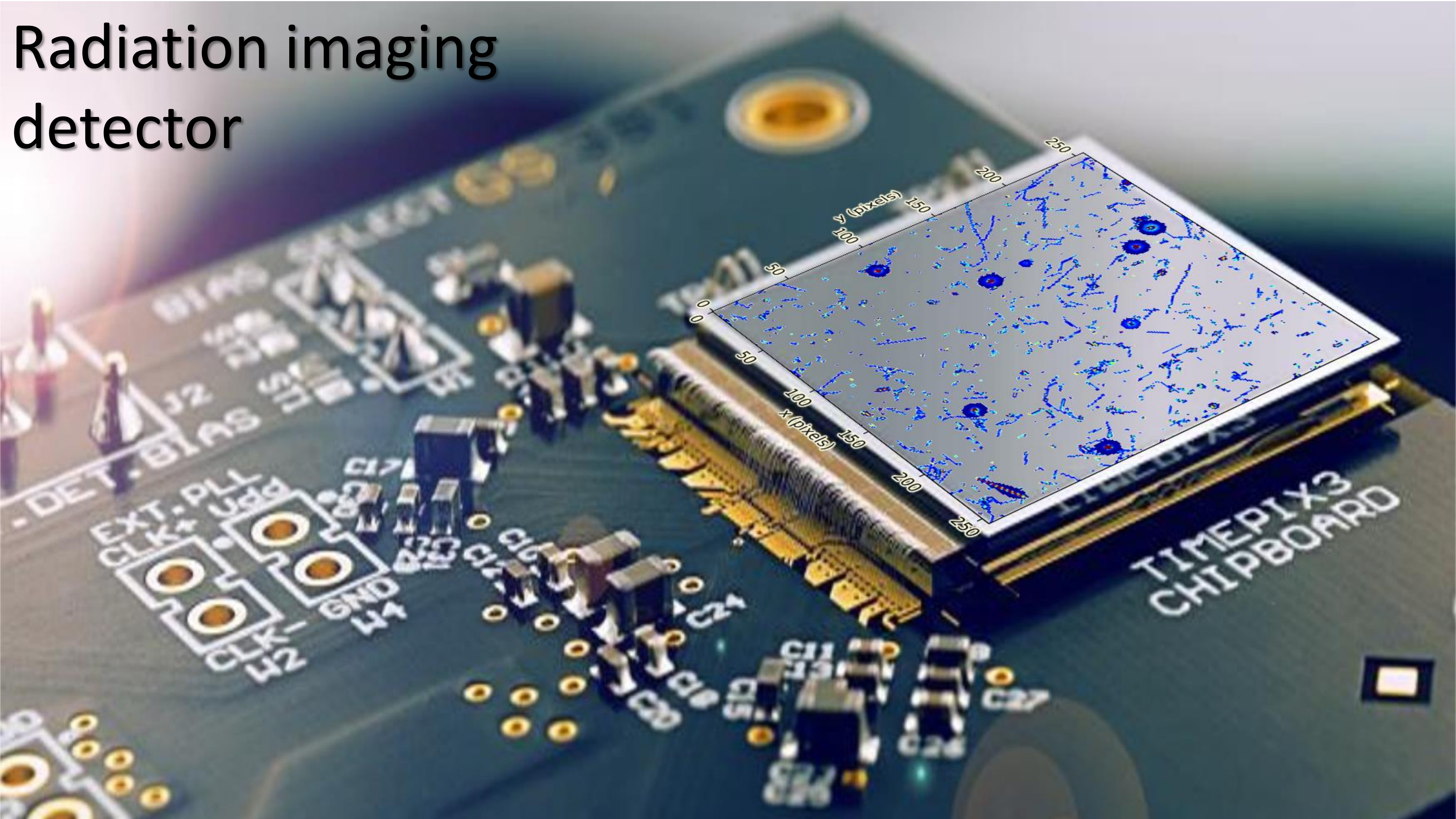

Pattern recognition

Pattern recognition together with dE/dX information allows determination of incident particle type - and energy?

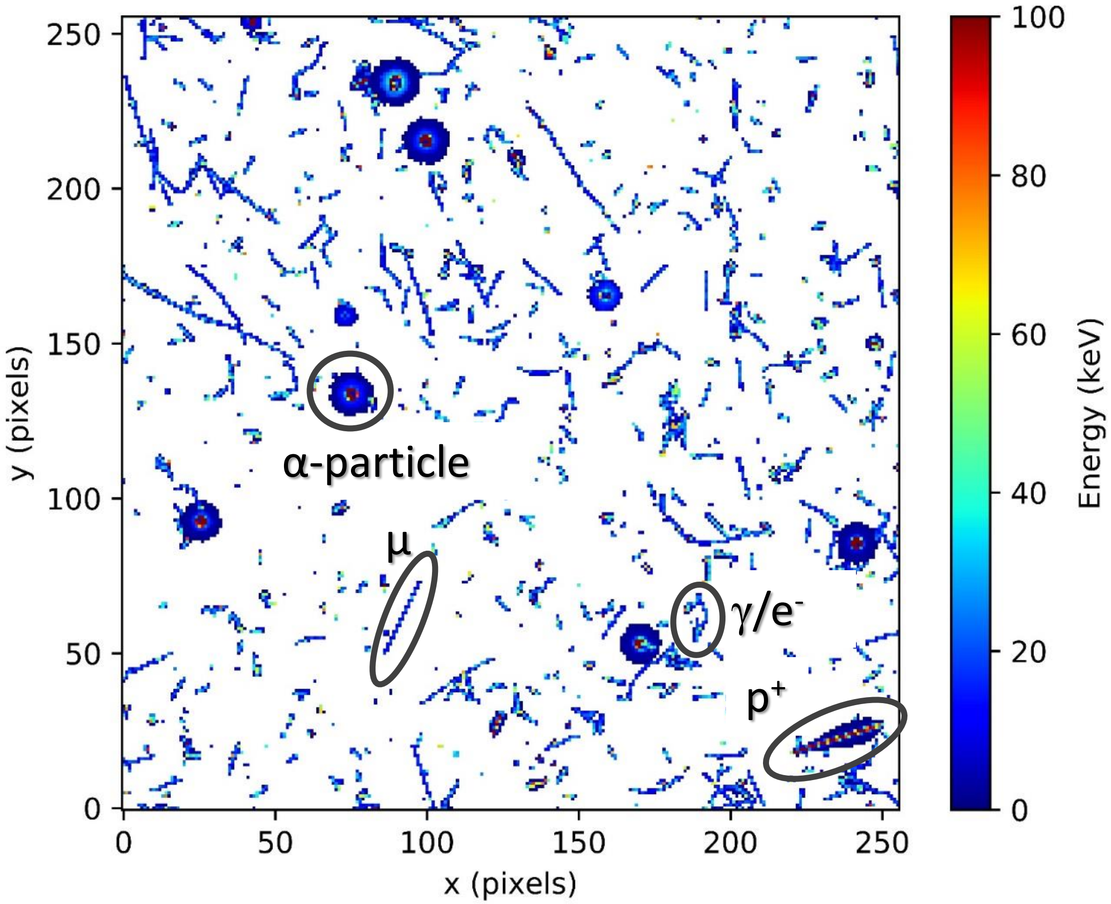

60 minutes measurement at an altitude of 2 700 m

T. Holy, et al. *Pattern recognition of tracks induced by individual quanta of ionizing radiation in Medipix2 silicon detector,* Nucl. Inst. Meth. Phys. Res. A, 591(1):287 – 290, 2008.

(1) Dot		Low energy X- and γ-rays, low energy electrons
(2) Small blob		X- and γ-rays, electrons
(3) Curly track		γ-rays and electrons (MeV)
(4) Heavy Blob		Highly ionizing particles with short range (α, protons, ...)
(5) Heavy track		Highly ionizing particles (protons, ions, ...)
(6) Straight track		Energetic light charged particles (μ, minimum ionizing light ions, ...)

Working principle:

Detector response to highly ionizing radiation

Analysis of δ-ray signal or Bragg-behavior further enhances particle separation capability

$$\left\langle -\frac{dE}{dx} \right\rangle = Kz^2 \frac{Z}{A} \frac{1}{\beta^2} \left[\frac{1}{2} \ln \frac{2m_e c^2 \beta^2 \gamma^2 W_{max}}{I^2} - \beta^2 - \frac{\delta(\beta\gamma)}{2} \right]$$

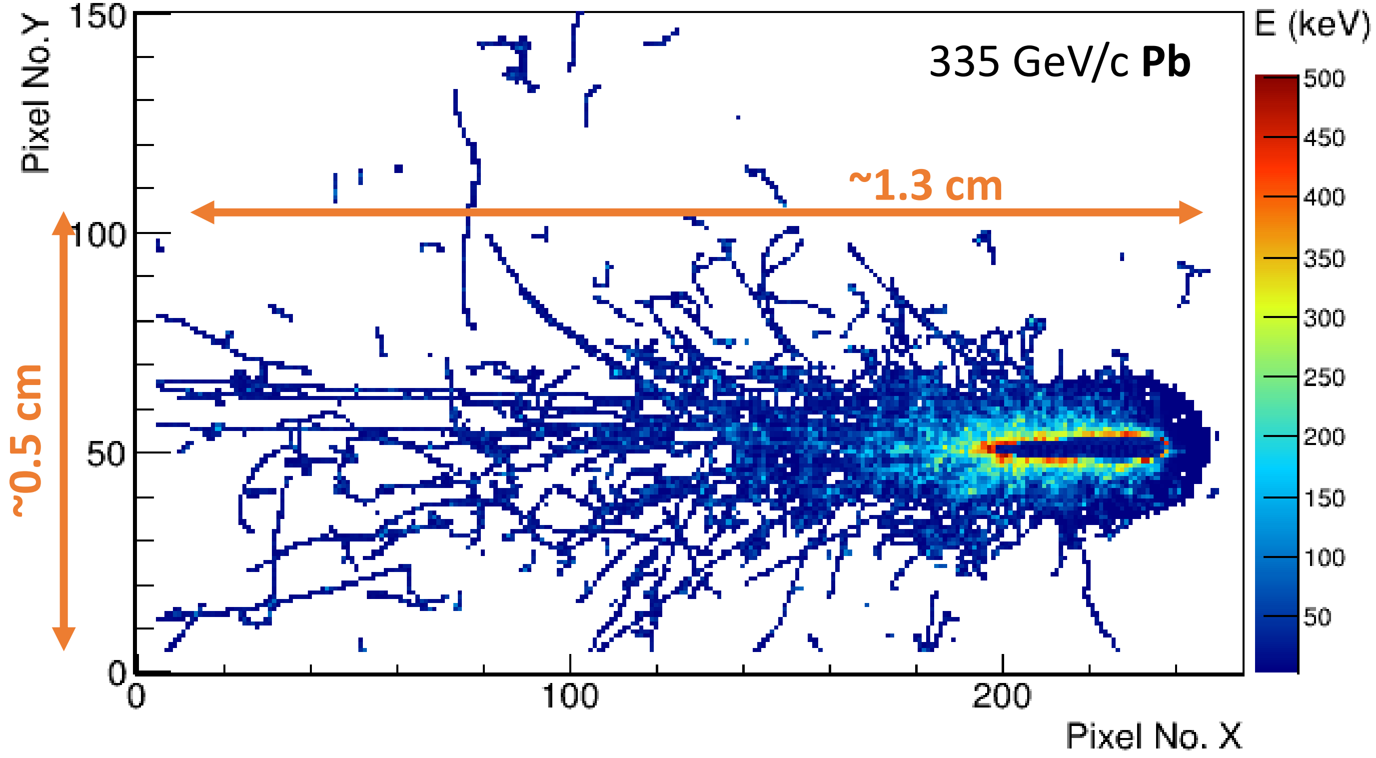

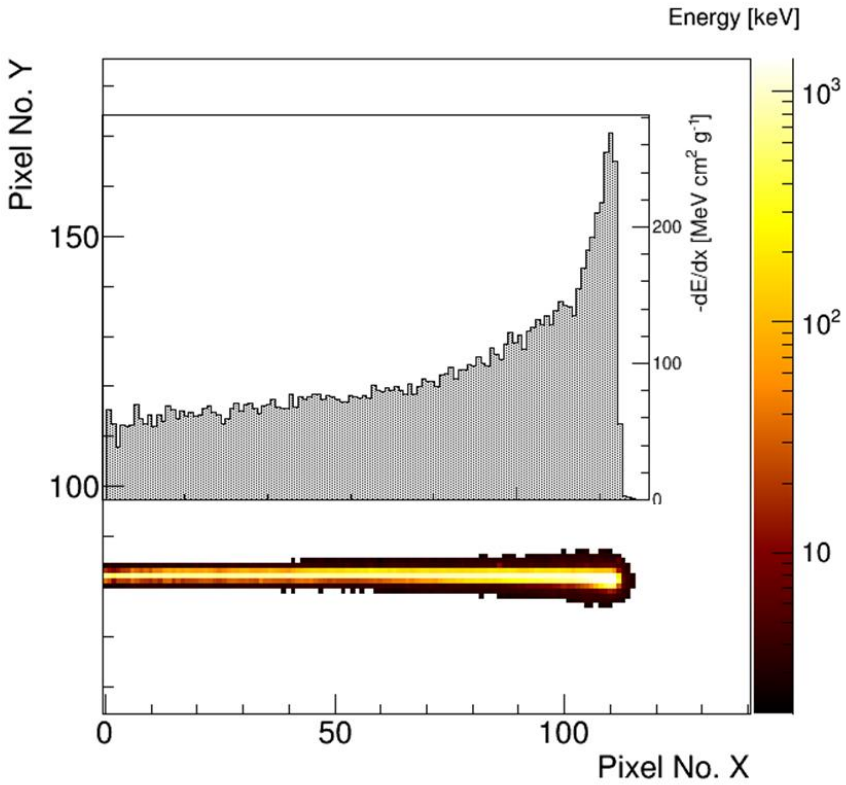

Increased energy deposit in the medium at the end of its range (**Bragg-Peak**)
Example: **350 MeV/A He track.**

Timepix and Timepix3

- 256 x 256 pixels with 55 µm pitch (1.98 cm^2)
- Sensor layer (Silicon, GaAs, CdTe, ...) flip-chip bump bonded to the ASIC

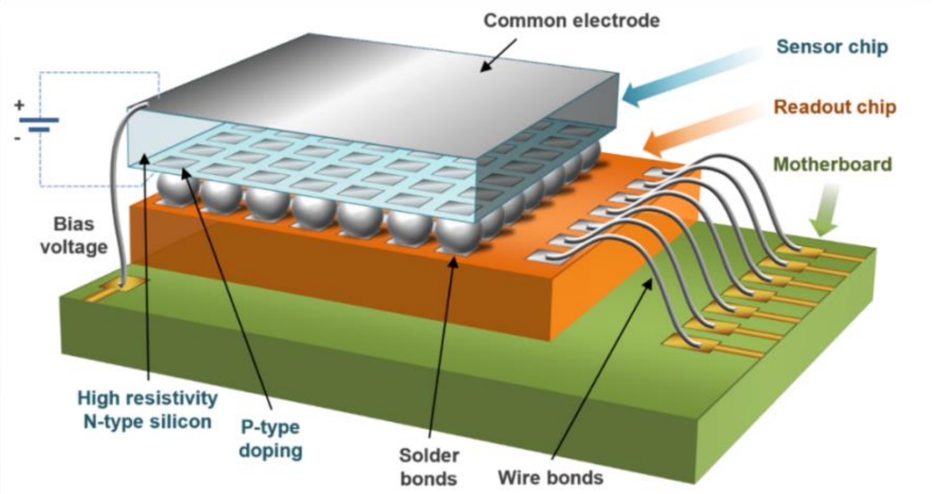

Timepix

- Frame based readout (92 fps) – dead time > 11 ms
- Measurement of **energy or time** (Δt = 20.8 ns)
- Threshold for noise free measurement: 3-5 keV

Timepix3

- Data-driven readout (Max. count rate 40 Mpix/s)
- Per-pixel dead time of 475 ns
- Measurement of **energy and time** (Δt = 1.56 ns)
- Threshold for noise free measurement: 3-5 keV

Timepix3 with chipboard.

Solid-state Time-Projection Chamber:

3D reconstruction of particle tracks

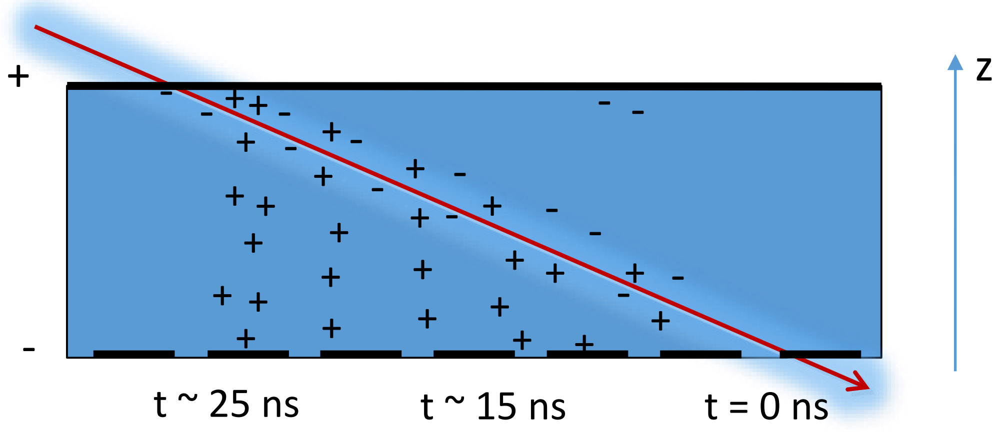

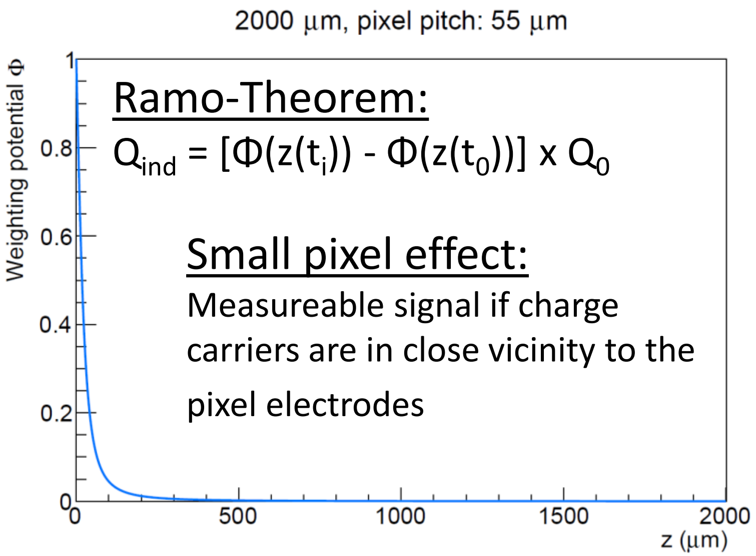

Ramo-Theorem:

$Q_{ind} = [\Phi(z(t_i)) - \Phi(z(t_0))] \times Q_0$

Small pixel effect:

Measureable signal if charge carriers are in close vicinity to the pixel electrodes

Charge carrier drift motion:

e^- and h^+ drift described by

$$v_e = -\mu_e \times E(z)$$
$$v_h = \mu_h \times E(z)$$

$\mu_{e/h}$: Mobility of e^-/h^+

Electric field parametrization:

$$\text{Si:}\quad \vec{E}(z) = \frac{U_B}{d}\vec{e_z} + \frac{2U_{dep}}{d^2}\left(\frac{d}{2} - z\right)\vec{e_z}\,;$$

$$\text{CdTe:}\quad \vec{E}(z) = \frac{U_B}{d}\vec{e_z}$$

U_B: Bias voltage; U_{dep}: Depletion voltage; d: Sensor thickness

→ Look-up table: $z(t_{meas.}, E_{meas.})$

Bergmann et al. Eur. Phys. J. C (2017) 77: 421. https://doi.org/10.1140/epjc/s10052-017-4993-4
Bergmann et al., Eur. Phys. J. C (2019) 79: 165. https://doi.org/10.1140/epjc/s10052-019-6673-z

Test beam measurement:
3D track reconstruction – 500 µm thick silicon

<u>120 GeV/c pion tracks accompanied by δ-rays:</u>

z-resolution:

σ_z ~ 30 µm

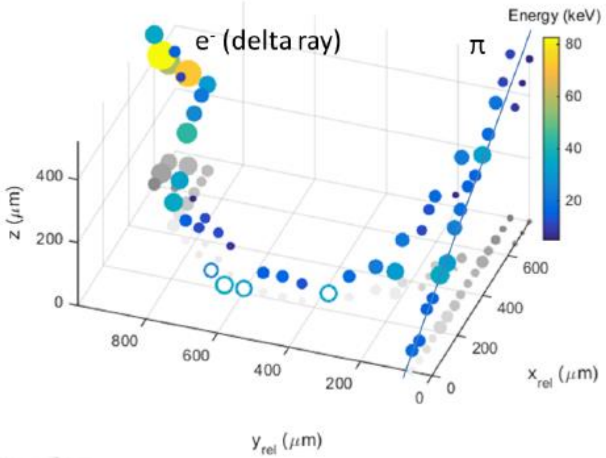

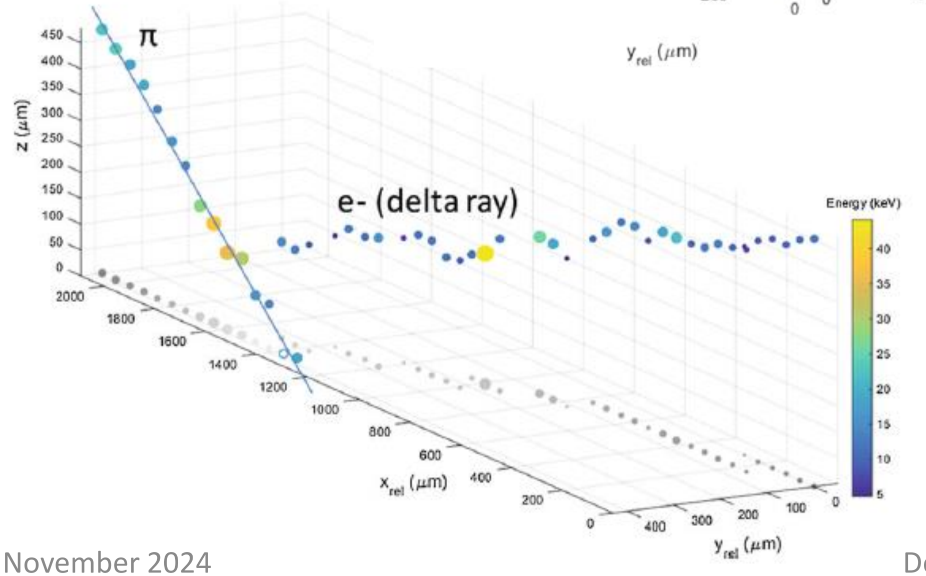

<u>A cosmic µ measured in the Prague laboratory:</u>

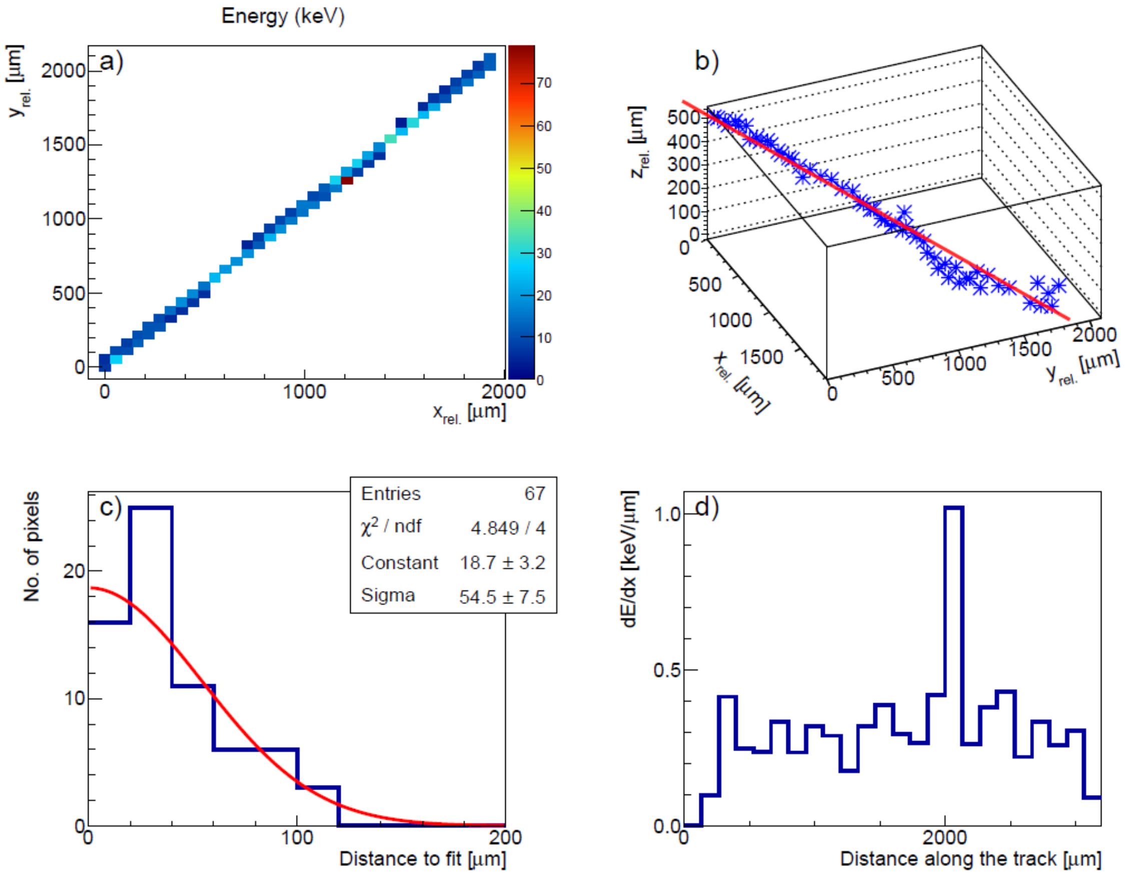

Bergmann et al. Eur. Phys. J. C (2017) 77: 421.
https://doi.org/10.1140/epjc/s10052-017-4993-4

Test measurement:

3D track reconstruction – 2 mm CdTe

Bergmann et al., Eur. Phys. J. C (2019) 79: 165.
https://doi.org/10.1140/epjc/s10052-019-6673-z

$E_{dep} = 5.66$ MeV $e^{-/+}$ like event

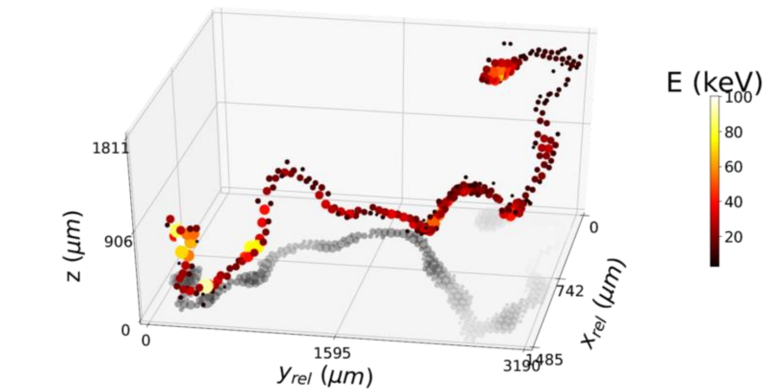

$E_{dep} = 3.96$ MeV   pair production (!?)

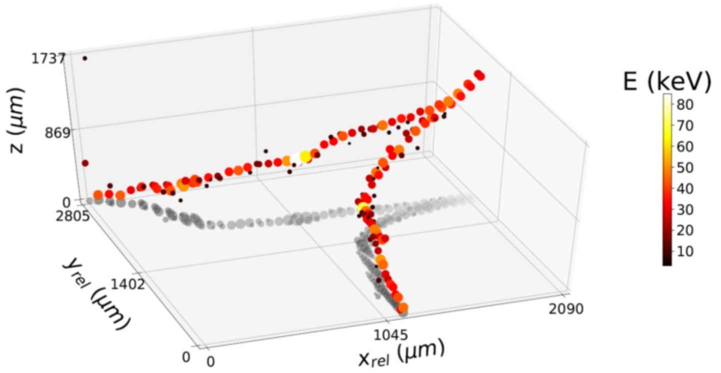

$\frac{dE}{dx} = 1.24 \frac{\text{MeVcm}^2}{\text{g}}$ cosmic μ

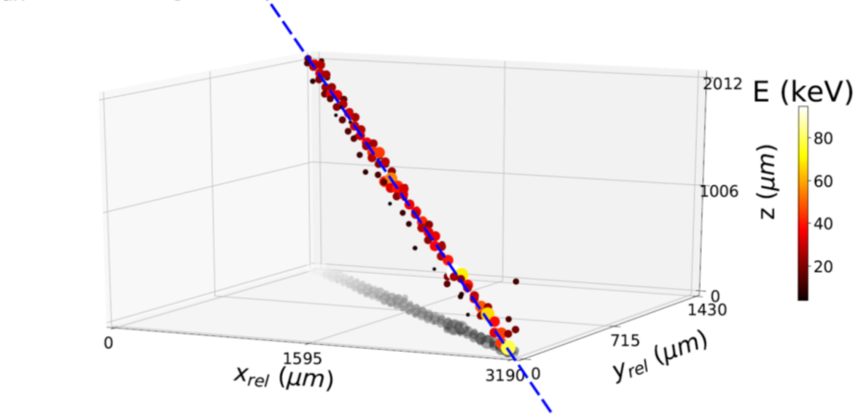

$E_{dep} = 37.06$ MeV   fragmentation

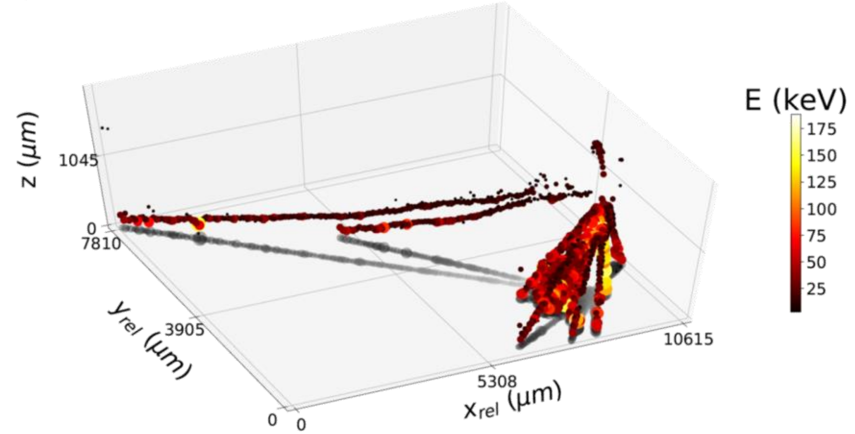

Trajectory reconstruction precision <200 μm at 1 m distance

z-resolution: σ_z ~ 60 μm

→ Improved determination of track directions

→ Improved separation of different particle classes

Chapter 1
Measurements with table-top experiments

Spatial and temporal coincidencing schemes

D. Turecek *et al* 2020 *JINST* **15** C01014

3D reconstruction:

Application as a single-layer Compton Camera

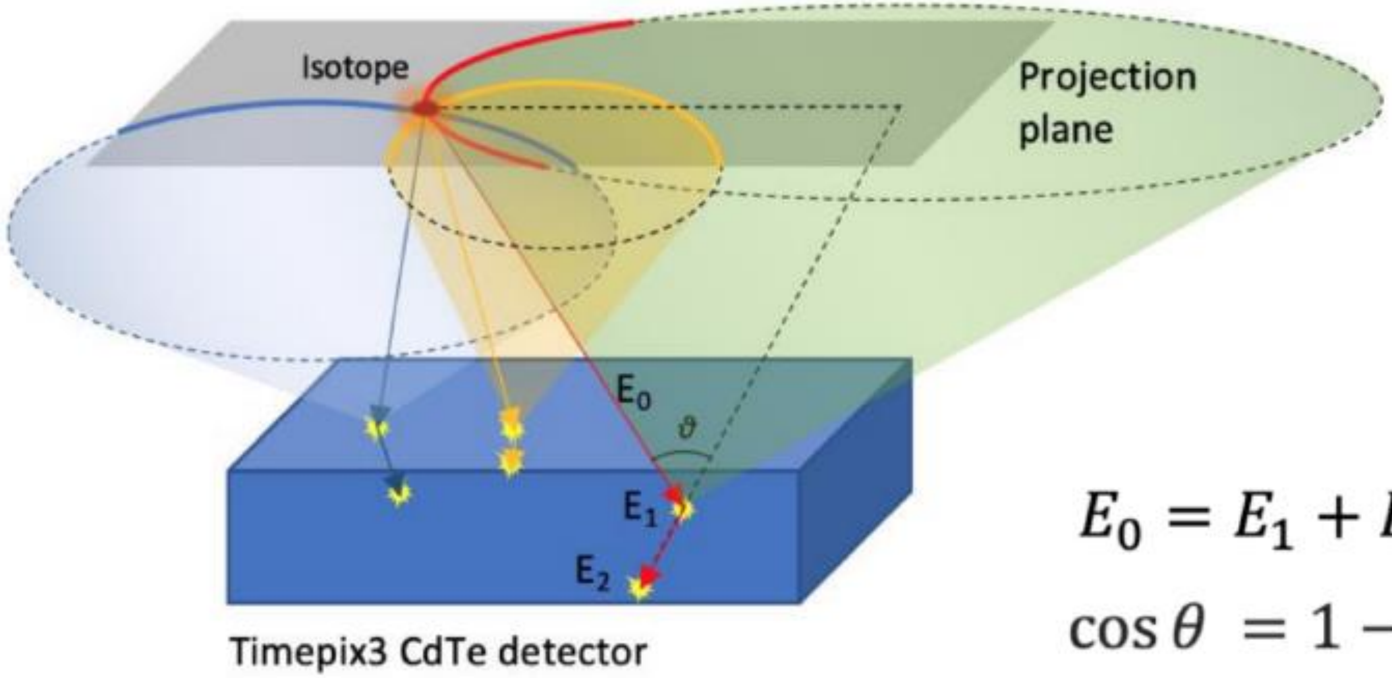

$$E_0 = E_1 + E_2$$

$$\cos\theta = 1 - m_e c^2 \frac{E_1}{E_2(E_1 + E_2)}$$

- Temporal coincidence detection of compton electron and scattered photon
- Energy information for apex calculation through kinematics reconstruction
- Vector between interactions defines axis

P Smolyanskiy *et al* 2024 *Phys. Scr.* **99** 015301

3D reconstruction:
Single-layer Compton Camera -

5 mm CZT Timepix3 (110 µm pitch) irradiated with a ^{22}**Na** at different lateral displacement.

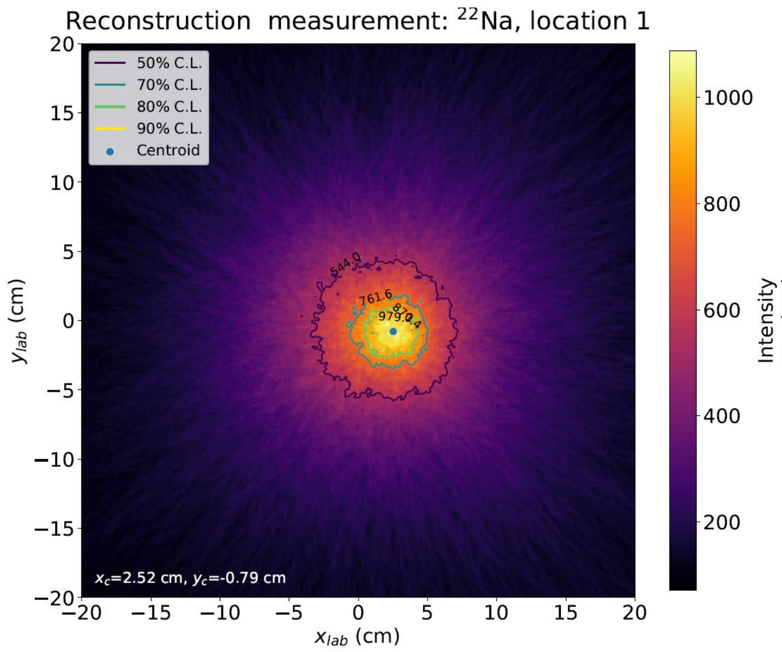

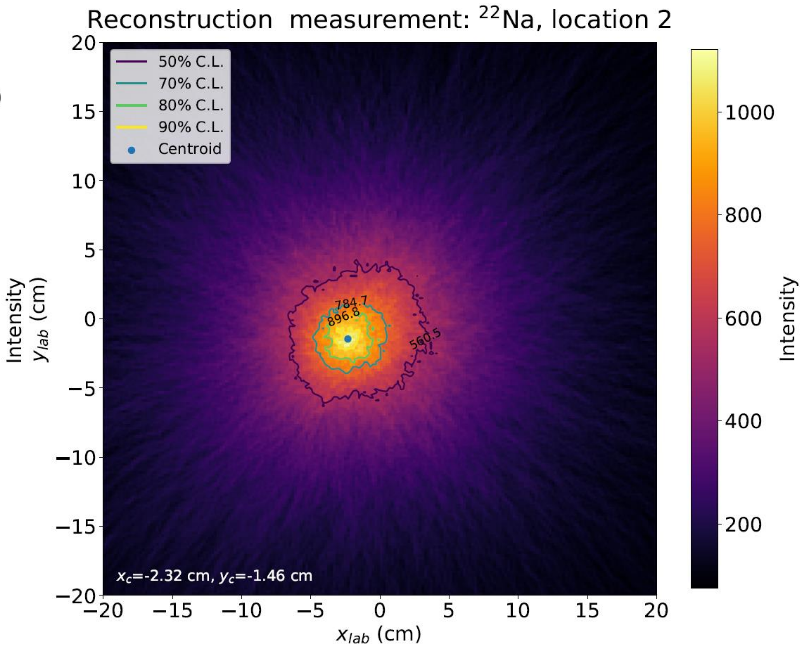

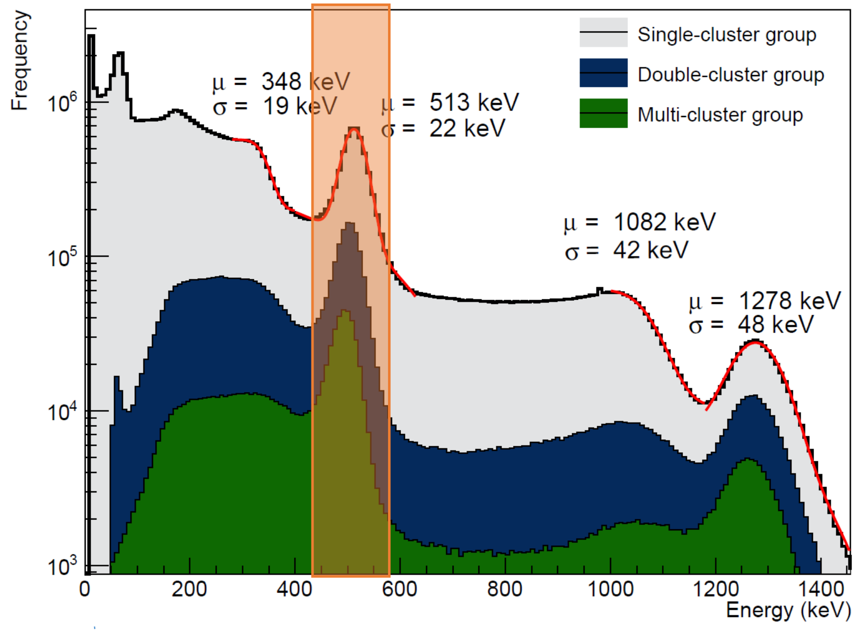

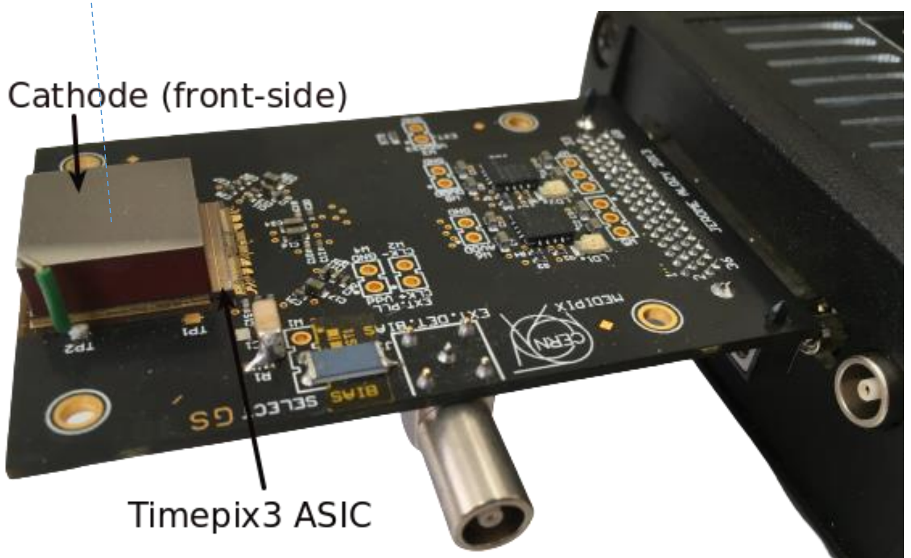

T. Michel, J. Durst, J. Jakubek, “X-ray polarimetry by means of Compton scattering in the sensor of a hybrid photon counting pixel detector,” NIMA 603, Issue 3, pp 384-392 (2009) https://doi.org/10.1016/j.nima.2009.02.032

Timepix3 Compton polarimeter - principle

Differential cross section for Compton scattering off an electron is described by the Klein-Nishina formula:

$$\frac{d\sigma}{d\Omega} = \frac{1}{2} r_0^2 \frac{E^2}{E_0^2} \left(\frac{E}{E_0} + \frac{E_0}{E} - 2 \cdot \sin^2\theta \cos^2\phi \right)$$

Φ is the angle between the electric field vector of the incoming photon and the scattering plane

$$M(\beta) = A\cos^2(\beta - \Phi_0) + B$$

$$\rightarrow \mu = \frac{A}{A+2B} \quad \text{(modulation)}$$

Degree of linear polarization $P = \frac{\mu}{\mu_{100}}$

Detected Compton-scatter pair

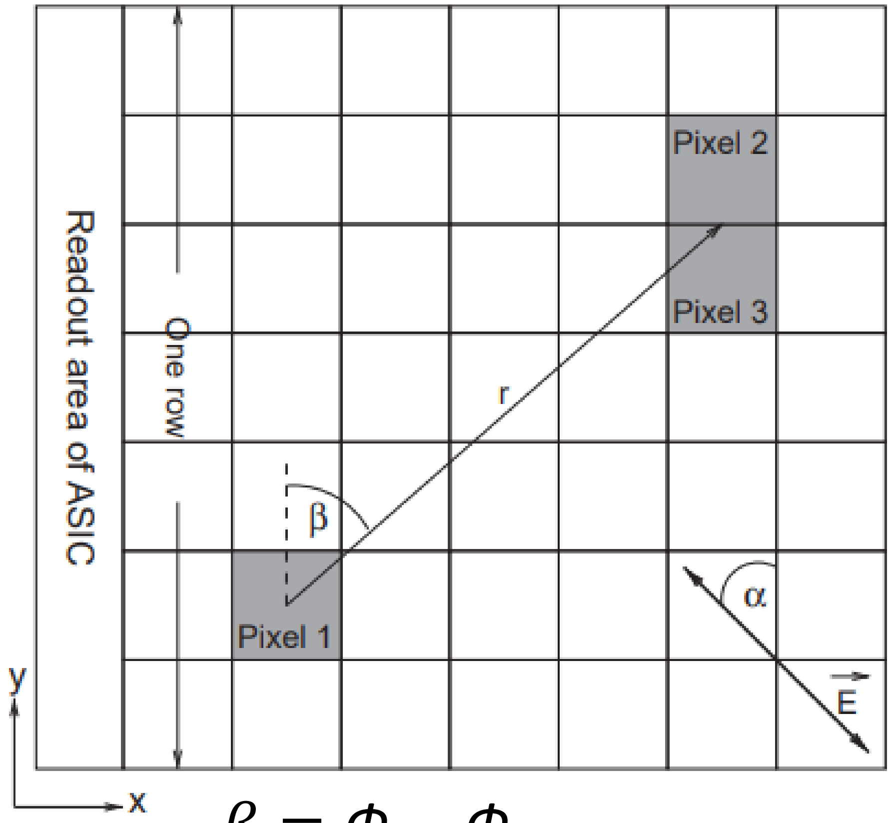

$$\beta = \Phi - \Phi_0$$

Bergmann et al. *Instruments* 2024, **8**(1), 17; https://www.mdpi.com/2410-390X/8/1/17

Timepix3 Compton polarimeter - principle

Summer student project of
Jindra Jelinek

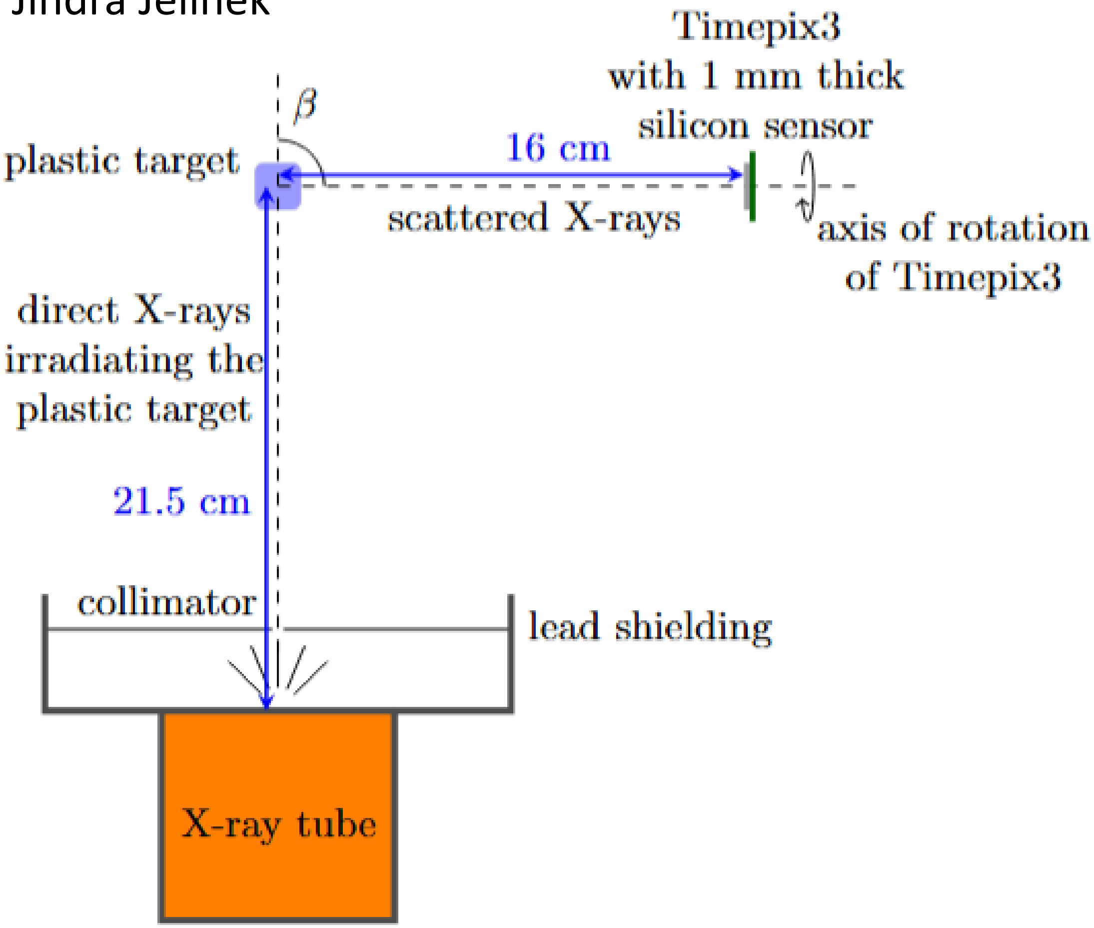

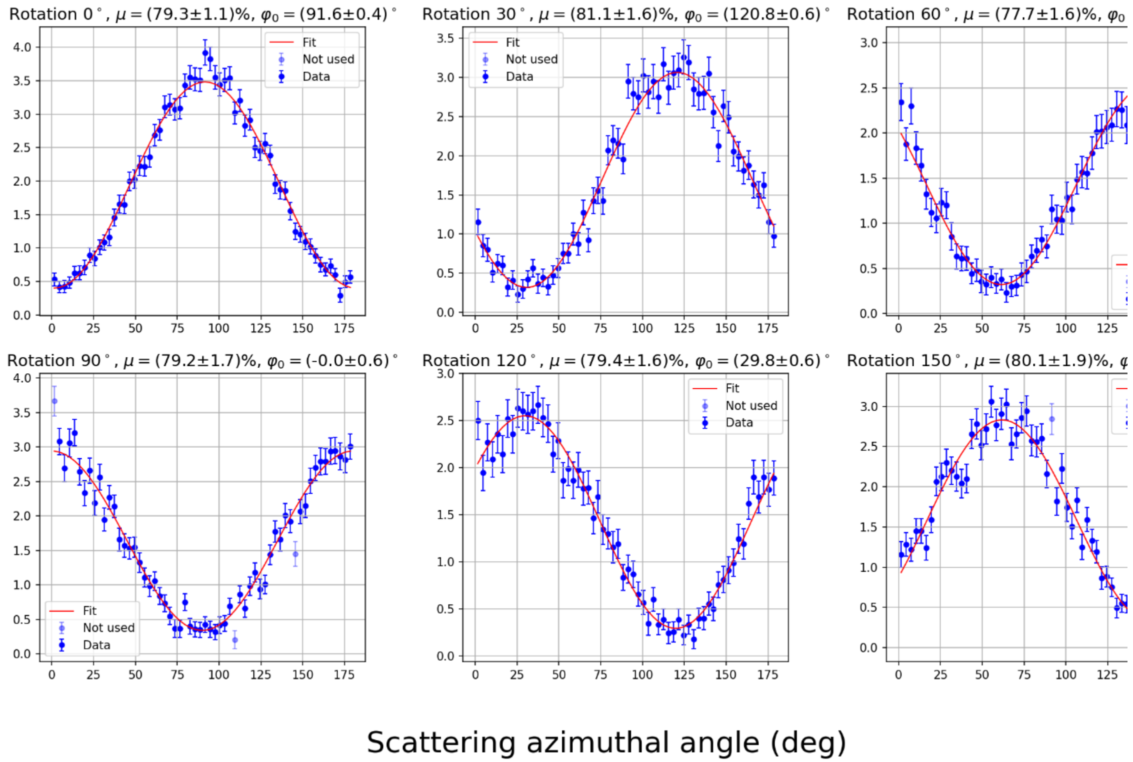

$$M(\beta) = A\cos^2(\beta - \Phi_0) + B$$

$$\mu_{meas} = 80\%$$

Precision measurement of the ^{212}Po and ^{214}Po half-life times with Timepix3

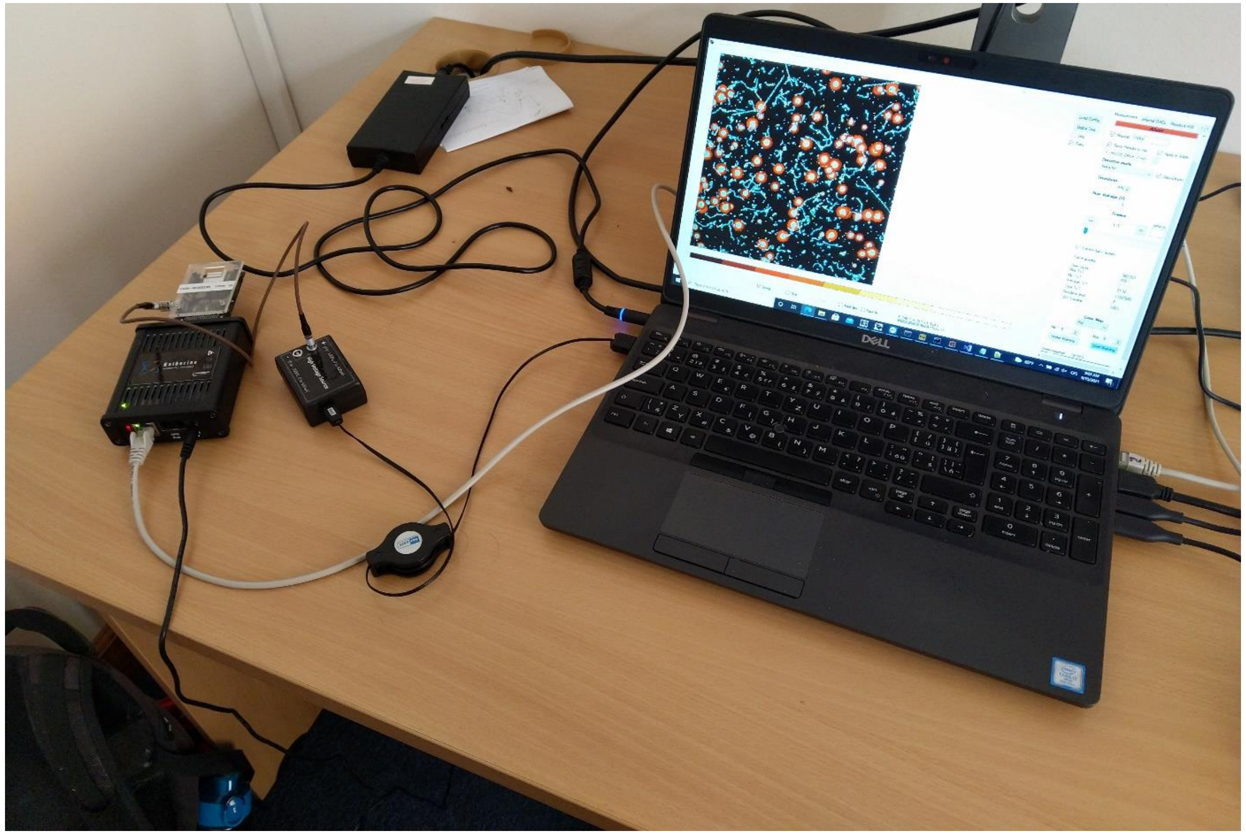

B. Bergmann, and J. Jelinek, "Measurement of the ^{212}Po, ^{214}Po and ^{212}Pb half-life times with Timepix3", *Eur. Phys. J. A* **58**, 106 (2022).
https://doi.org/10.1140/epja/s10050-022-00757-z

The polonium decay signature

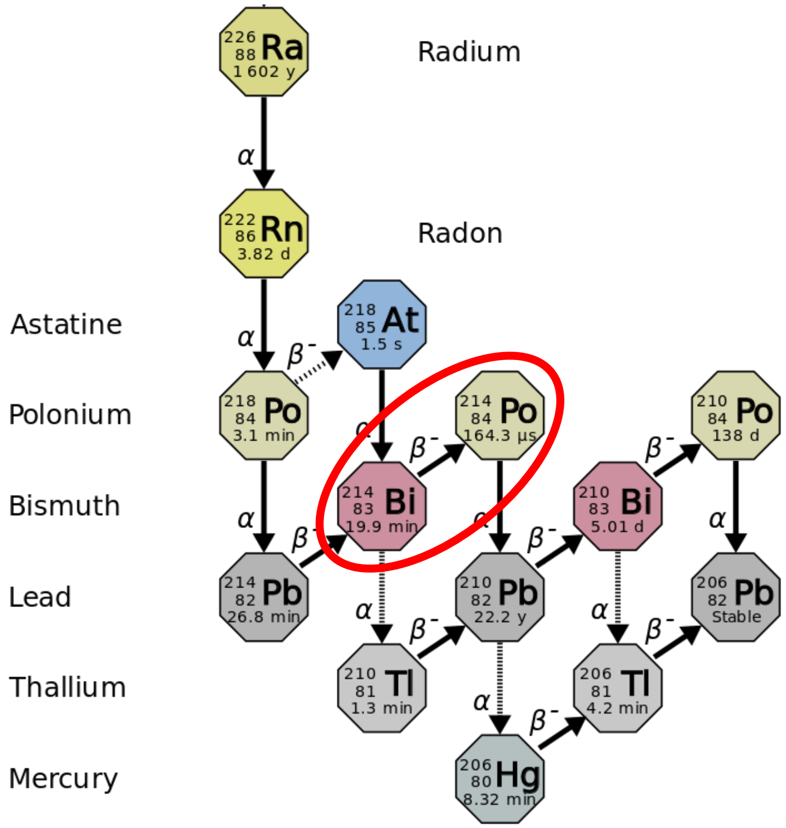

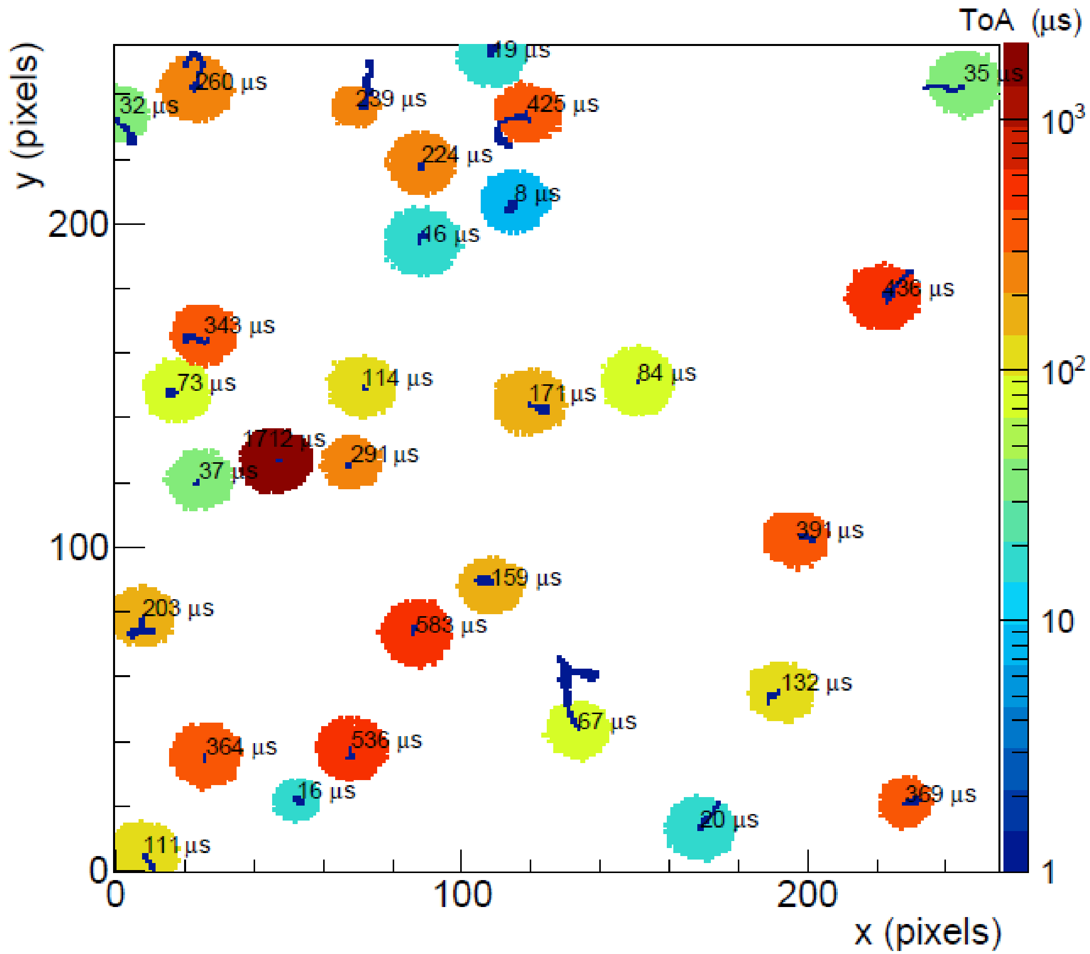

Measurements at the National Radiation Protection Institute (SURO)

$$^{222}\mathrm{Rn} \xrightarrow[Q_\alpha=5.6\,\mathrm{MeV}]{3.82\,\mathrm{d}} {}^{218}\mathrm{Po} \xrightarrow[Q_\alpha=6.1\,\mathrm{MeV}]{3.0\,\mathrm{min}} \mathbf{^{214}Pb}$$

$$\xrightarrow[Q_\beta=1.0\,\mathrm{MeV}]{26.9\,\mathrm{min}} \mathbf{^{214}Bi} \xrightarrow[Q_\beta=3.3\,\mathrm{MeV}]{19.8\,\mathrm{min}} \mathbf{^{214}Po}$$

$$\xrightarrow[Q_\alpha=7.8\,\mathrm{MeV}]{163\,\mu\mathrm{s}} {}^{210}\mathrm{Pb}$$

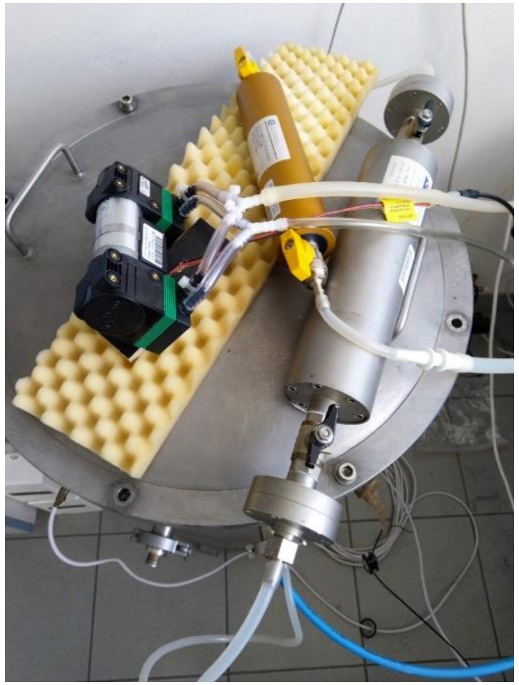

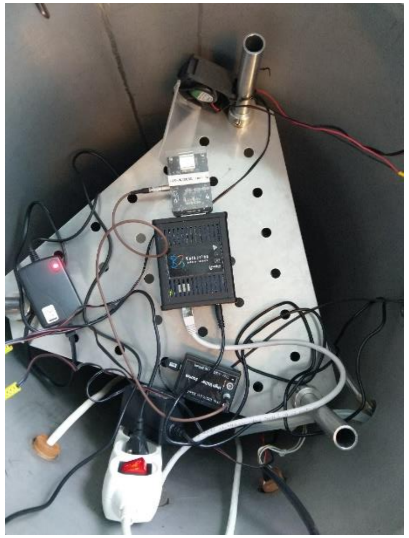

$$^{220}\mathrm{Rn} \xrightarrow[Q_\alpha=6.4\,\mathrm{MeV}]{55.8\,\mathrm{s}} {}^{216}\mathrm{Po} \xrightarrow[Q_\alpha=6.9\,\mathrm{MeV}]{0.15\,\mathrm{s}} \mathbf{^{212}Pb}$$

$$\xrightarrow[Q_\beta=0.57\,\mathrm{MeV}]{10.6\,\mathrm{h}} \mathbf{^{212}Bi} \xrightarrow[Q_\beta=2.3\,\mathrm{MeV}\ (64\%)]{60.6\,\mathrm{min}} \mathbf{^{212}Po}$$

$$\xrightarrow[Q_\alpha=9.0\,\mathrm{MeV}]{295\,\mathrm{ns}} {}^{208}\mathrm{Pb}$$

B. Bergmann, and J. Jelinek, "Measurement of the ^{212}Po, ^{214}Po and ^{212}Pb half-life times with Timepix3", *Eur. Phys. J. A* **58**, 106 (2022).
https://doi.org/10.1140/epja/s10050-022-00757-z

Delayed coincidence spectra - ^{212}Po and ^{214}Po

Nuclear Data Sheets (2020) [17]†	294.3(8)
This work (2021)	295.0(3)

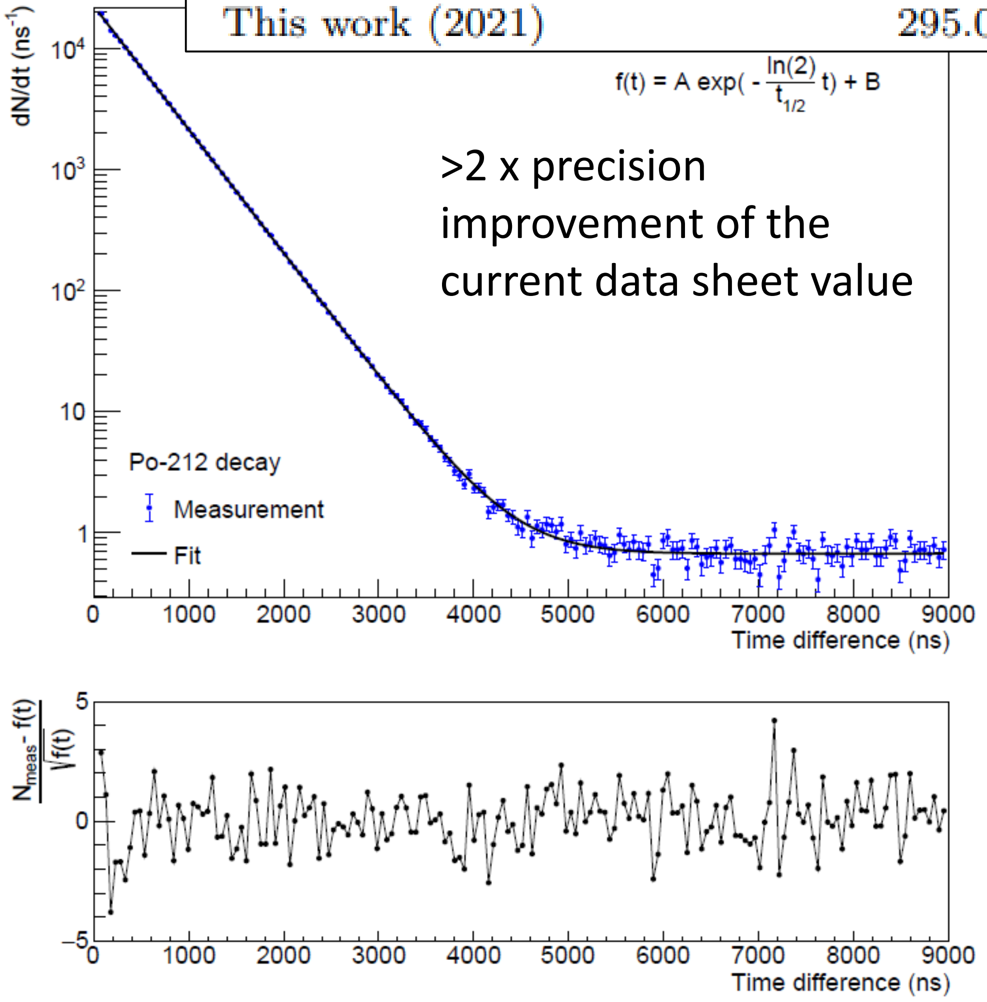

>2 x precision improvement of the current data sheet value

Nuclear Data Sheets (2021) [18]§	163.46(4)
This work (2022)	163.64(10)

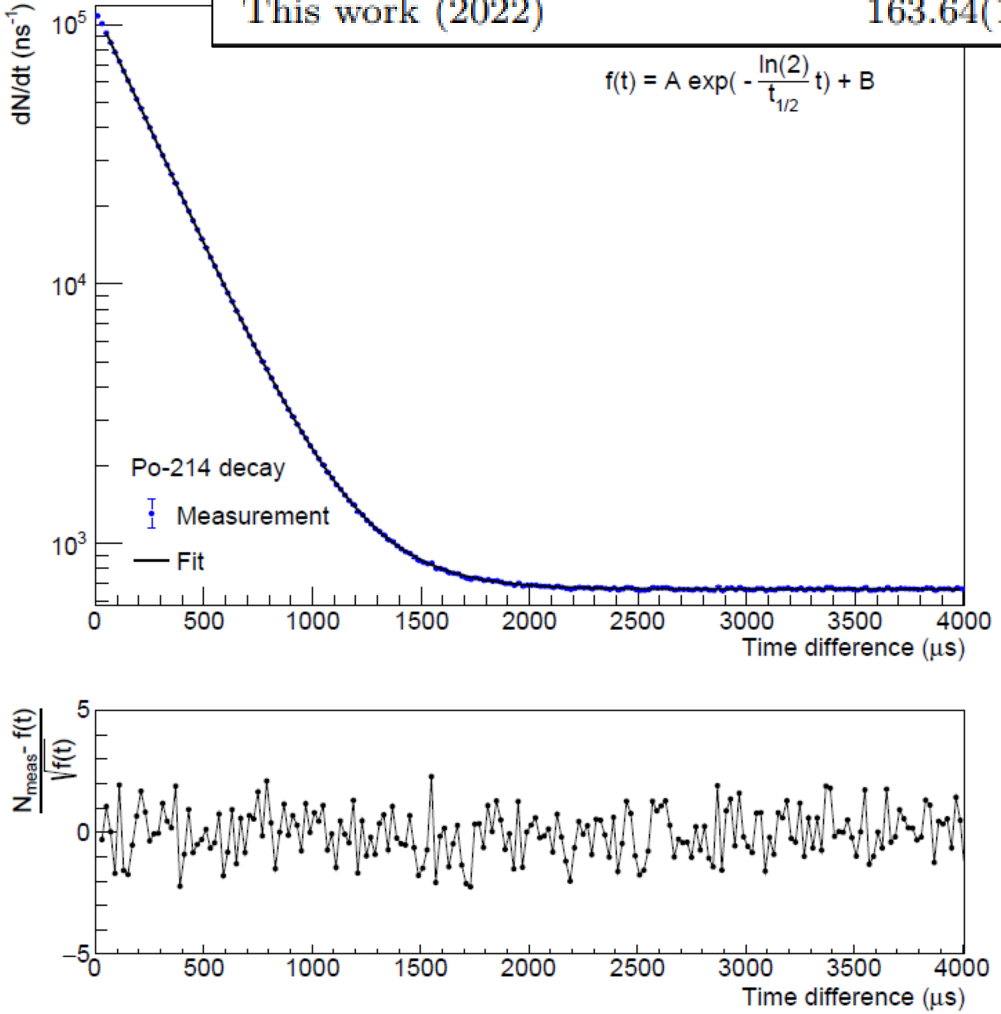

Measurement of the life time of excited states of ^{57}Fe

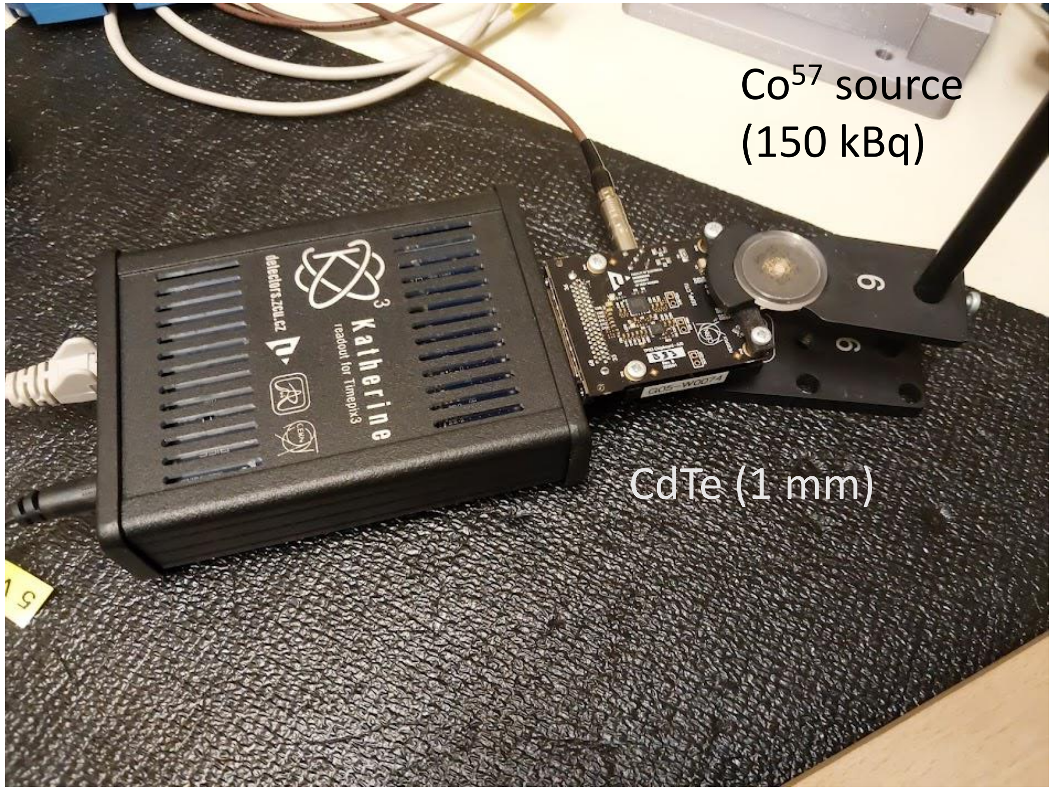

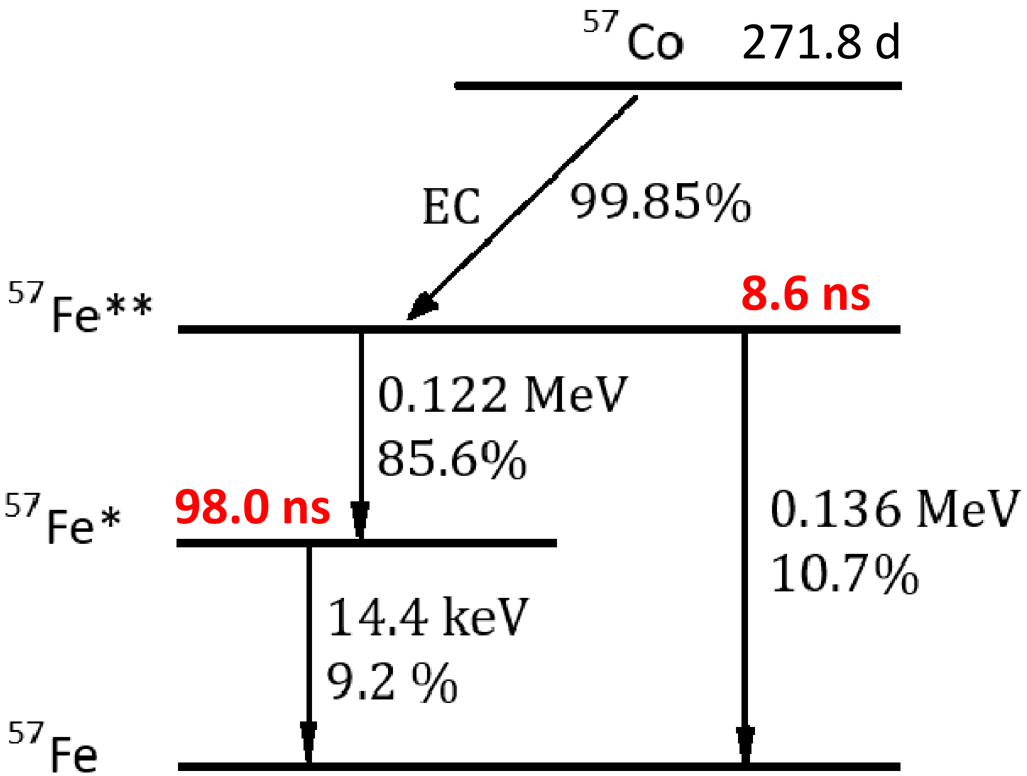

Energy spectrum and signals for half life time measurement

Energy spectrum measured with CdTe

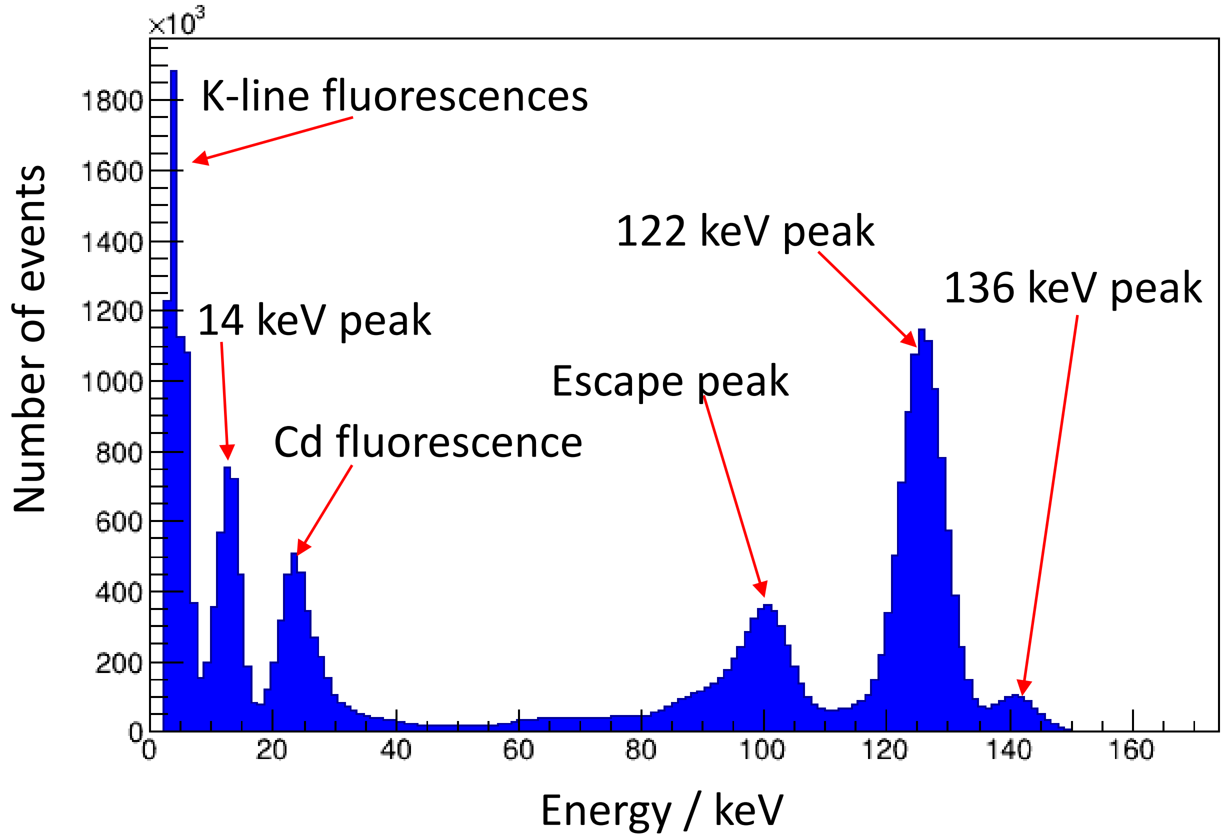

Electron capture decay leaves the daughter atom in an excited state with vacancies in inner orbitals.

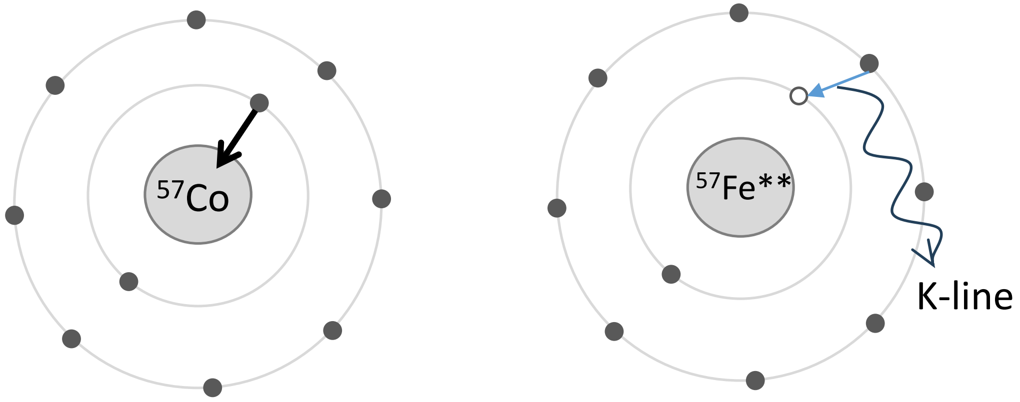

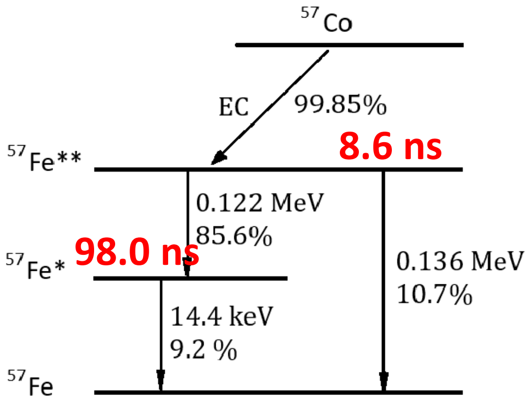

Half life time signals

^{57}Fe** through the delayed coincidence of the

- 6 keV and 136 keV
- 6 keV and 122 keV

^{57}Fe* through delayed coincidence of

- 122 keV and 14.4 keV

Results

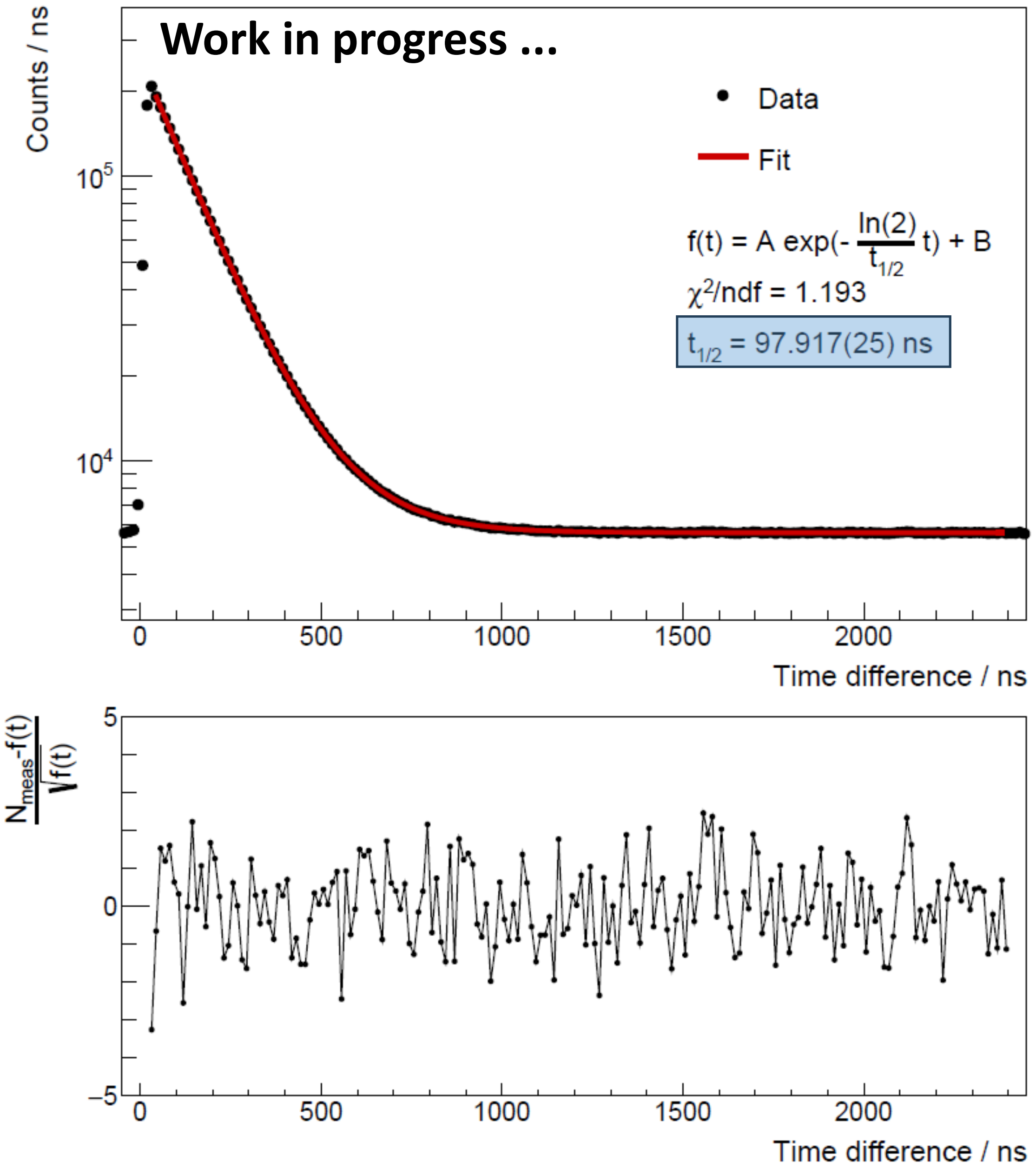
Work in progress ...
Data
Fit
f(t) = A exp(- ln(2)/t1/2 t) + B
χ2/ndf = 1.193
t1/2 = 97.917(25) ns
Counts / ns
Time difference / ns
Nmeas-f(t) / √f(t)
Time difference / ns

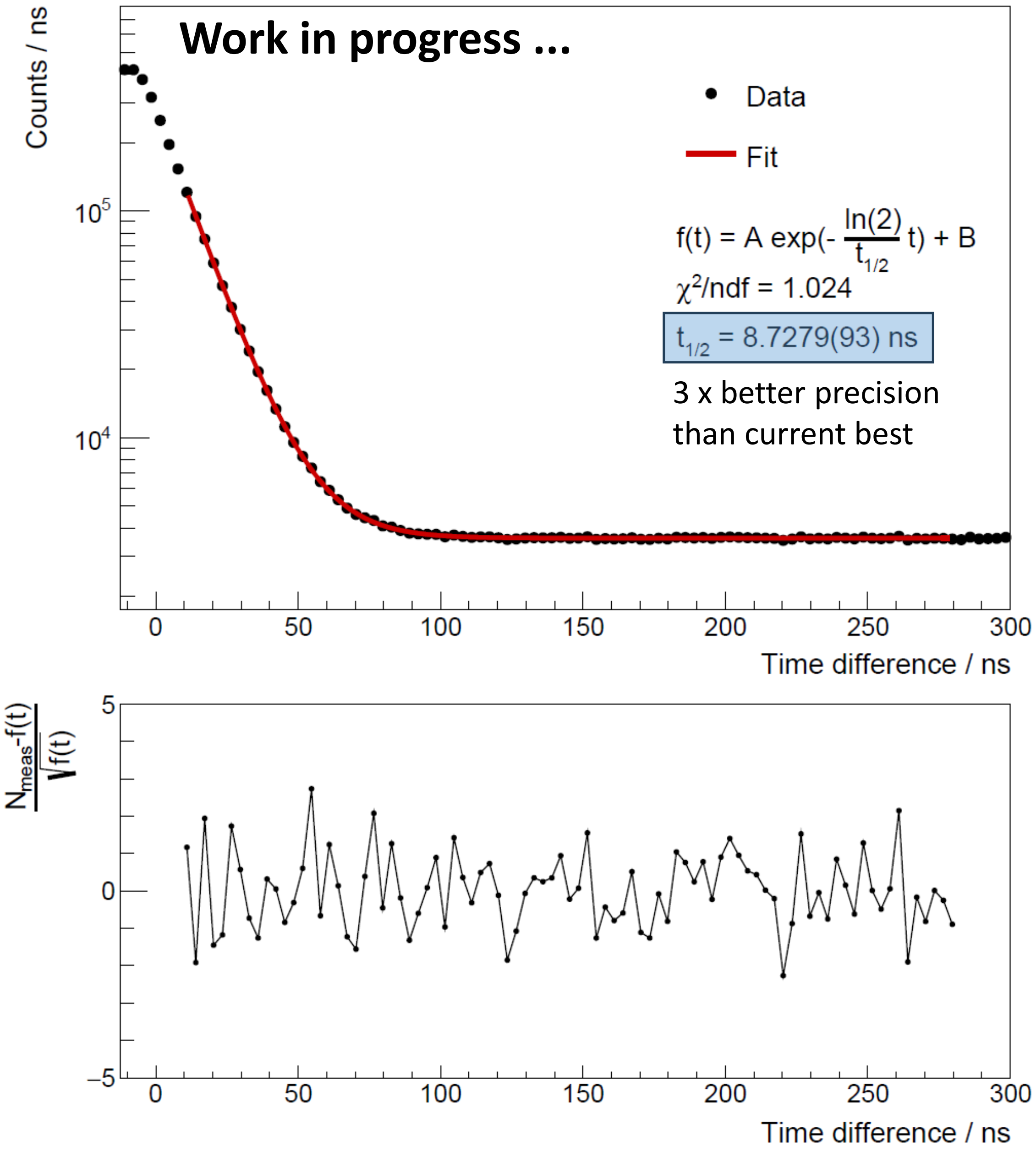
Work in progress ...
Data
Fit
f(t) = A exp(- ln(2)/t1/2 t) + B
χ2/ndf = 1.024
t1/2 = 8.7279(93) ns
3 x better precision
than current best
Counts / ns
Time difference / ns
Nmeas-f(t) / √f(t)
Time difference / ns

Chapter 2

Radiation field decomposition in low earth orbit

Electron & proton discrimination

Proton spectrum measurement

Radiation environment in LEO

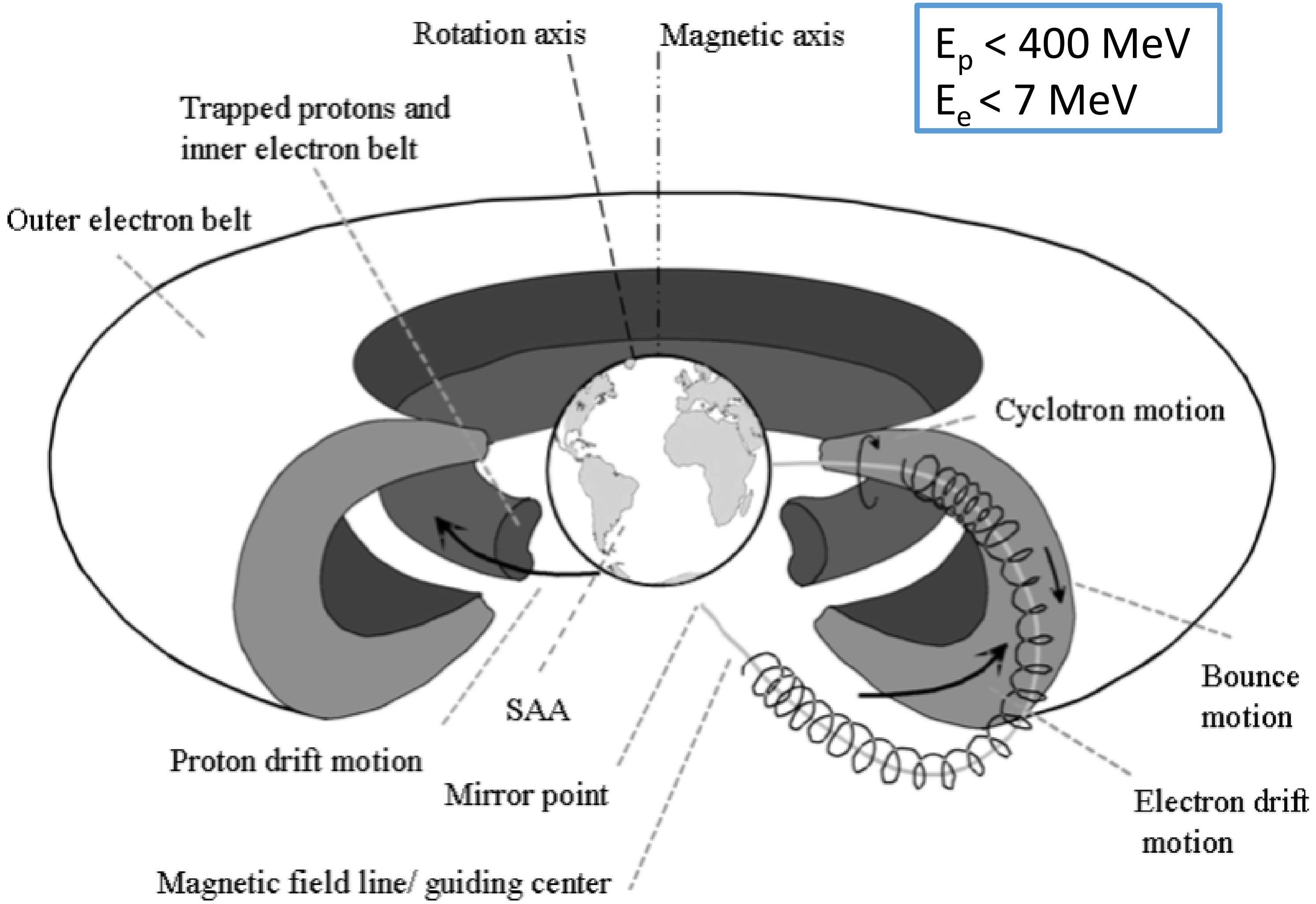

$E_p < 400$ MeV
$E_e < 7$ MeV

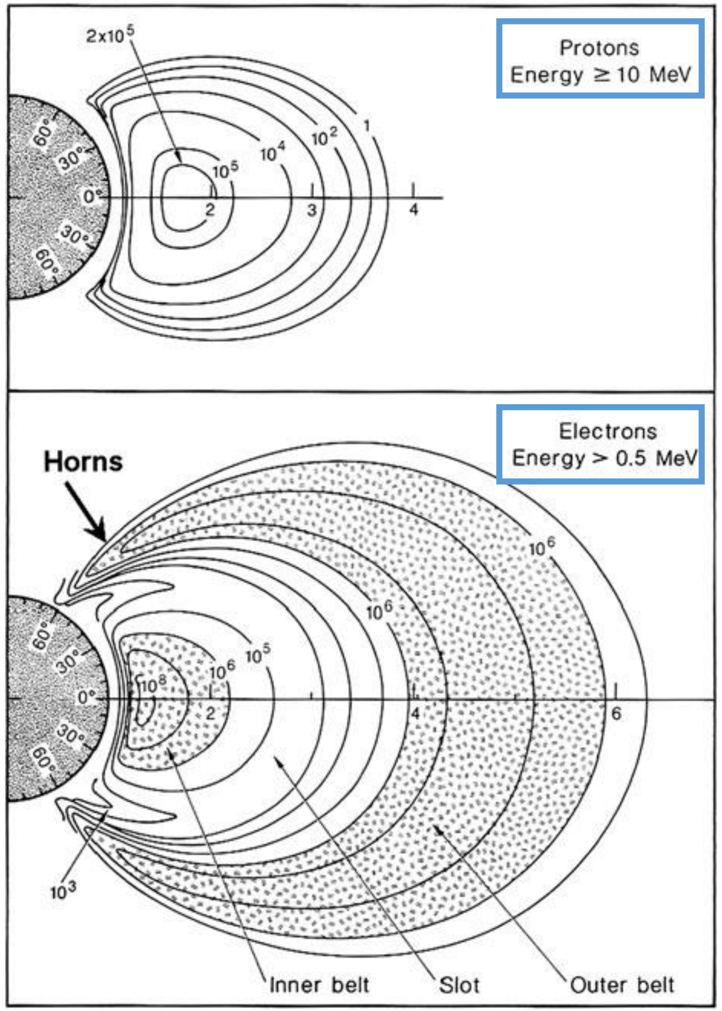

Mauk, B.H., Fox, N.J., Kanekal, S.G. et al. Space Sci Rev (2013) 179: 3.

Space Application of Timepix Radiation Monitor (SATRAM)

- **First Timepix in open space**
- Power consumption of **2.5 W**
- Total mass **380 g** (107 x 70 x 55 mm)
- Platform technology demonstrator

10 x times lower mass budget than space environment monitors with similar capabilities

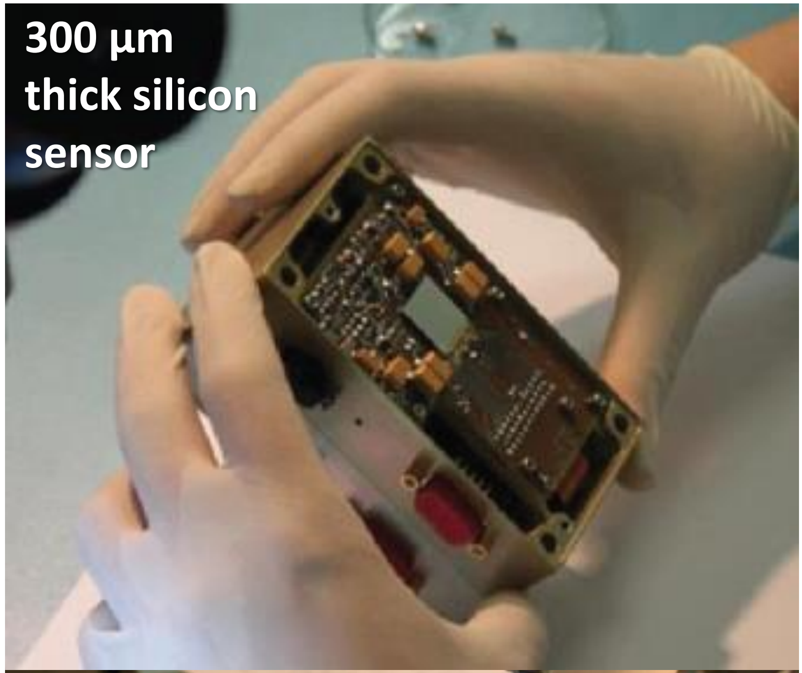

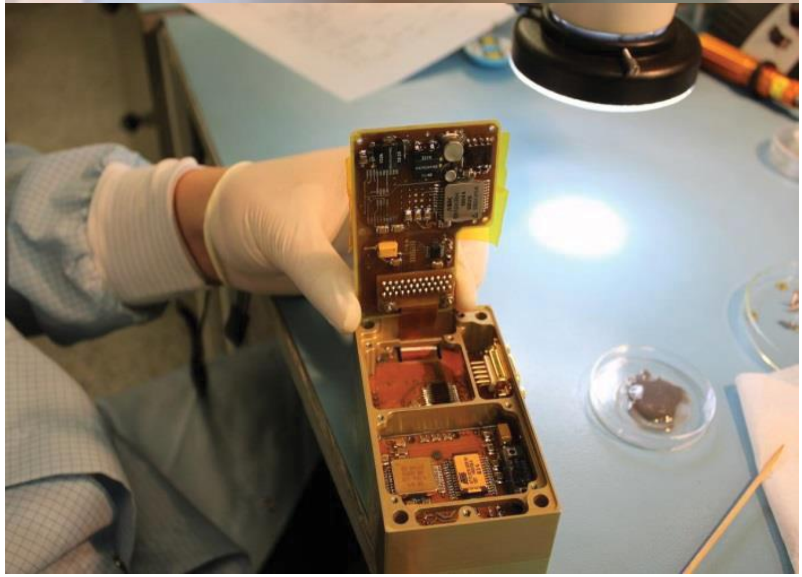

Proba-V

- Minisatellite (158 kg)
- Altitude ~ 820 km (LEO)
- 101.21 minutes orbit duration
- Inclination 98.6°
- Sun-synchronous
- Launched 7th March 2013

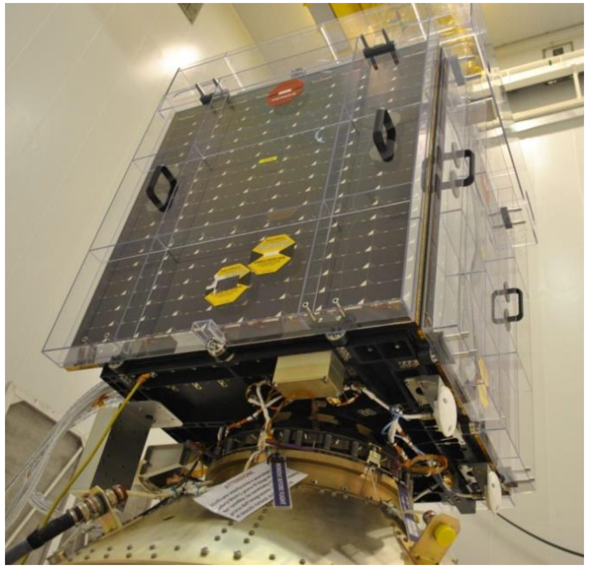

https://satram.utef.cvut.cz/

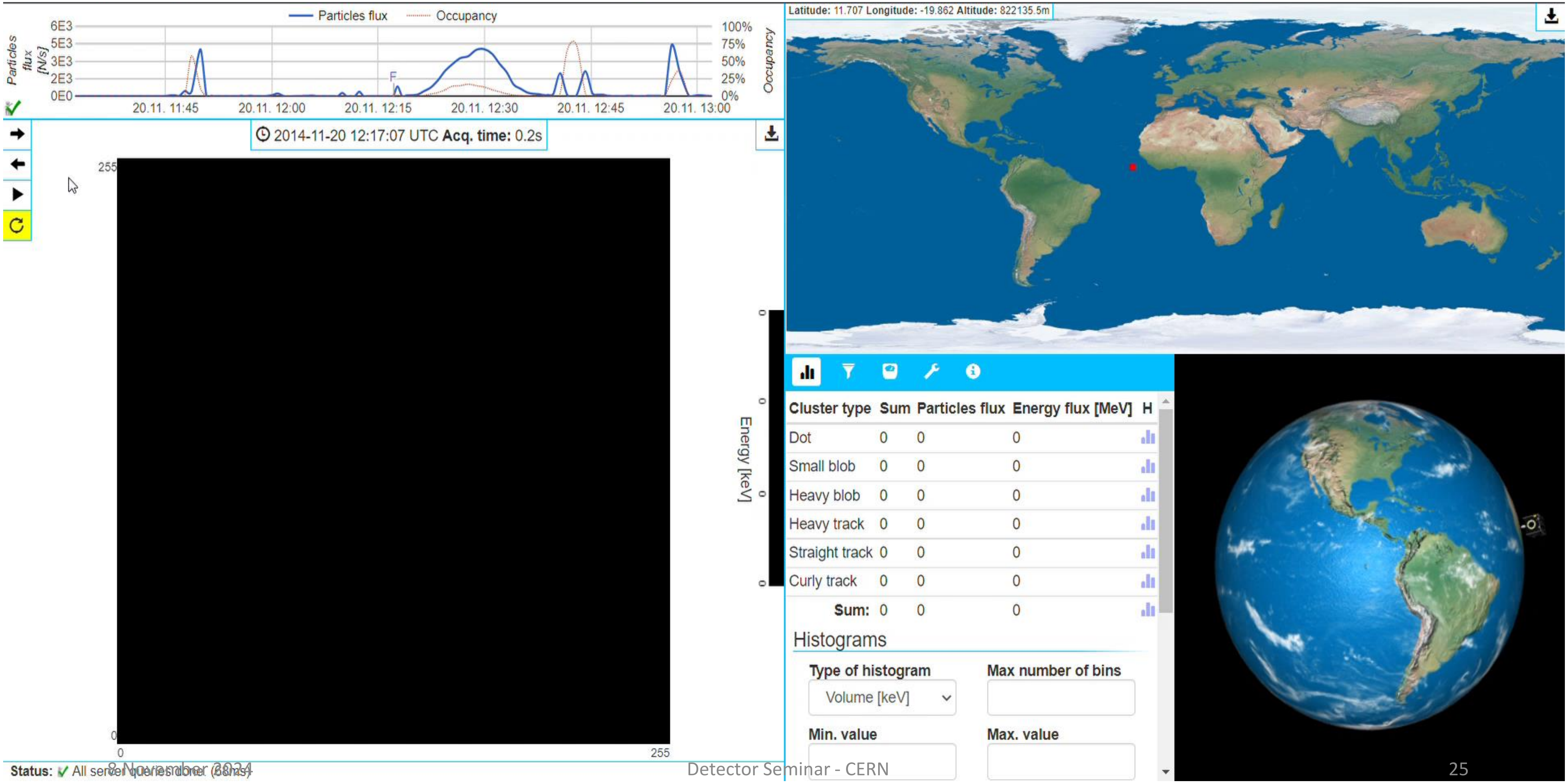

SATRAM - Average dose rate 2015-2018 (mGy/h) - Orbit: 820 km

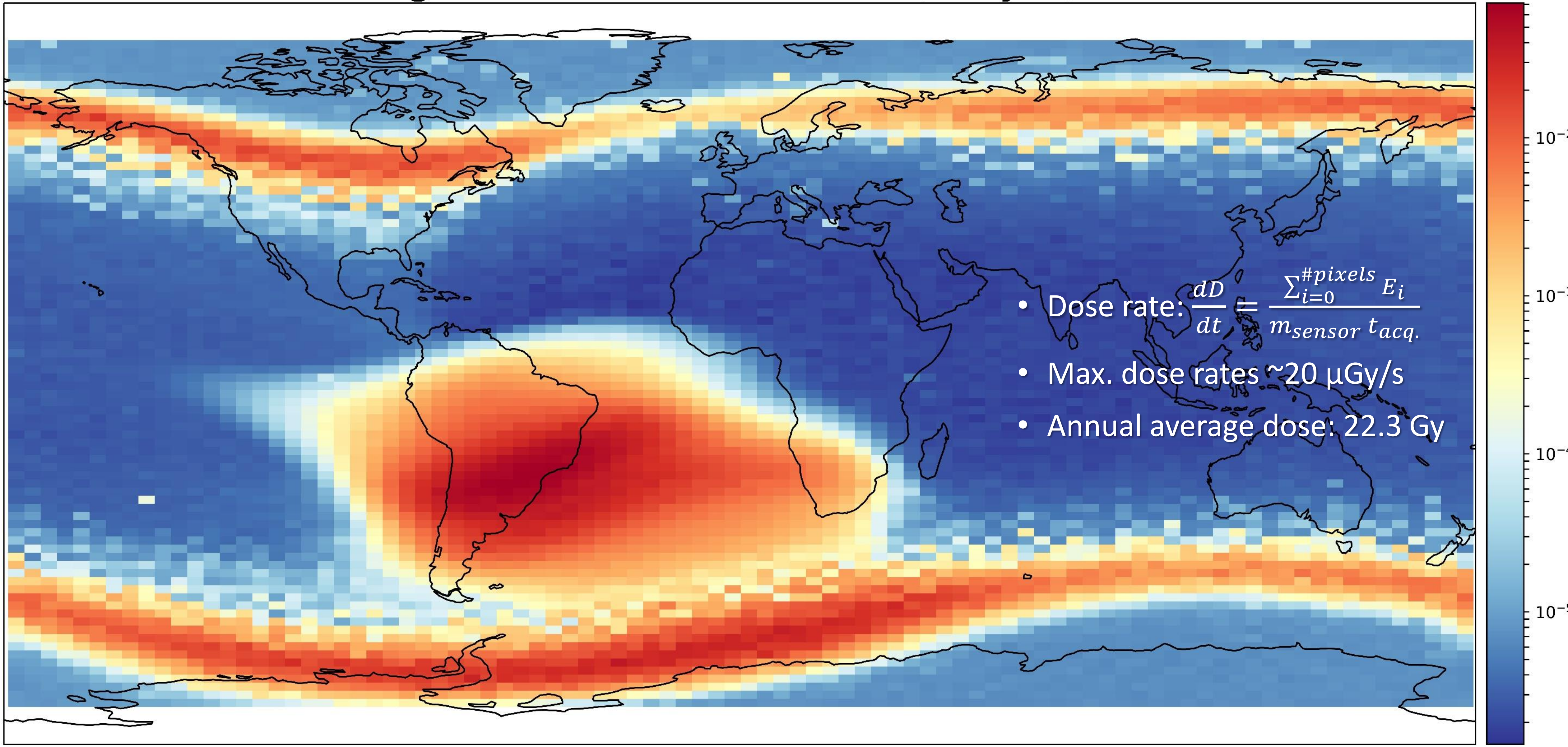

- Dose rate: $\frac{dD}{dt} = \frac{\sum_{i=0}^{\#pixels} E_i}{m_{sensor}\, t_{acq.}}$
- Max. dose rates ~20 µGy/s
- Annual average dose: 22.3 Gy

dE/dX and particle c

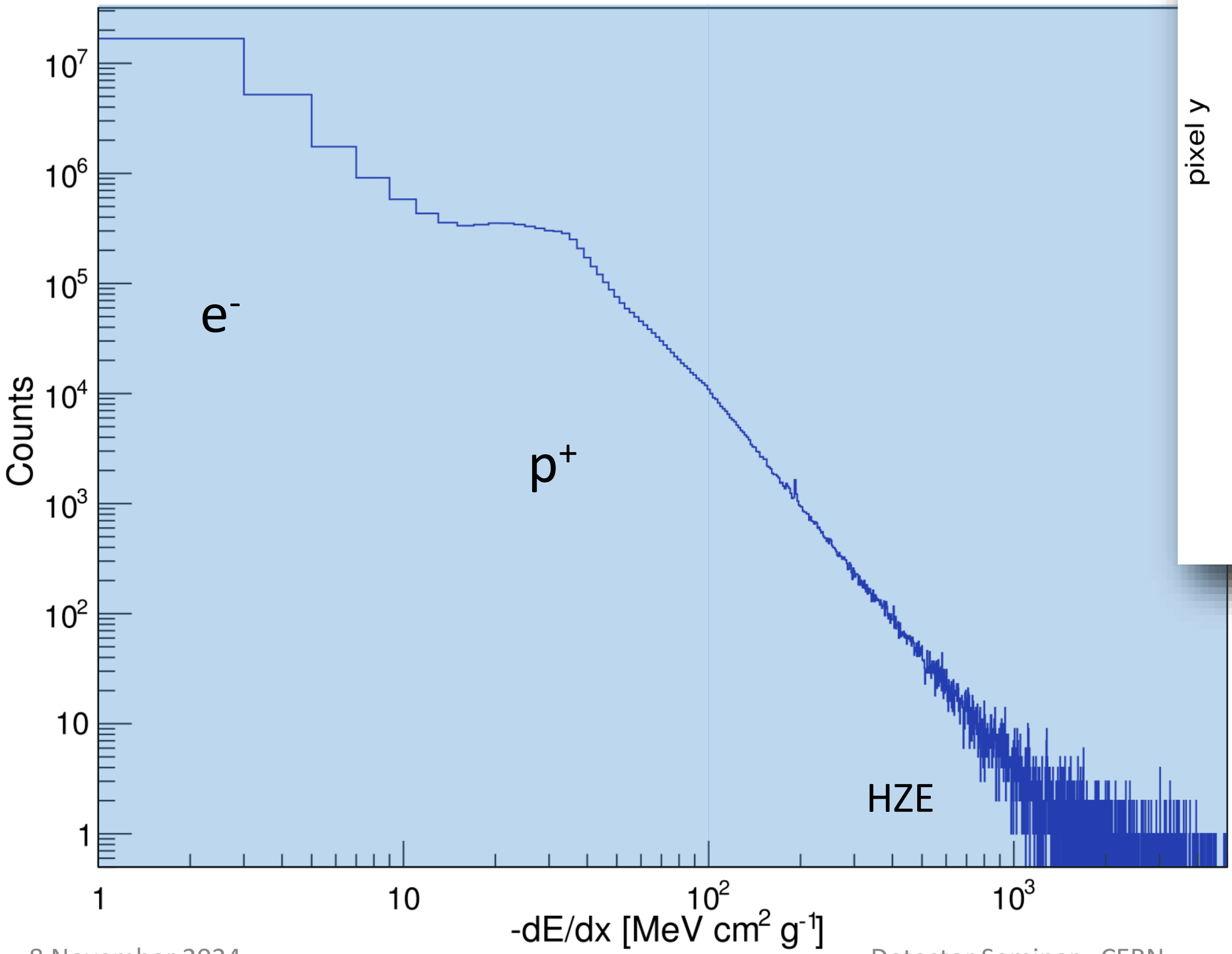

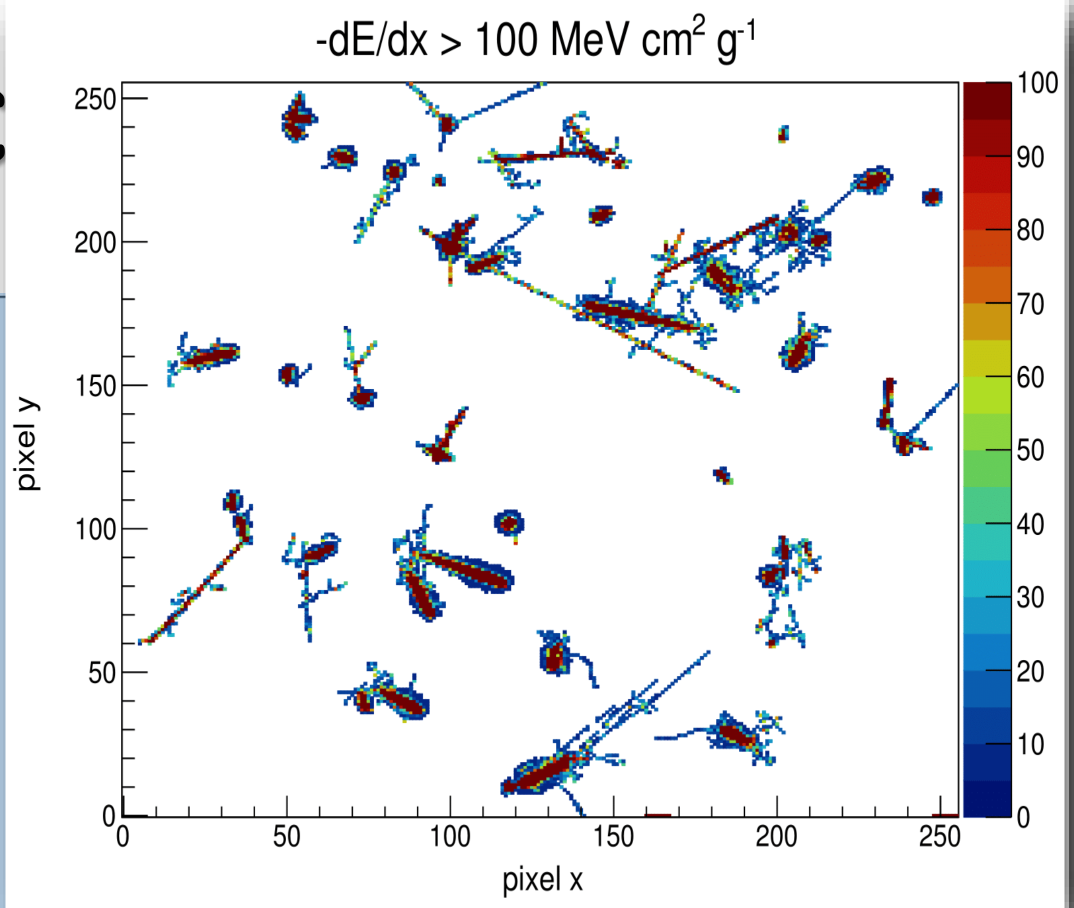

*St. Gohl et al., "Study of the radiation fields in LEO with the Space Application of Timepix Radiation Monitor (SATRAM)", Advances in Space Research **63**, Issue 5, pp. 1646-1660, (2019).*

Electron and proton flux maps

e^- fluxes 3 orders of magnitude larger than p^+ fluxes

→ Even small e^- misclassification distort p^+ flux measurement

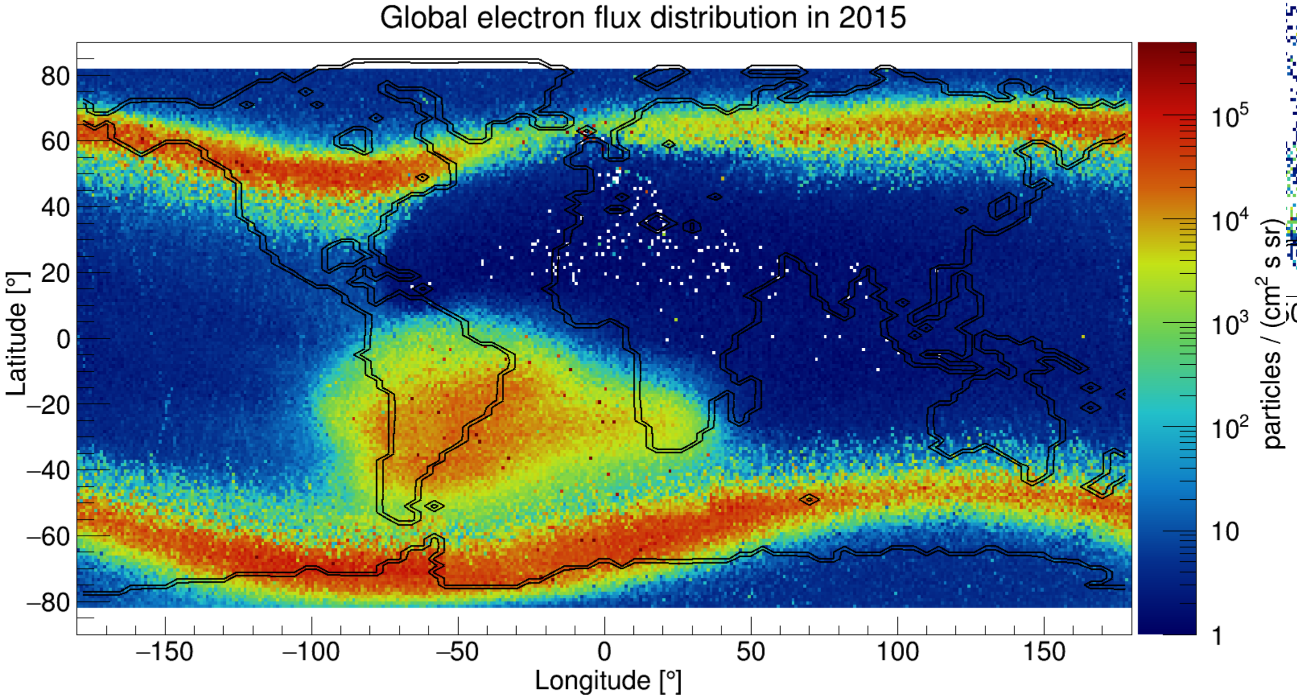

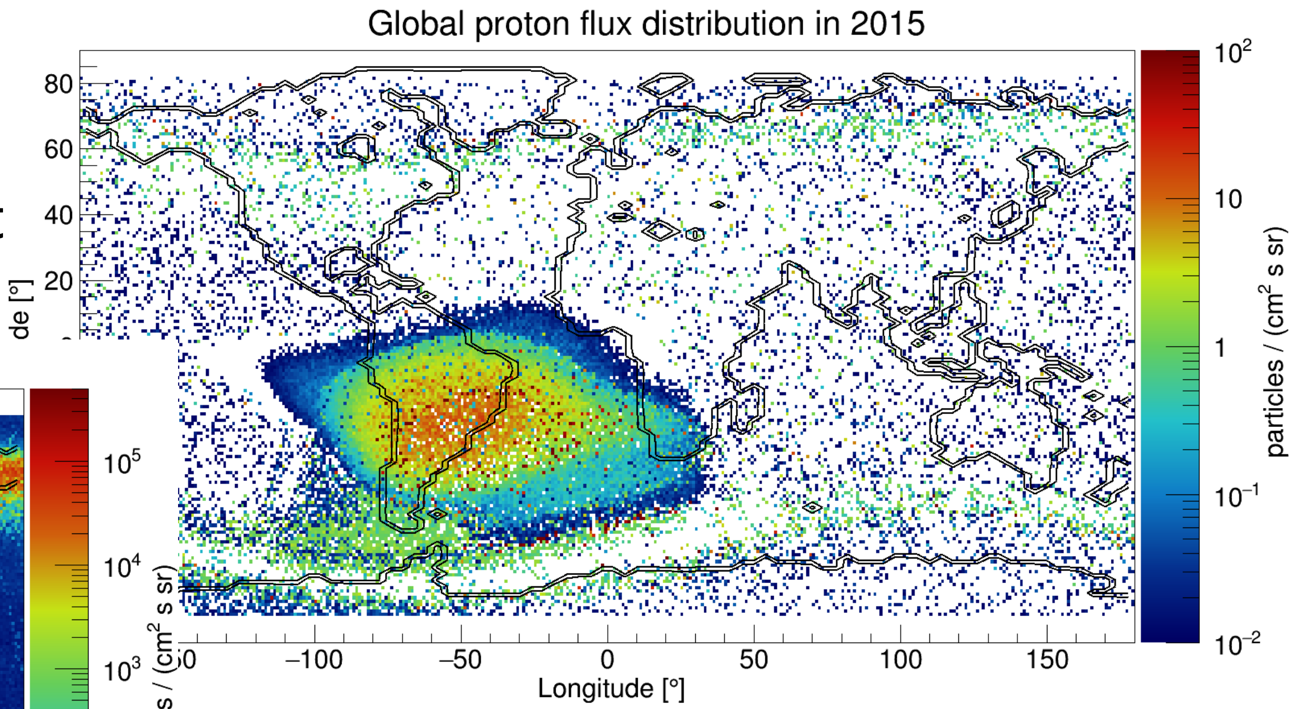

St. Gohl et al., "Study of the radiation fields in LEO with the Space Application of Timepix Radiation Monitor (SATRAM)", Advances in Space Research ***63****, Issue 5, pp. 1646-1660 (2019).*

Proton energy spectrum reconstruction using dE/dX unfolding

Response Matrix

$$n(E) = R\,\phi(C)$$

Particle Spectrum

Measured dE/dx Spectrum

Solved by

$$R^T n(E) = \Phi(C)$$

Typical unfolding codes:

- Matrix inversion
- Richardson Lucy
- Gold deconvolution
- **Bayesian unfolding***

*G. D'Agostini, "A multidimensional unfolding method based on Bayes' theorem" Nucl. Inst. Meth. A **362**, 2-3, pp. 487-498 (1995) https://doi.org/10.1016/0168-9002(95)00274-X dE/dX unfolding:

Response matrix

- Simulated in omnidirectional particle field for **e⁻** (E_e < 6 MeV) and **p⁺** (E_p < 400 MeV)
- Methodology verification in monoenergetic proton beams

Energy (MeV)	125	175	225
σ (MeV)	17	25	42

Resolution averaged over polar angles of 0, 45, 70 and 85 degrees

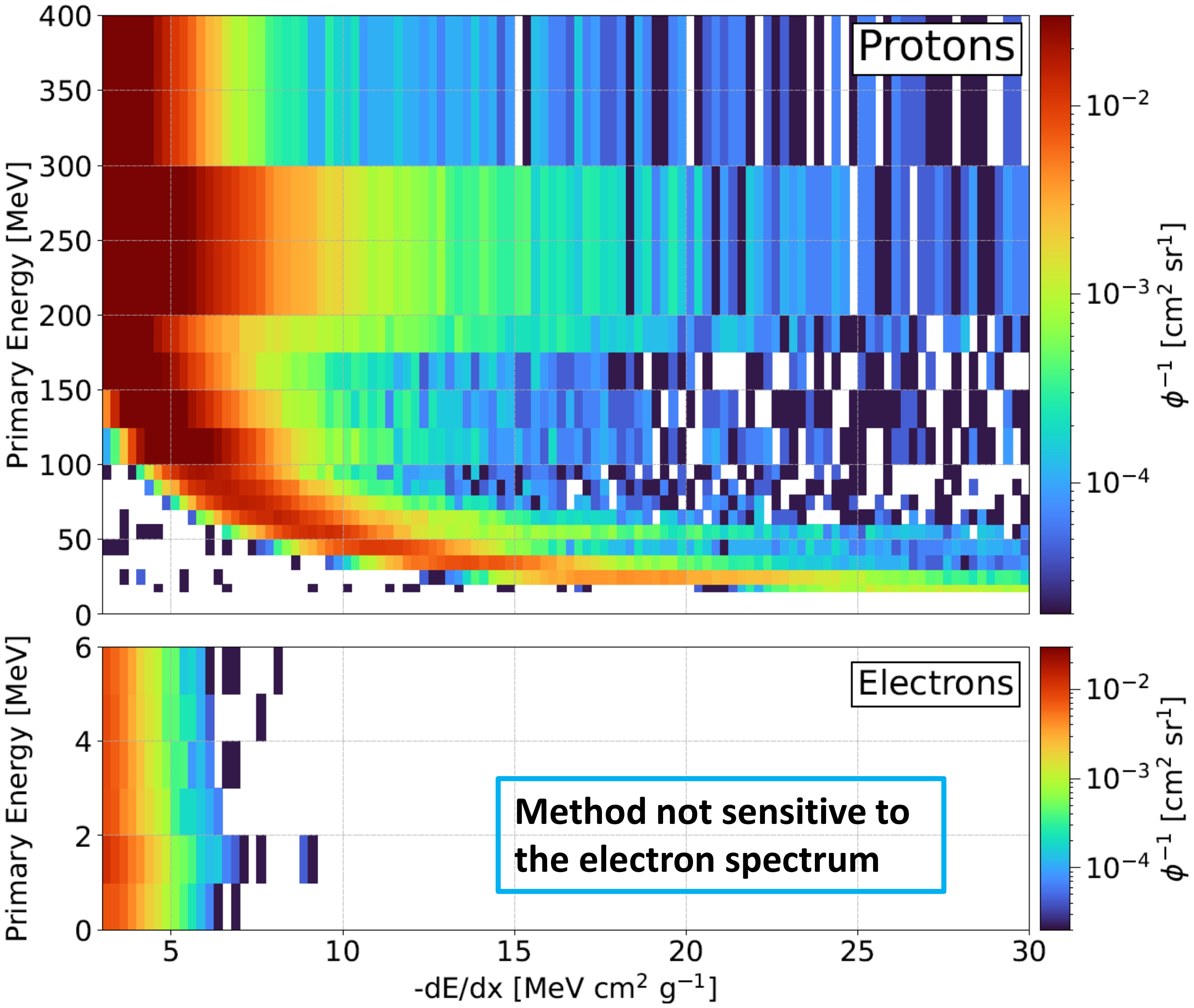

dE/dX unfolding:

Application to measured SATRAM data

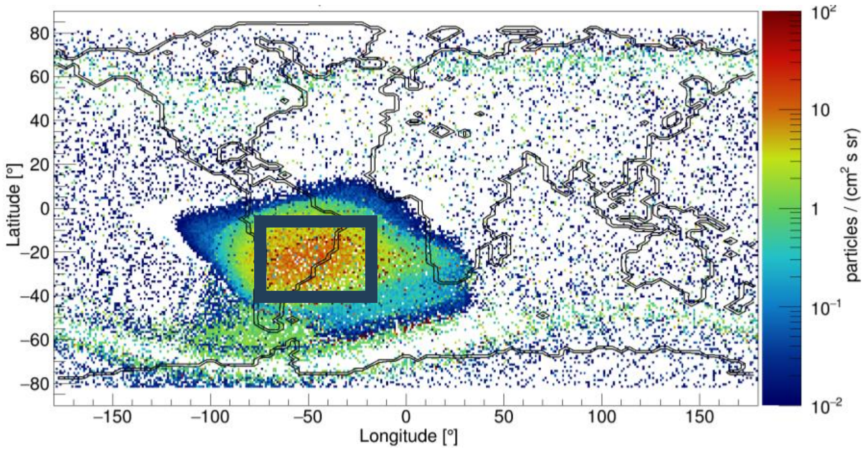

22,784 frames of 2 ms (**t_{meas} = ~46 s**) were found in the selected geographic region in the years 2014-2018.

The electron background was estimated by scaling the unfolded dE/dX spectrum from simulation to the amount of detected e^- signatures.

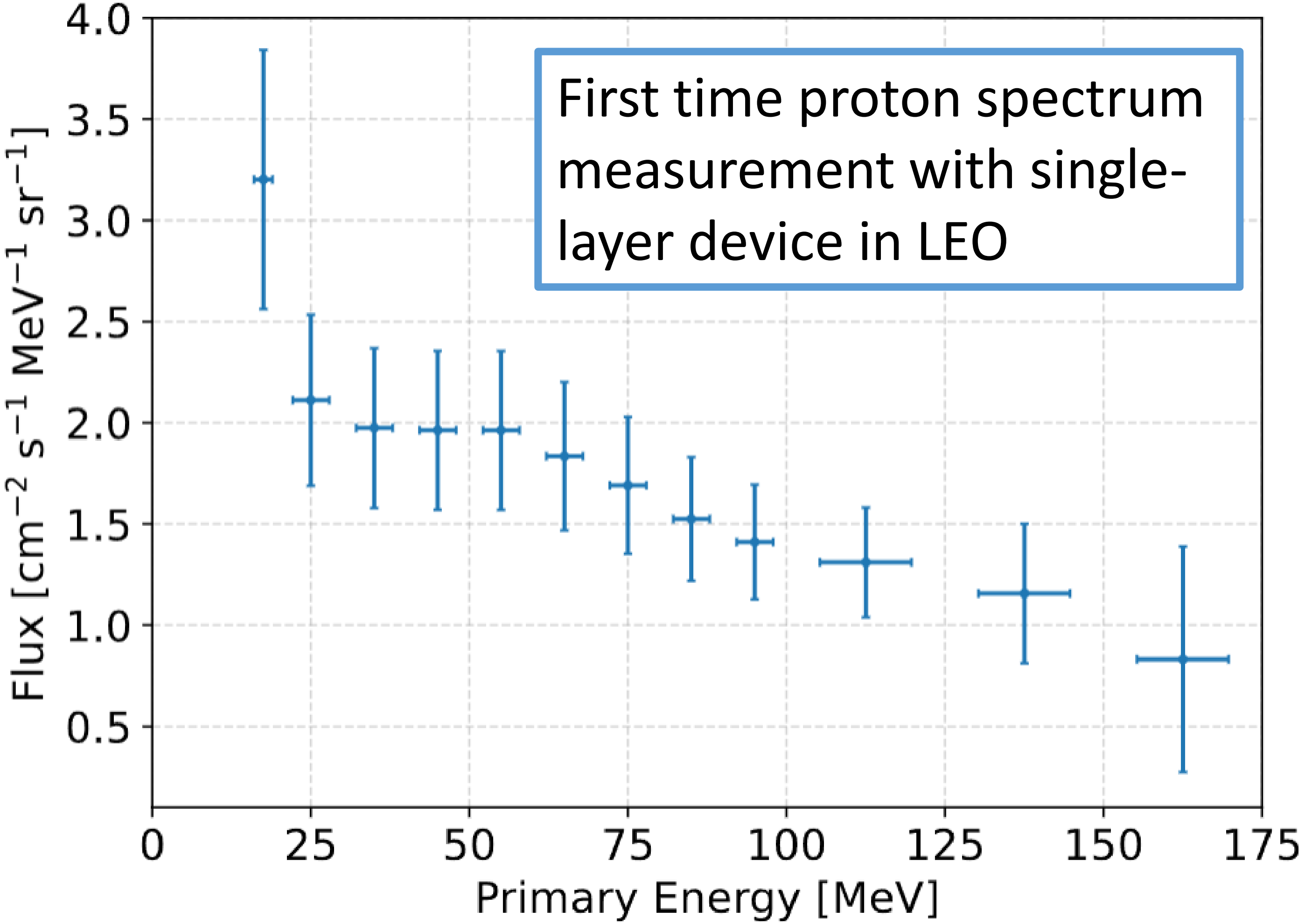

Bergmann et al. *Instruments* 2024, **8**(1), 17; https://www.mdpi.com/2410-390X/8/1/17

Chapter 3

Radiation field decomposition for luminosity measurement in ATLAS

The value of pattern recognition for neutron-gamma discrimination and bunch-sensitive luminosity measurement

Neutron detection with Timepix:

ATLAS-Timepix3 device design

- **^{6}LiF** (89% Li enrichment): ^{6}Li + n → α + ^{3}H + 4.78 MeV
- **PE** (~ 1 mm): recoil protons from elastic scattering
- **PE + Al** (80 µm): fast neutrons above 3.5 MeV
- **Free:** Background subtraction (non-neutron field and neutron interactions in silicon)

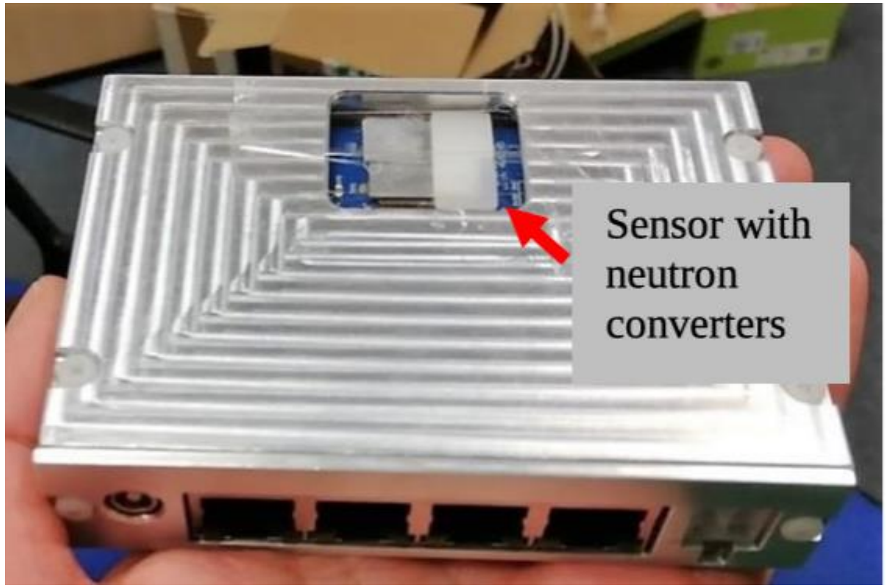

Pattern recognition

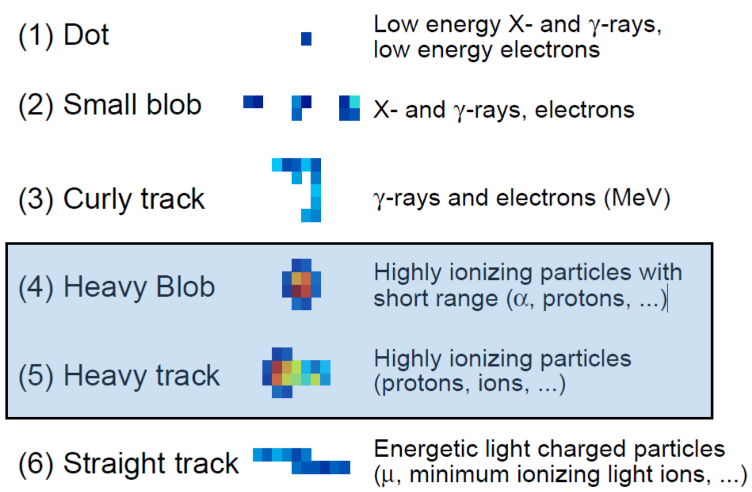

Proper selection of neutron converters and application of pattern recognition allows for **reliable neutron-γ separation**

Neutron detection with Timepix:

Converter effect and γ-discrimination

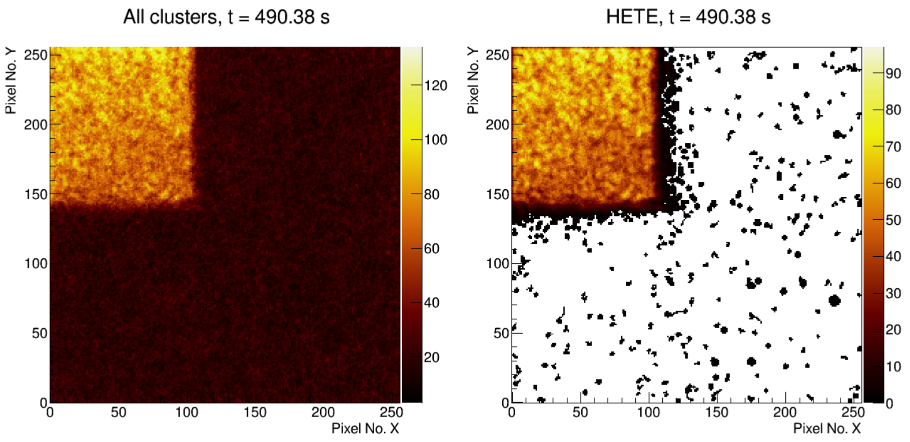

Thermal neutrons (E_n~ 25 meV)

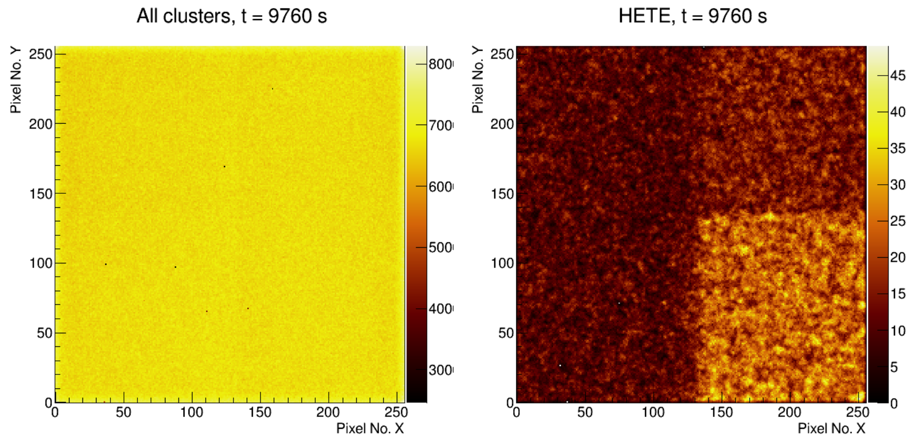

AmBe (E_{mean} = 4.2 MeV)

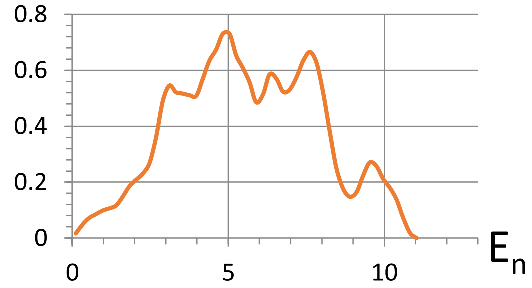

^{252}Cf (E_{mean} = 2.2 MeV)

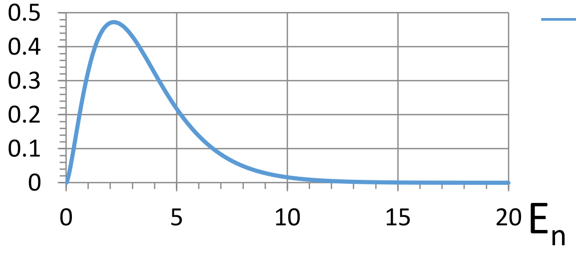

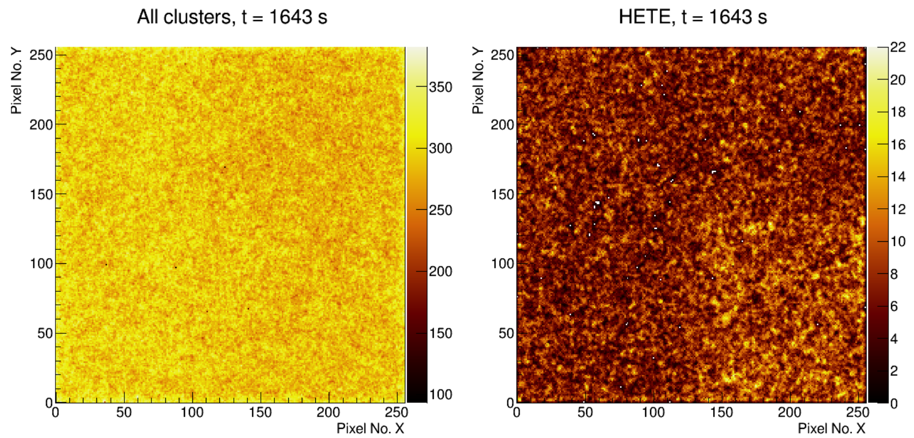

Neutron converter efficiencies

Converter efficiency:

$$\varepsilon_i = \frac{N_i - {}^{A_i}/_{A_{Si}} N_{Si}}{\Phi_{source} t}$$

i: converter region LiF, PE, PE+Al

Converter efficiency calibration was done in time-of-flight experiments at

- The **Los Alamos neutron Science Center** (LANSCE) neutrons 1-600 MeV
- **n_TOF at CERN:** neutrons meV – 400 MeV

Neutron spectrum hardness assessment through comparison of signal in the PE regions

P. Smolyanskiy *et al* 2024 *JINST* **19** C02016

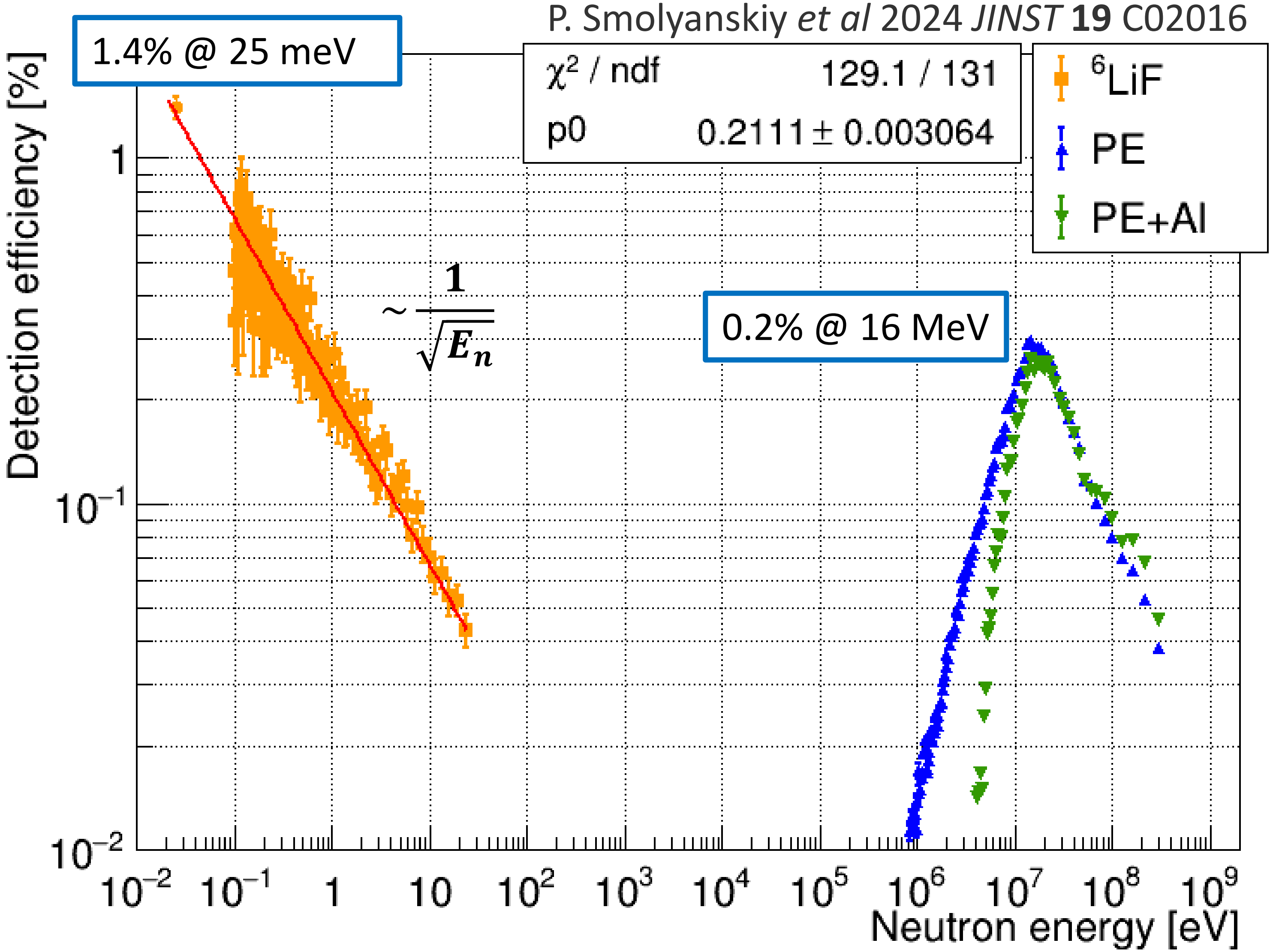

Timepix(3) in ATLAS

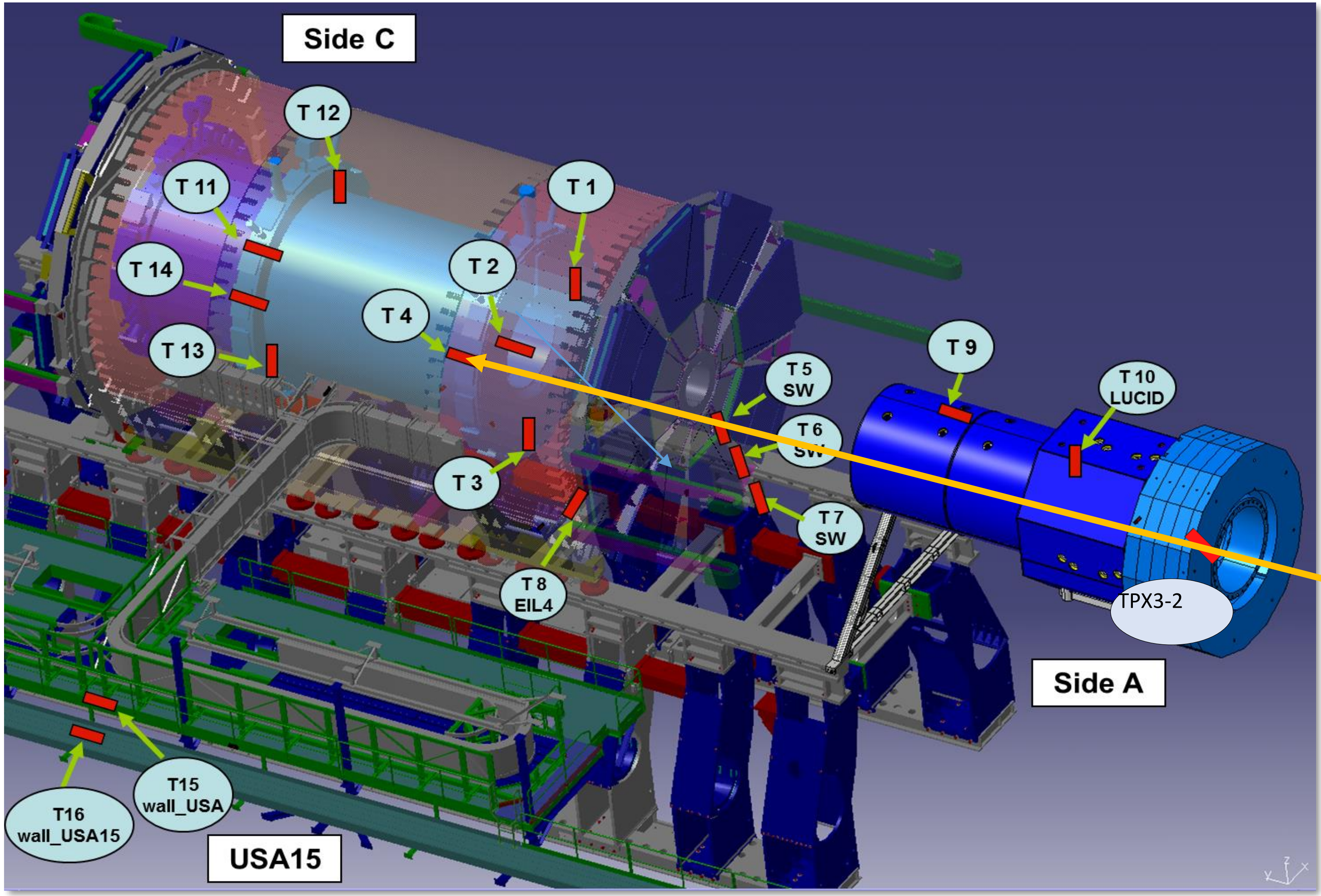

Timepix and Timepix3 **detector networks** were installed in the ATLAS experiment

- Study the radiation fields during and after collision periods
- Measurement of the luminosity

ATLAS environment

Continuous measurement of the radiation level

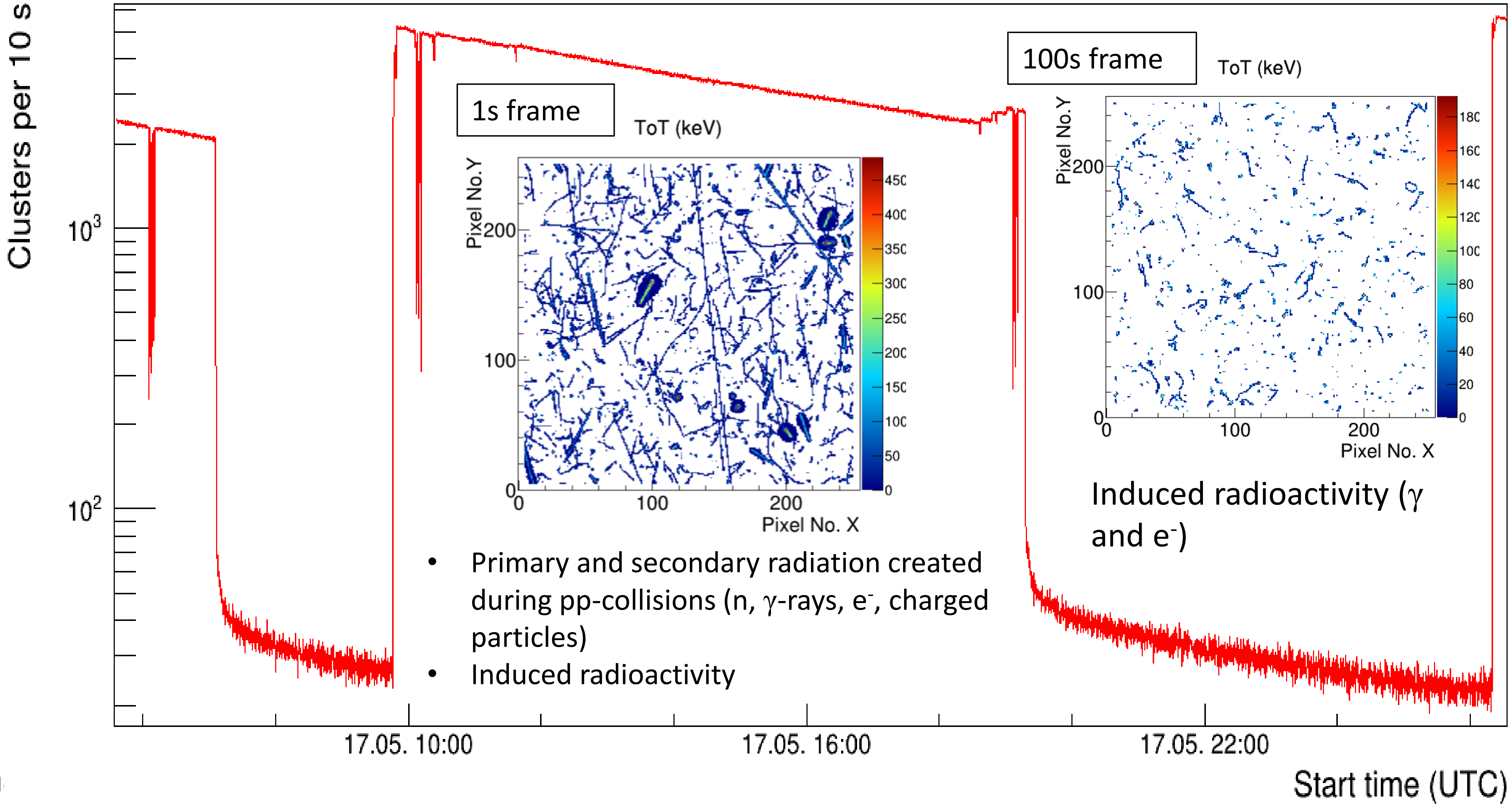

- Primary and secondary radiation created during pp-collisions (n, γ-rays, e⁻, charged particles)
- Induced radioactivity

Induced radioactivity (γ and e⁻)

Activation analysis:

Equation to describe the growth and decay of induced radioactivity

$$M_{act}^{i} = \underbrace{\sum_{k=1}^{n} M_{act}^{i-1,k} \times e^{-\lambda_k t}}_{\text{Decay of atoms activated before i-th time bin}} + \underbrace{\theta\left(M_{tot}^{i} - M_{act}^{i-1}\right) \times \sum_{k=1}^{n} \left(M_{tot}^{i} - M_{act}^{i-1,k}\right) \times \boldsymbol{Y}_k \times \left(1 - e^{-\lambda_k t}\right)}_{\text{Activation during i-th time bin (valid only during collisions)}}$$

Decay of atoms activated before i-th time bin

Activation during i-th time bin (valid only during collisions)

λ	**decay constant, $\lambda = \ln(2)/t_{1/2}$; $t_{1/2}$ is the half-life time**
Y_k	**activation yield; how many clusters do we have to measure to create on instable isotope *k***
i	index of the time bin
M_{tot}	total count rate measured in the given Timepix3 time bin (normalized to unit time)
M_{act}	count rate caused by all activation products
t	time period between the end of (*i-1*)-th bin and the end of *i*-th bin
$\theta(x)$	Heavyside-function

Activation analysis:

Determination of the input half-life times

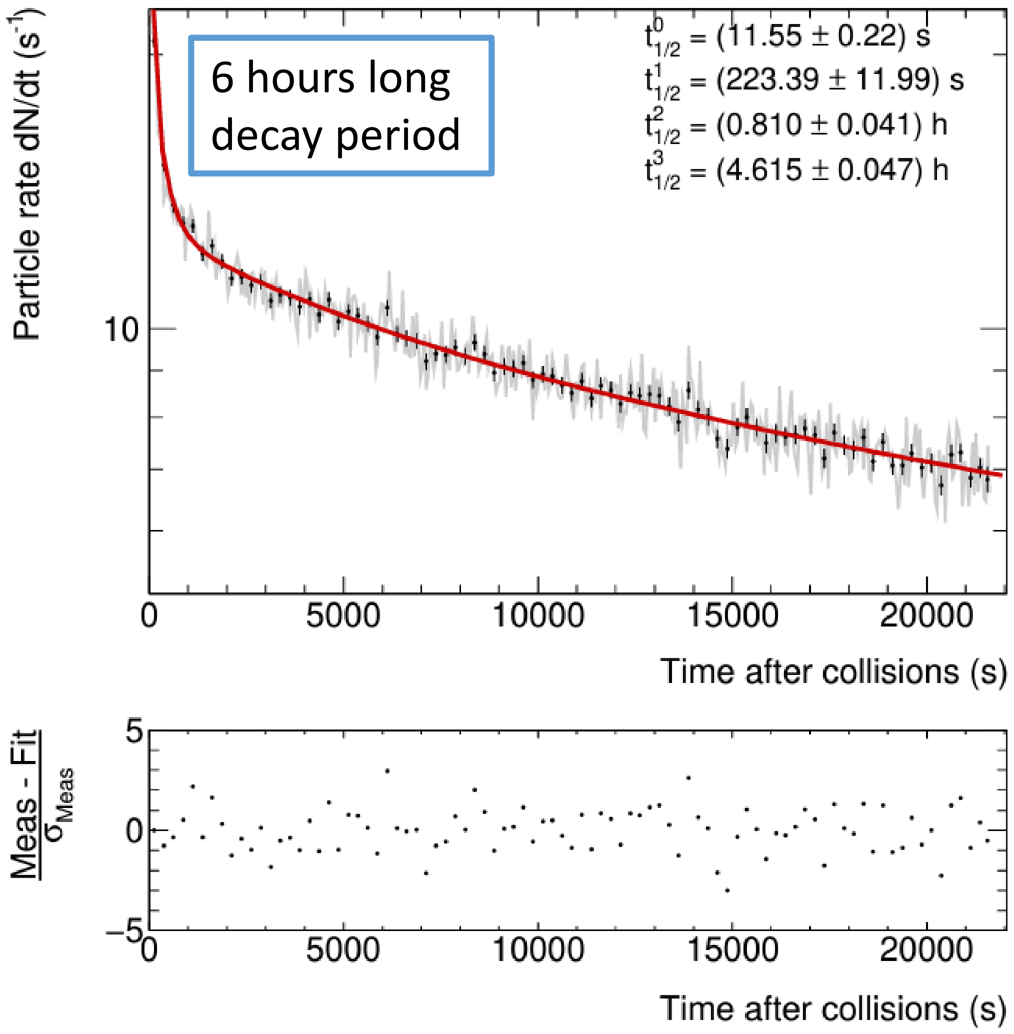

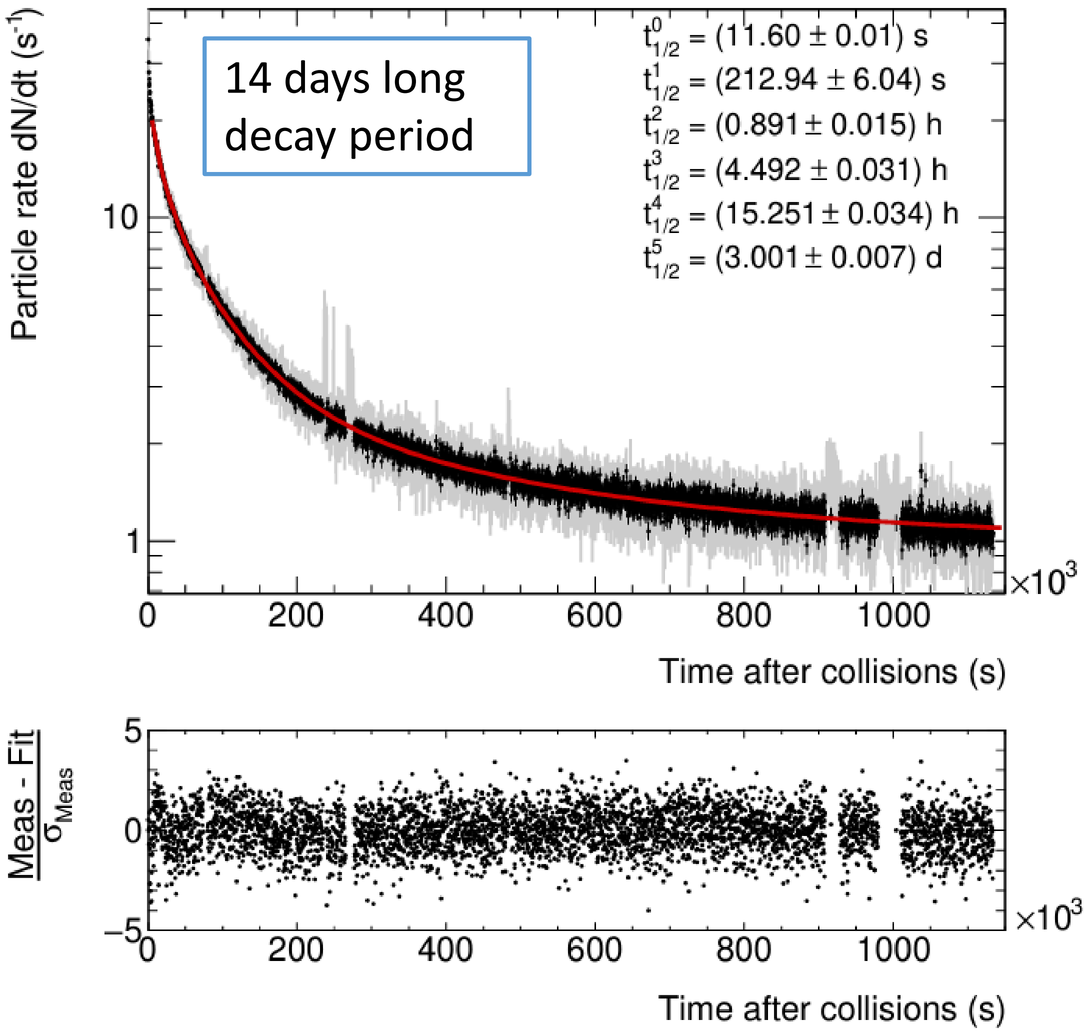

Activation analysis:
Application of the iterative formula to the measured data

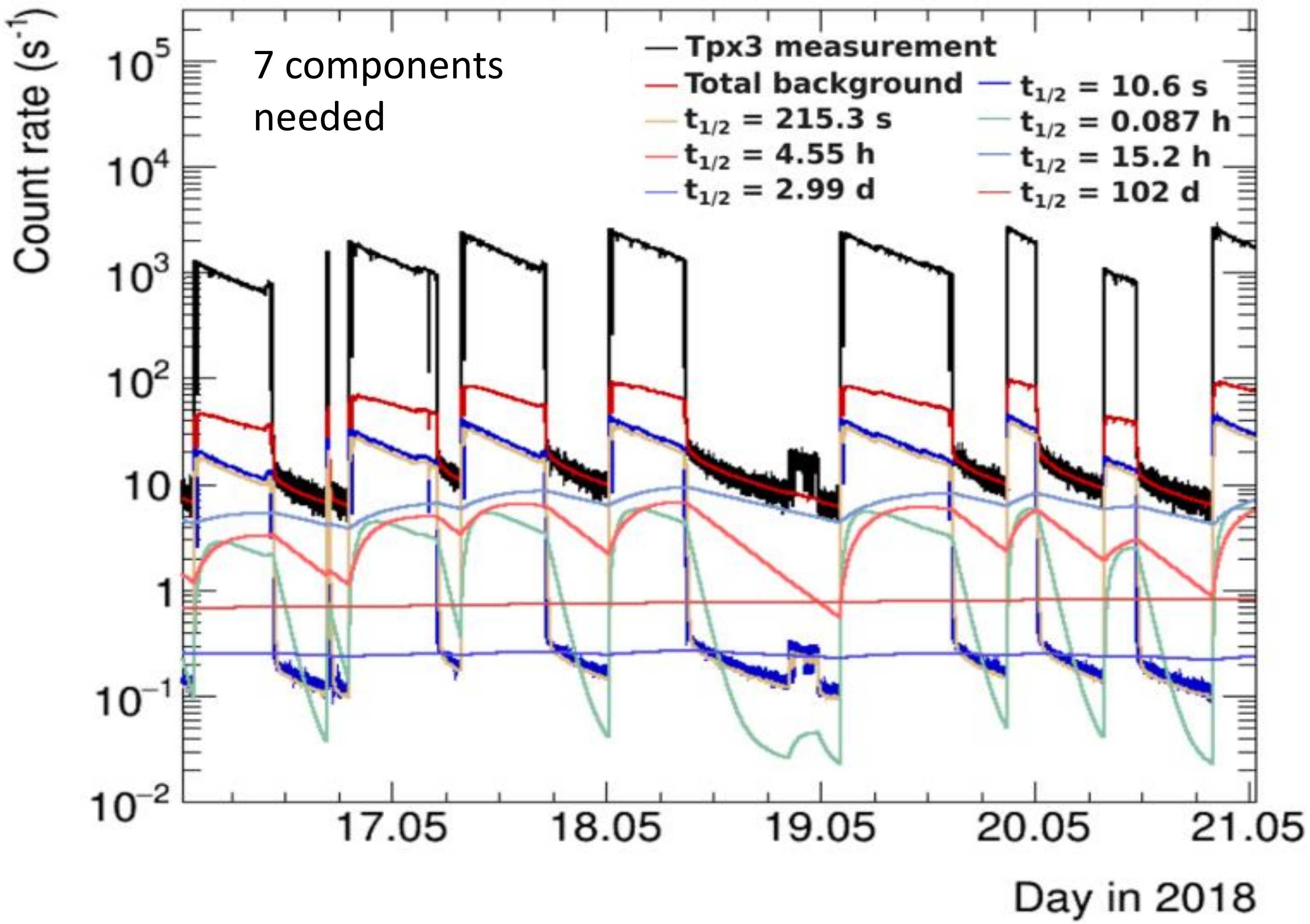

The count rate from activation at a specific point in time depends on:

- Previous collision periods
- Time from start/end of the collision period

Short half-lifes lead to systematic drift within a single run
Long half-lifes will be seen in long-term studies → baseline shift

The presented activation modelling is possible due to triggerless continuous measurement!

Thermal neutron signals in ATLAS

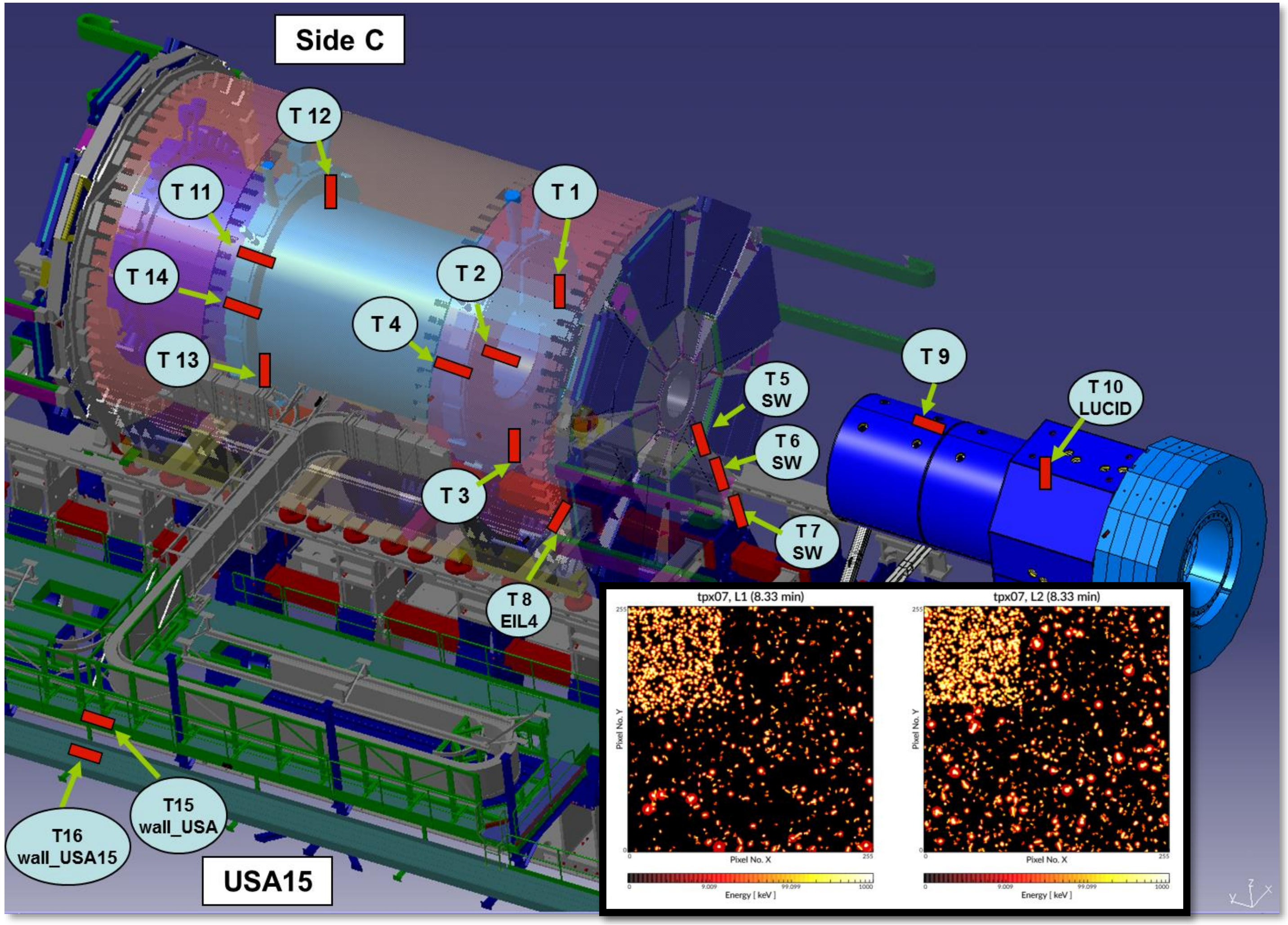

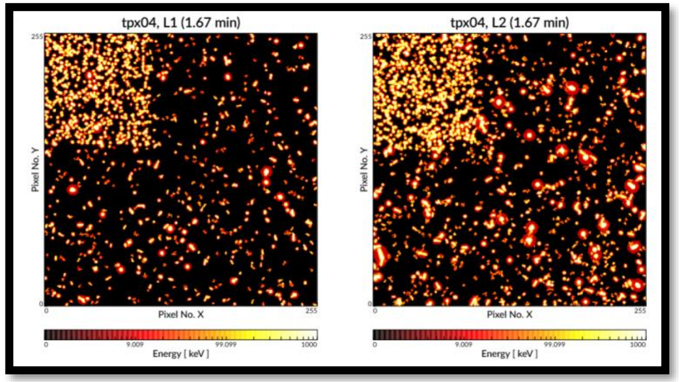

TPX04: Integral HETE frame (**1.67min**) measured on May 31, 2016

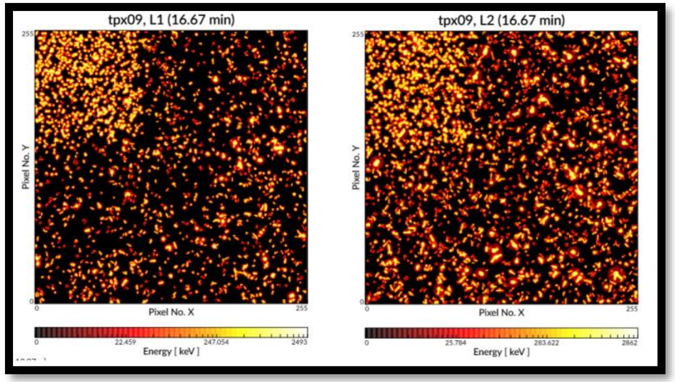

TPX09: Integral HETE frame (**16.67min**) measured on May 31, 2016

TPX07: Integral HETE frame (**8.33min**)

Thermal neutron fluxes in ATLAS

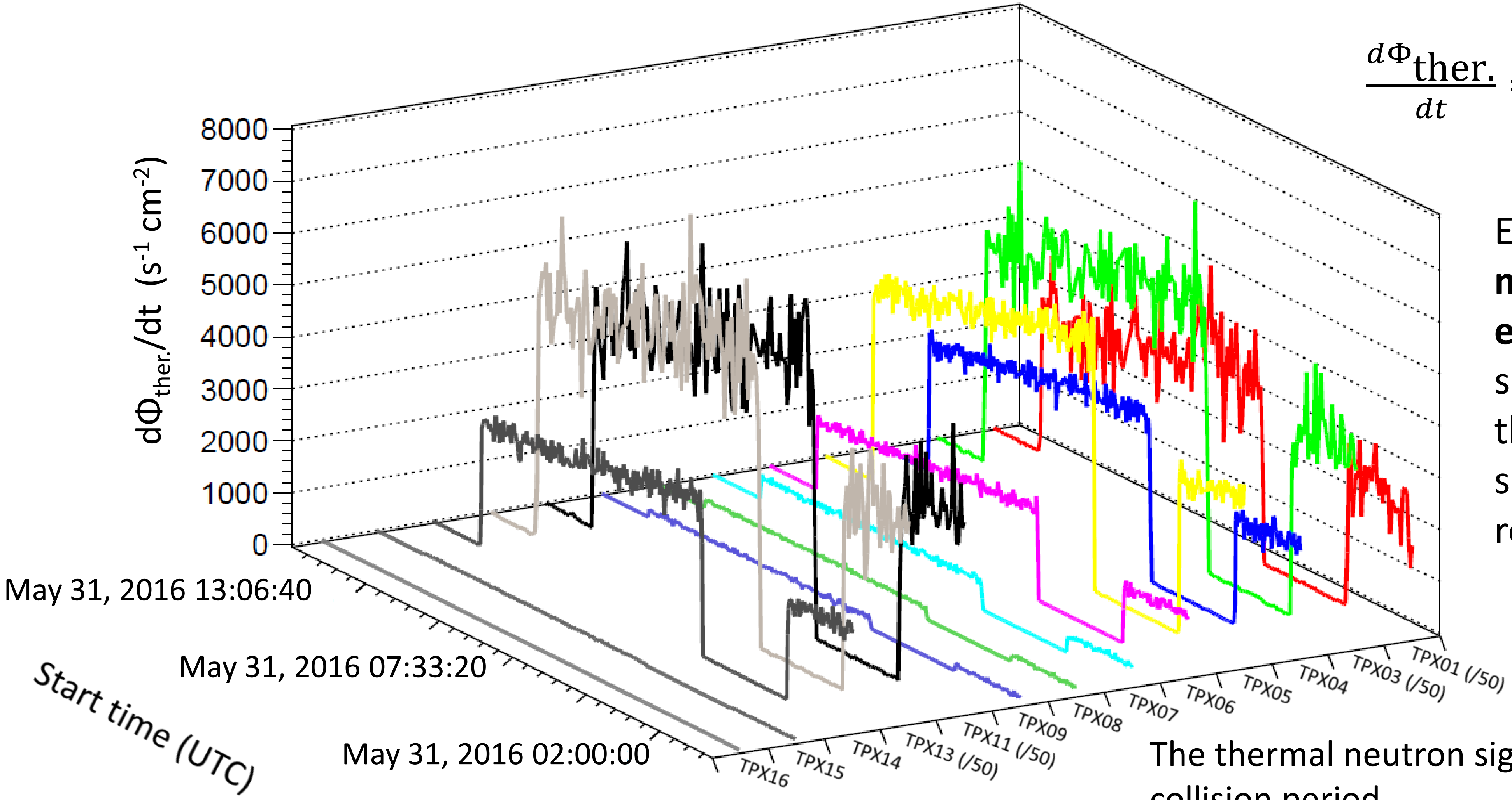

$$\frac{d\Phi_{ther.}}{dt} = \frac{N_{LiF}/A_{LiF} - N_{Si}/A_{Si}}{t_{meas.} \cdot \epsilon_{ther.}}$$

Even in the **most complex man-made radiation environments**, the neutron signal can be extracted thanks to the converter selection and pattern recognition.

The thermal neutron signal is a clear indicator for collision period

→ **Good signal for luminosity determination?**

Luminosity measurement during 2018 *pp* collisions at √s=13 TeV using Timepix3 in ATLAS

(Relative) luminosity measurement with Timepix3 in ATLAS

Luminosity measurement through the counting of particle traces (clusters) left in Timepix3.

$$\mathcal{L}_{\mathrm{Timepix3}} = C \ \frac{N_{\mathrm{clusters/TN}}}{t}$$

Scaling factor *C* determined by comparison of Timepix3 and $\mathrm{LUCID}_{\mathrm{C12}}$ run integrated luminosity during a anchor run.

Luminosity measurement

Evaluation of the short-term precision

Relative devitation of Timepix3 compared with $LUCID_{C12}$ within a Fill (lumi block by lumi block)

- Cluster counting with good agreement after activation subtraction
- Neutron counting not affected by activation but lower statistical precision

Reference data are from **ATLAS**, see also:
Aad, G., Abbott, B., Abeling, K. *et al.* Luminosity determination in *pp* collisions at √s=13 TeV using the ATLAS detector at the LHC. *Eur. Phys. J. C* **83**, 982 (2023). https://doi.org/10.1140/epjc/s10052-023-11747-w

Activation subtracted cluster counting

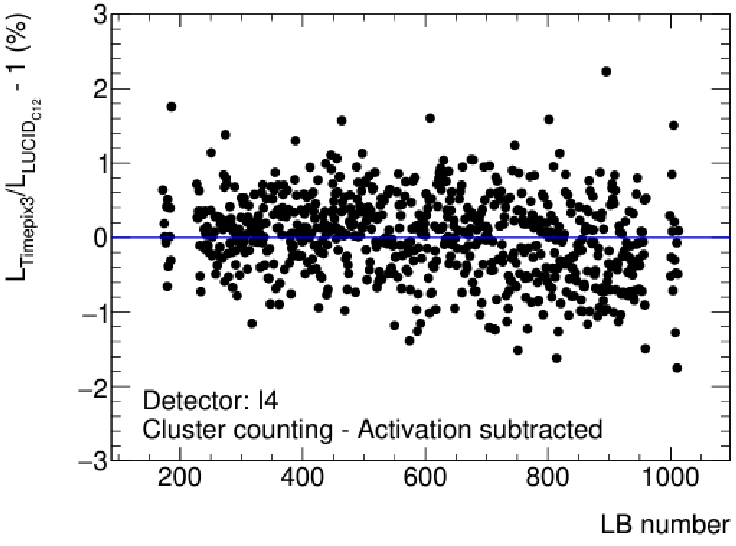

(a)

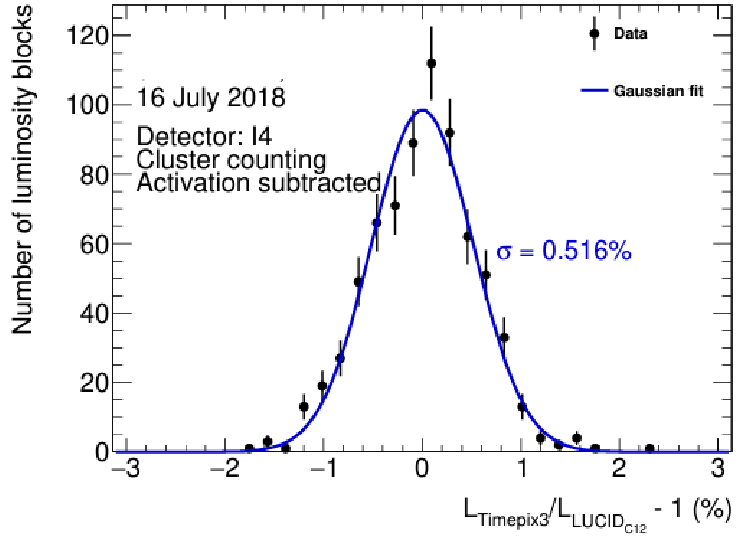

(b)

Thermal neutron counting

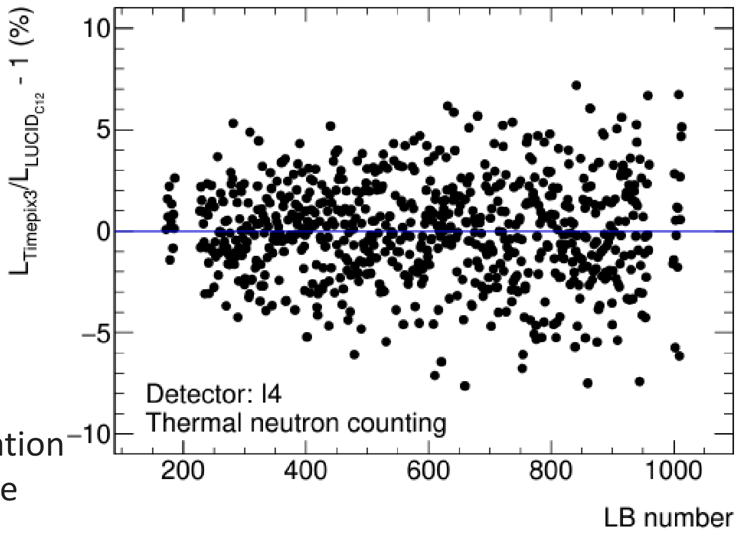

(c)

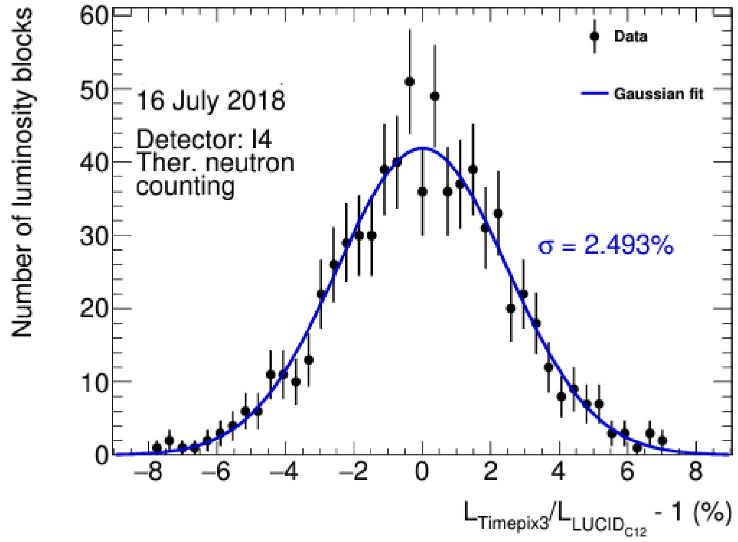

(d)

Timepix3 luminosity measurement:
Long-term stability

Reference data are from **ATLAS**, see also:
Aad, G., Abbott, B., Abeling, K. *et al.* Luminosity determination in *pp* collisions at √s=13 TeV using the ATLAS detector at the LHC. *Eur. Phys. J. C* **83**, 982 (2023).
https://doi.org/10.1140/epjc/s10052-023-11747-w

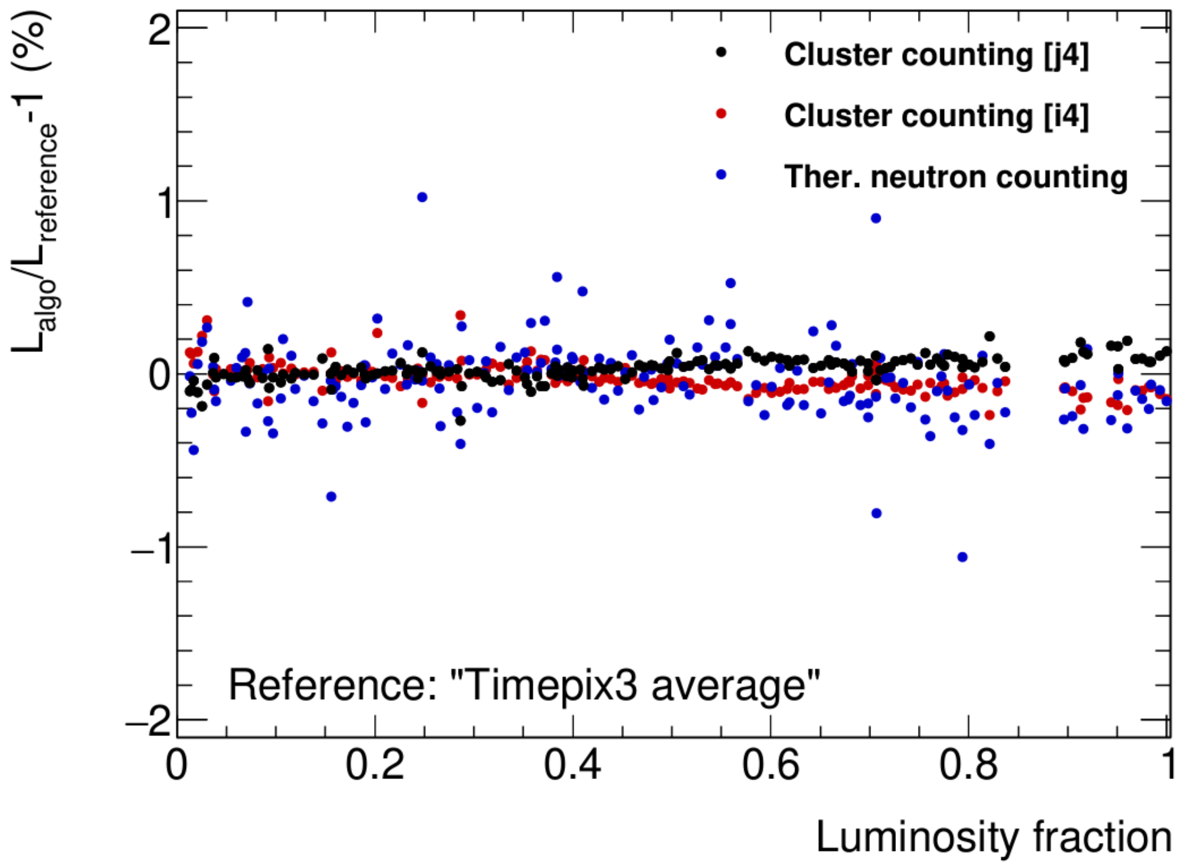

Systematic Timepix3-internal drift below 0.1% over the entire year.

Timepix3 fill-by-fill luminosity measurement is consistent with other luminometers.

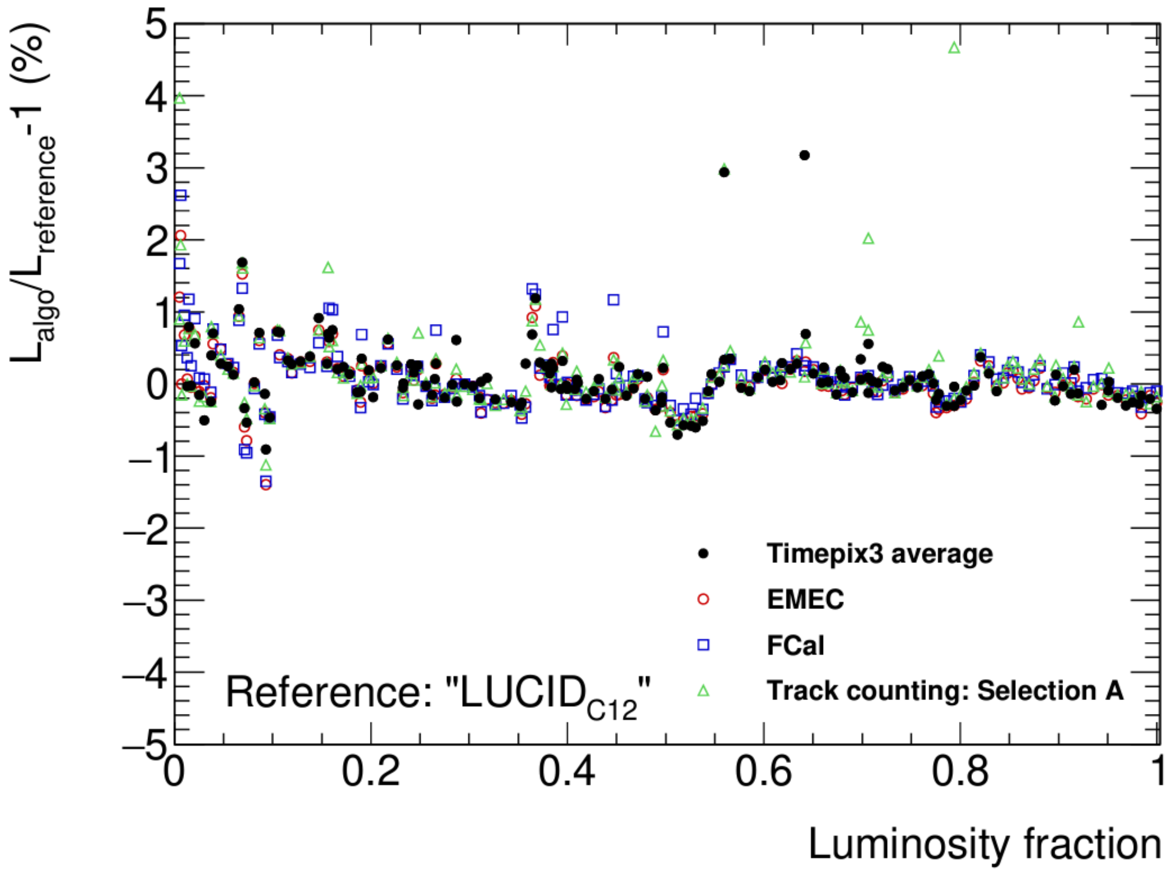

Resolving the bunch structure for luminosity measurement with BCID

Resolving bunches with ATLAS-Timepix3

Timepix3 detectors synchronized with LHC orbit clock allows to resolve bunch slots separated by 25 ns.

Time structure consists of **trains** of **filled** slots interruptd by empty slots

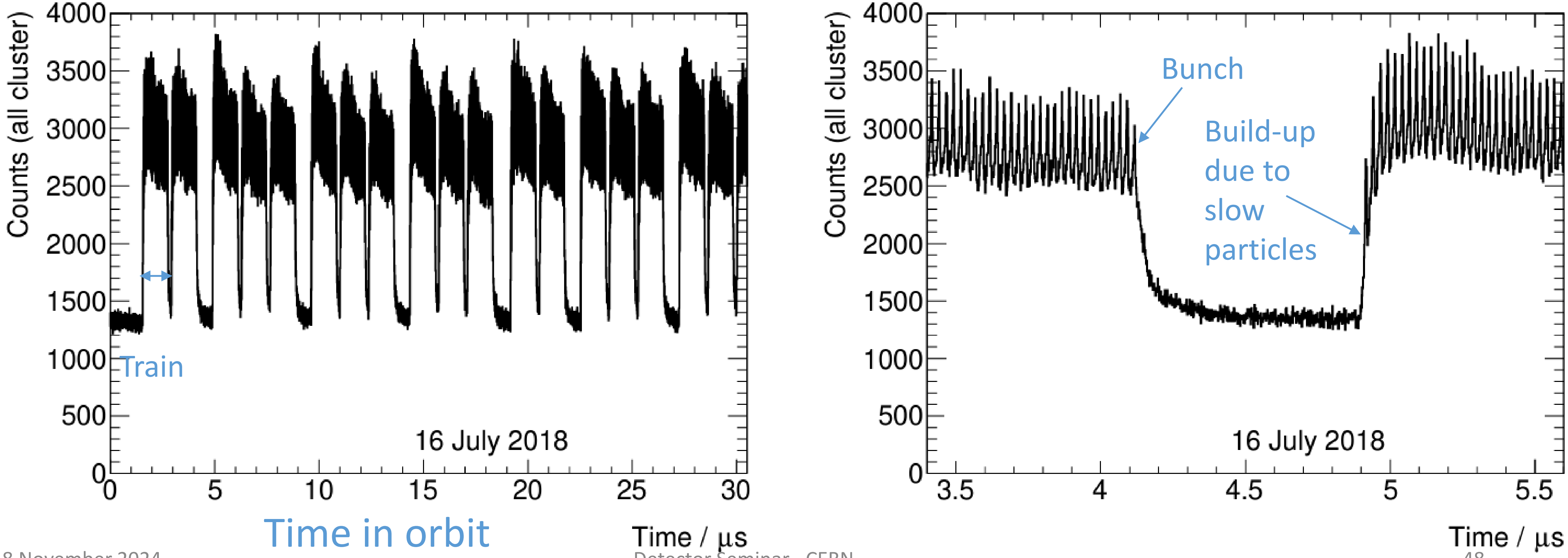

Decomposiong the temporal response

Isolated bunch

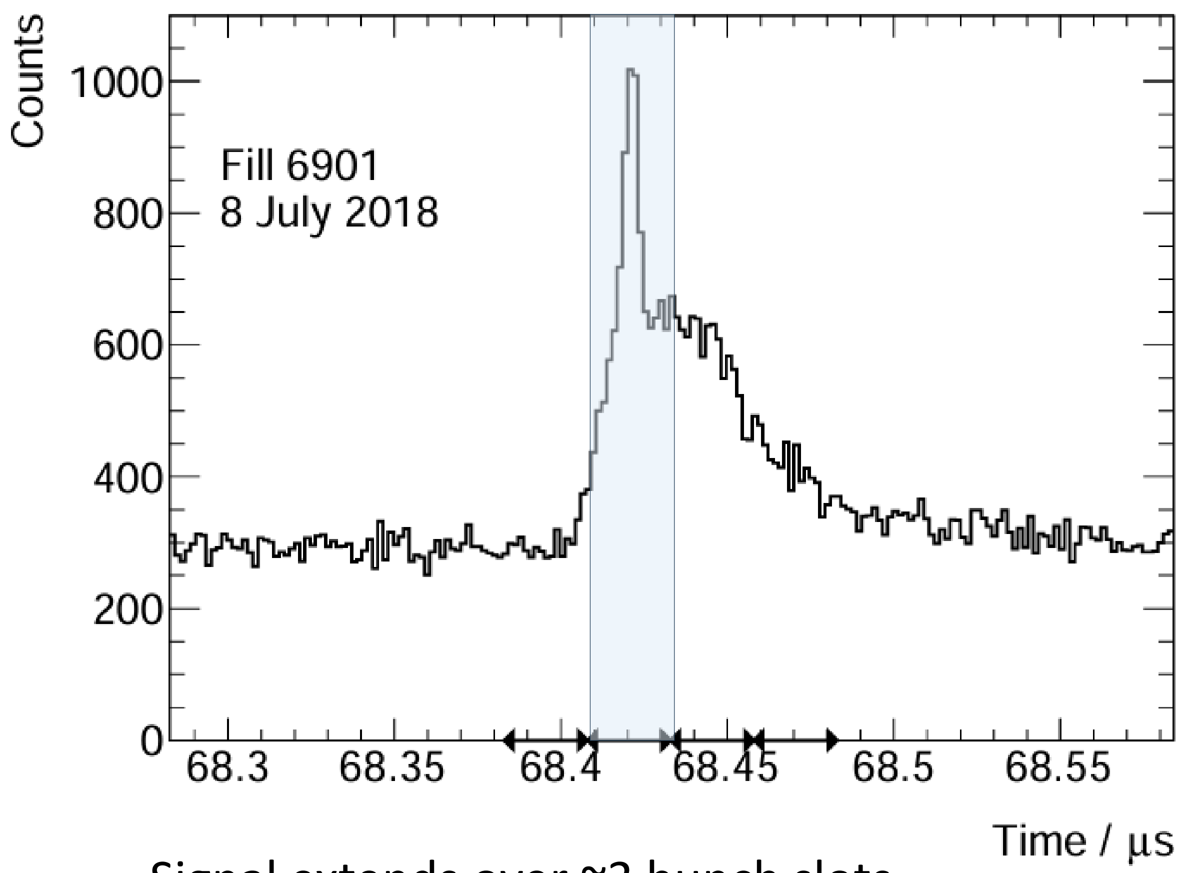

Signal extends over ~3 bunch slots

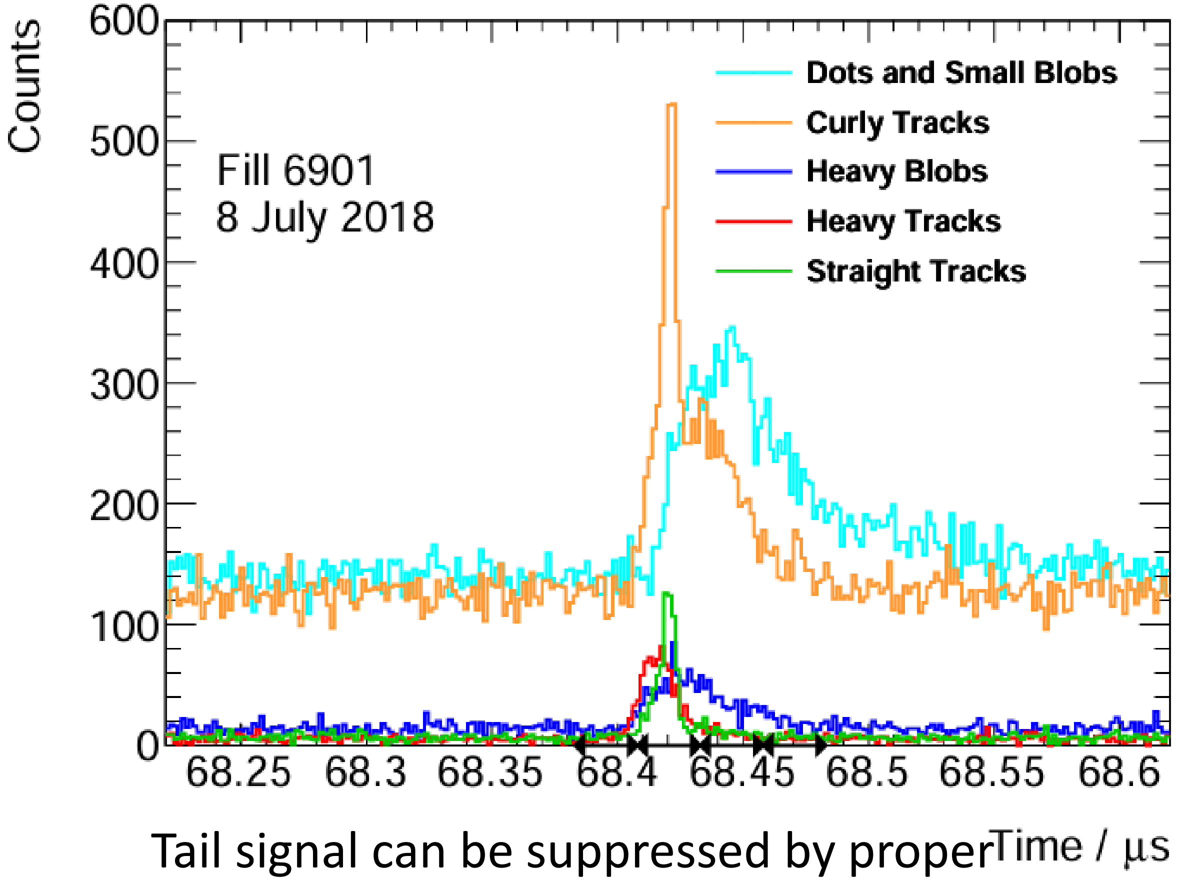

Tail signal can be suppressed by proper selection of the track category

Decomposiong the temporal response
Isolated bunch - Quantitative

Delayed-particle signal present a challenge for proper assignment of particle counts to BCID

→ Find the particle signature with best peak-to-tail ratio

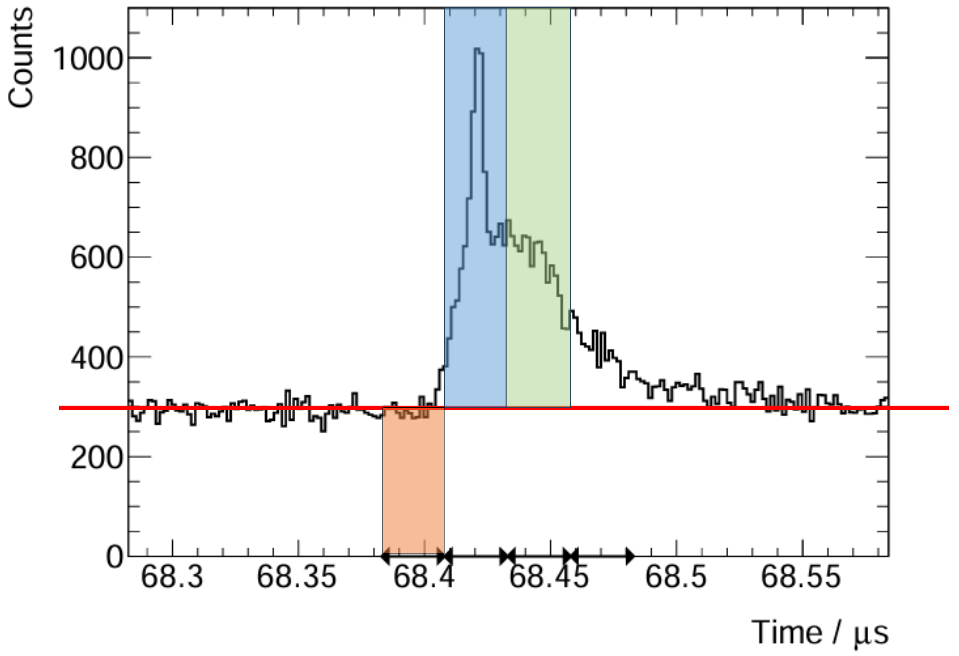

Category	$N_{\text{background}}$	N_{peak}	N_{tail}	$N_{\text{peak}}/N_{\text{background}}$	$N_{\text{tail}}/N_{\text{peak}}$
Dots	2159 ± 46	1164±34	5404±74	0.54±0.02	4.640±0.150
Small blobs	2445±49	1447±38	5897±77	0.59±0.02	4.080±0.120
Heavy blobs	465± 22	1103 ±33	882±30	2.37±0.13	0.800±0.036
Curly tracks	4101±64	5934±77	4326±66	1.45±0.03	0.730±0.015
Heavy tracks (HT)	162 ± 13	1494±39	310±18	9.22±0.76	0.210±0.013
Straight tracks (ST)	208 ± 14	1258±35	166±13	6.05±0.45	0.130±0.011
Signal (HT, ST)	**370±19**	**2752±74**	**476±30**	**7.44±0.44**	**0.173±0.012**

Bunch-by-bunch luminosity:

Time spectrum decomposition for luminosity determination

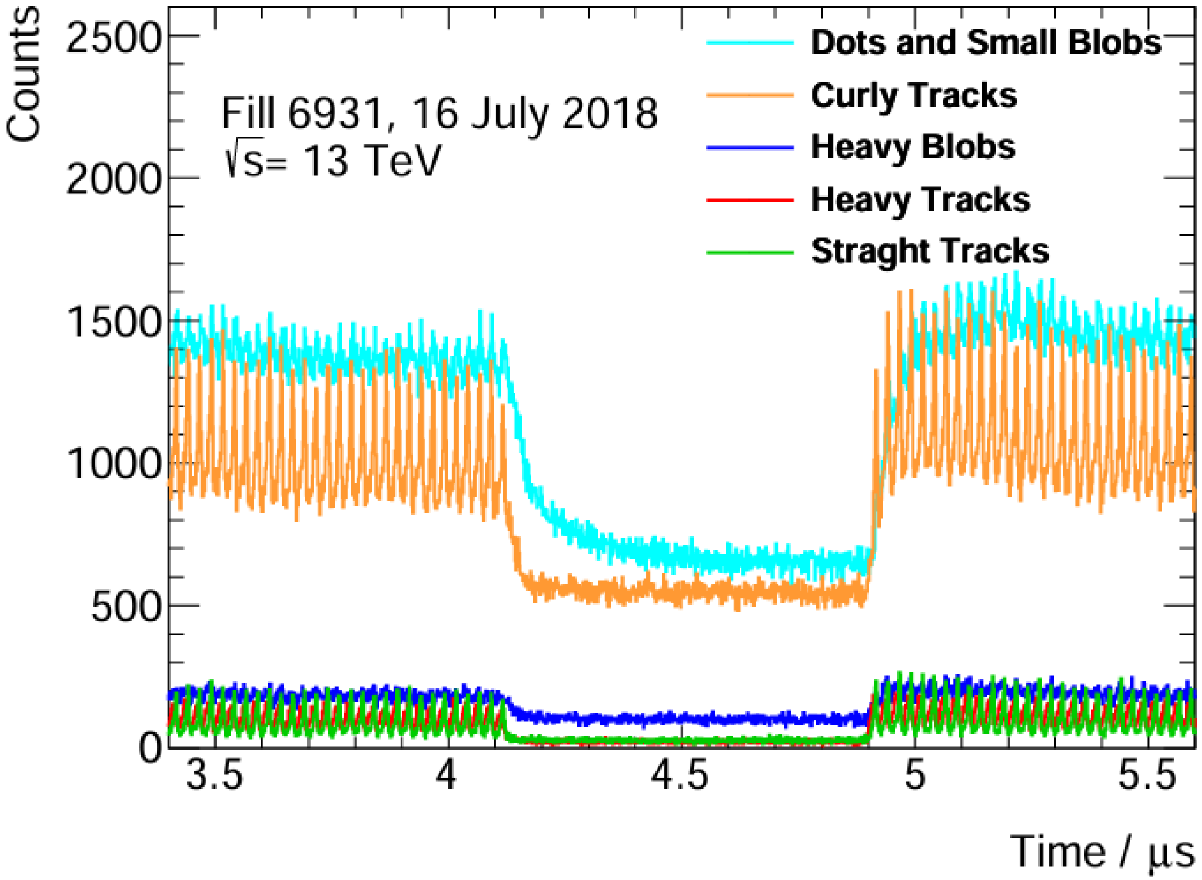

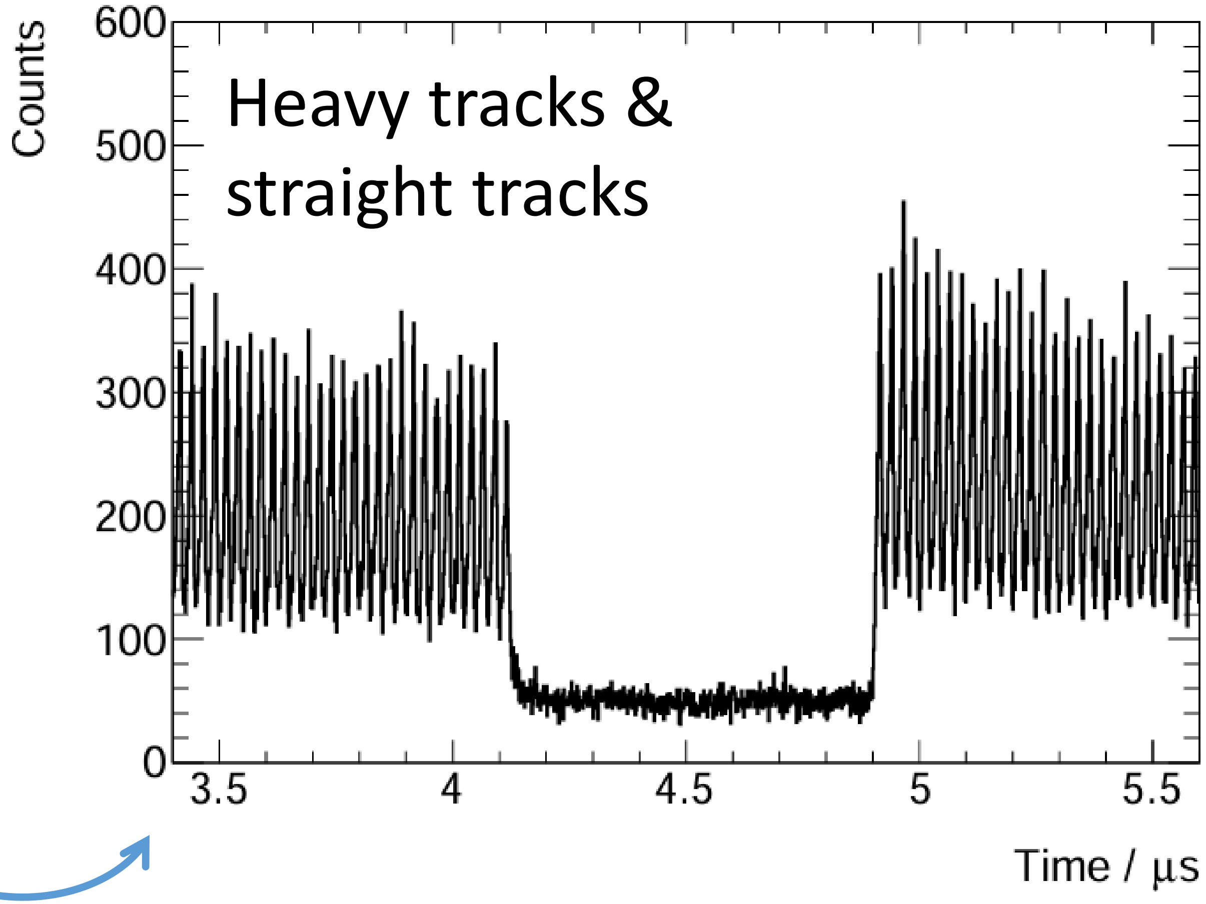

Selection of signatures of interest

Bunch-by-bunch luminosity:

Comparison with other lumino-meters

Reference data are from **ATLAS**, see also:
Aad, G., Abbott, B., Abeling, K. *et al.* ”Luminosity determination in *pp* collisions at √s=13 TeV using the ATLAS detector at the LHC.” *Eur. Phys. J. C* **83**, 982 (2023).
https://doi.org/10.1140/epjc/s10052-023-11747-w

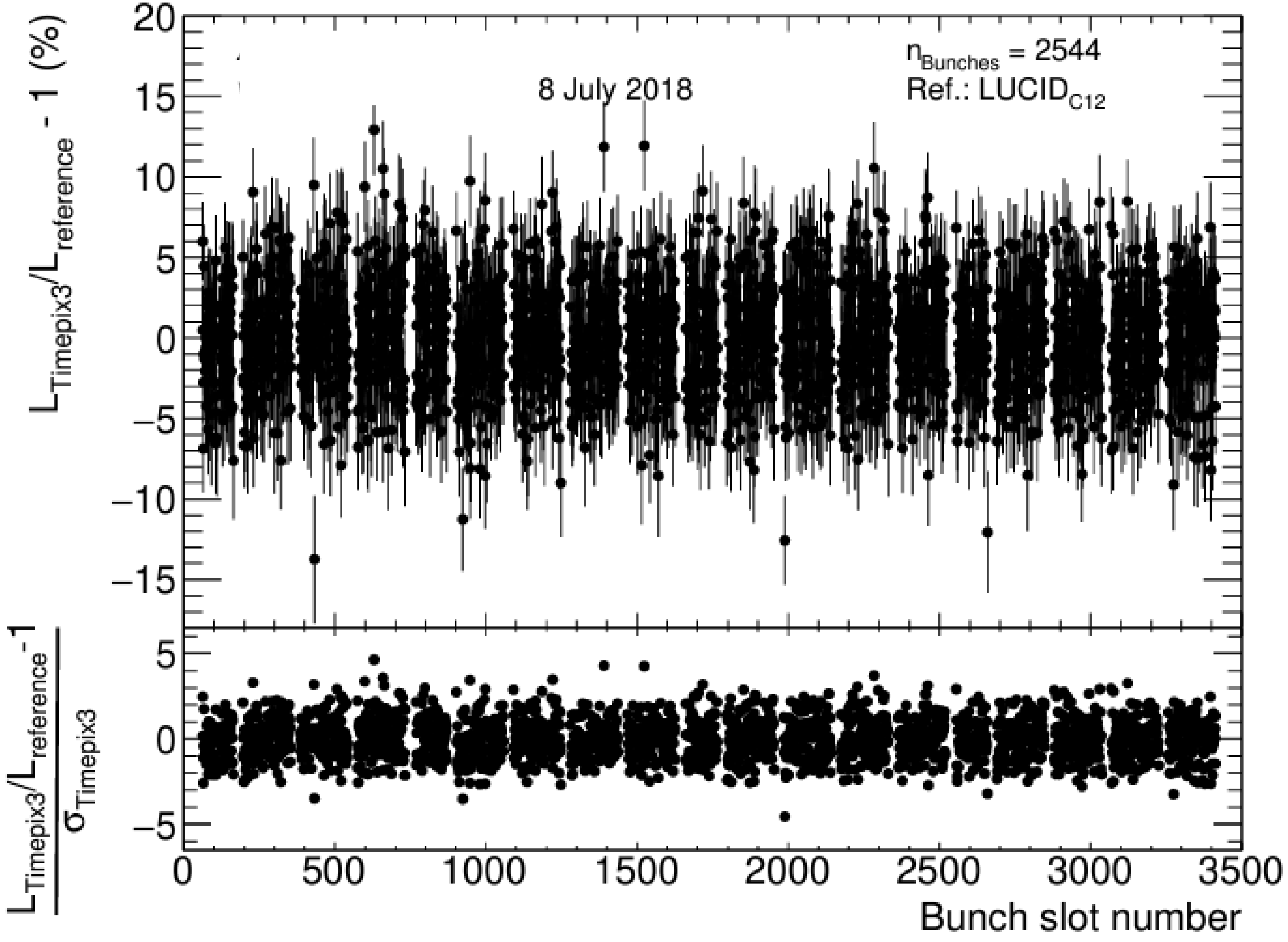

Overall good agreement both with LUCID and Track Counting
→ Precision is statistics limited

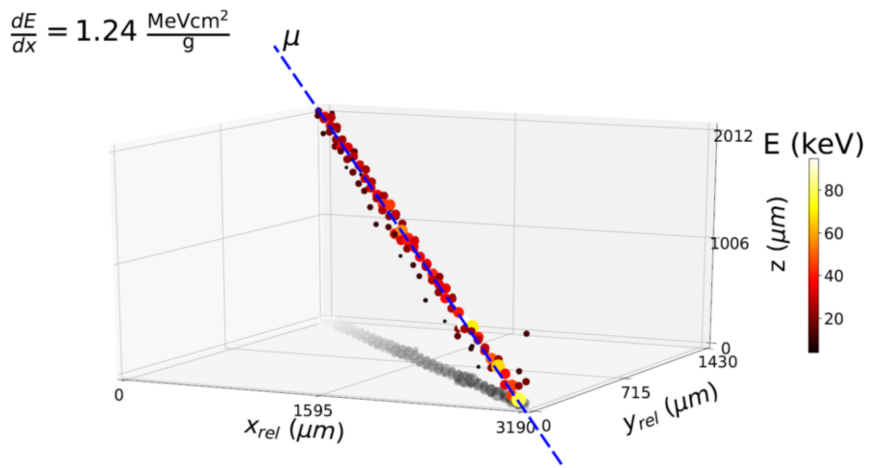

Chapter 4

Minimum ionizing particle tracking for interaction point length reconstruction

Timepix3 within MoEDAL

Installation of 2 Timepix3 detectors in MoEDAL in **September 2018**. Timepix3 are placed at 1.1 m distance to IP8 with a relatively unobstructed view

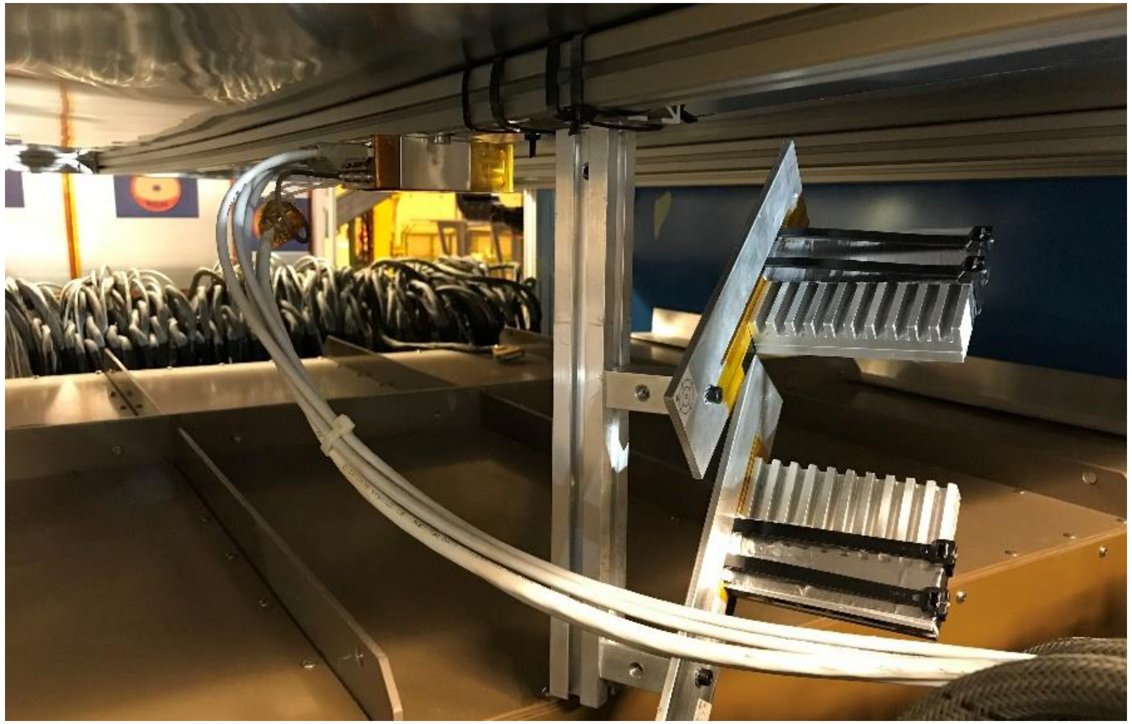

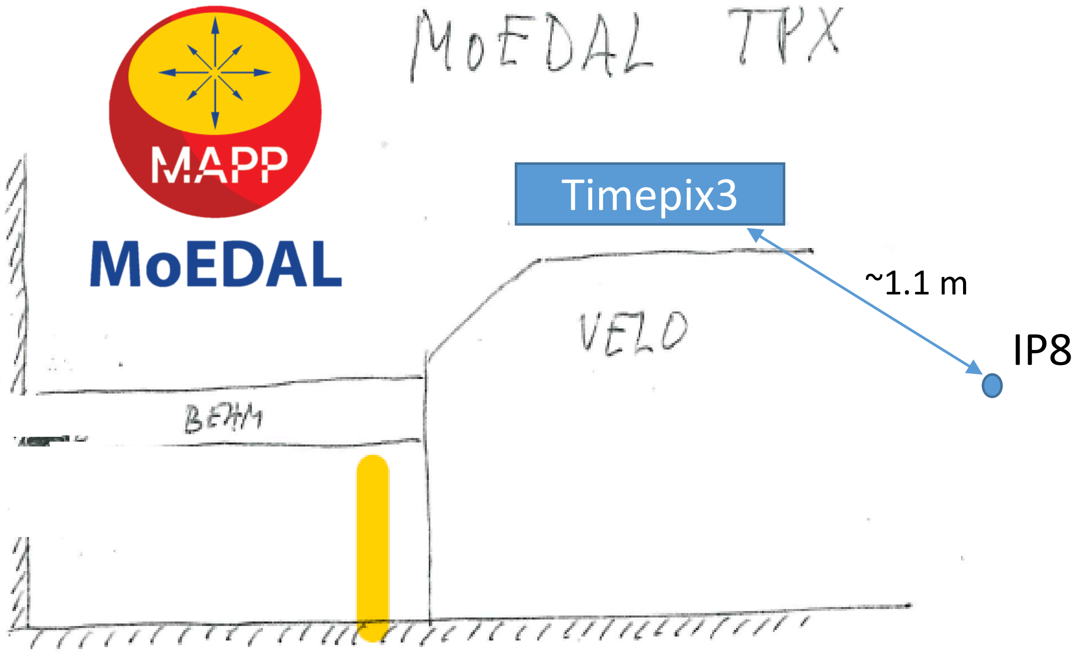

MoEDAL

Continuous quasi dead-time free measurement (in real time) keeping a permanent record of **all particle traces**

- Tracking and identification of **all** particles
- Online outlier detection to search for exotics (highly ionizing events)

Radiation Levels and radiation Field

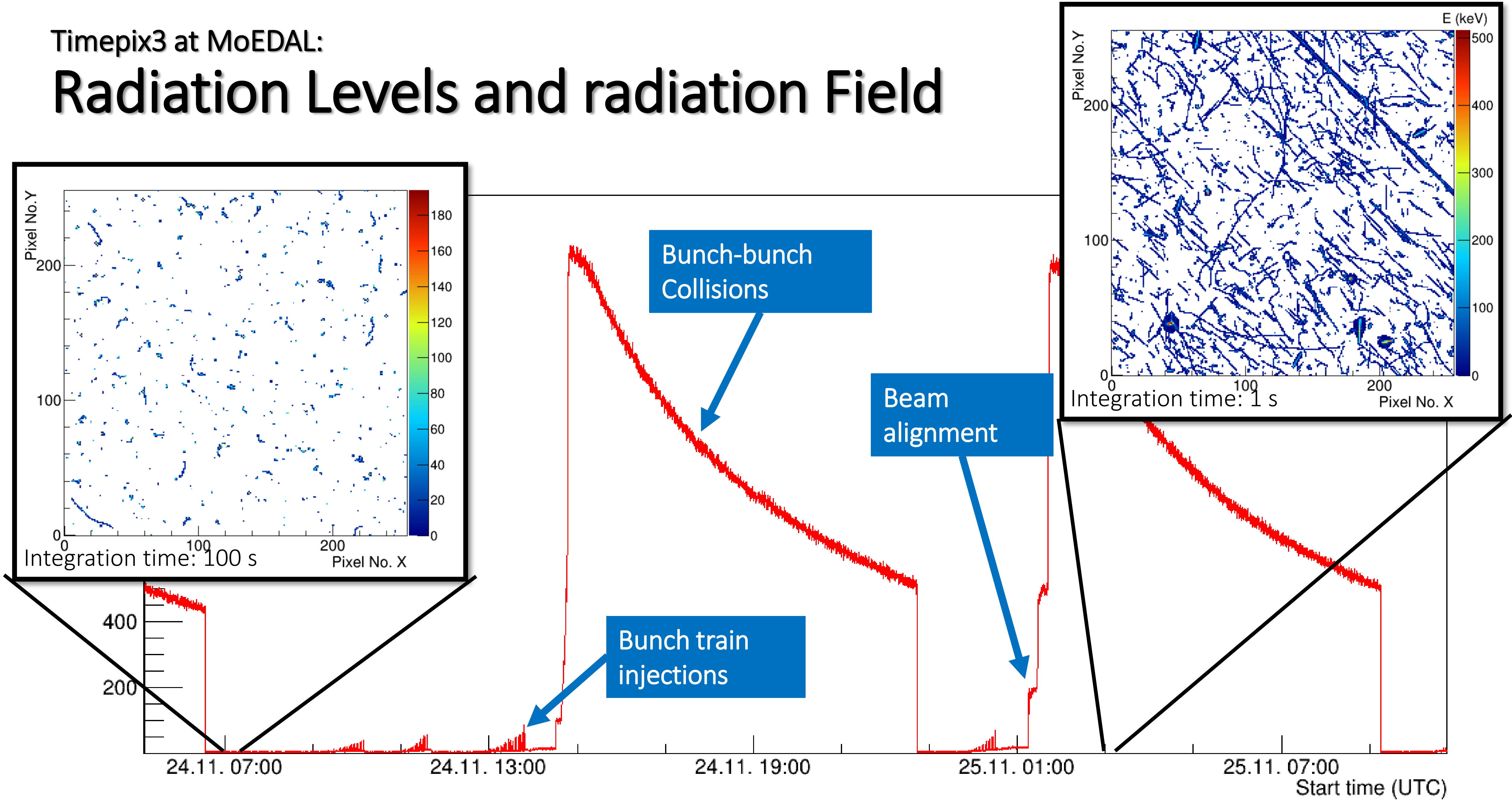

haracterization – during collisions

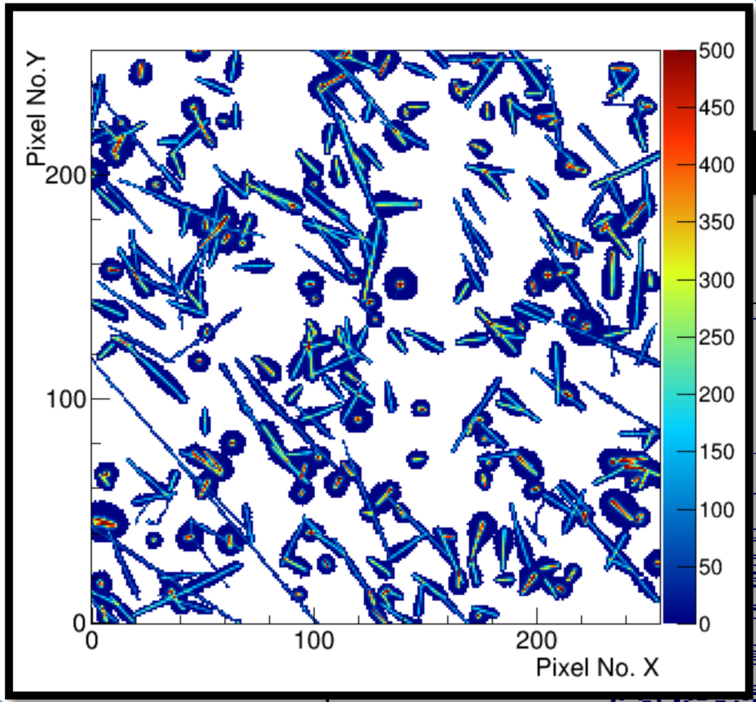

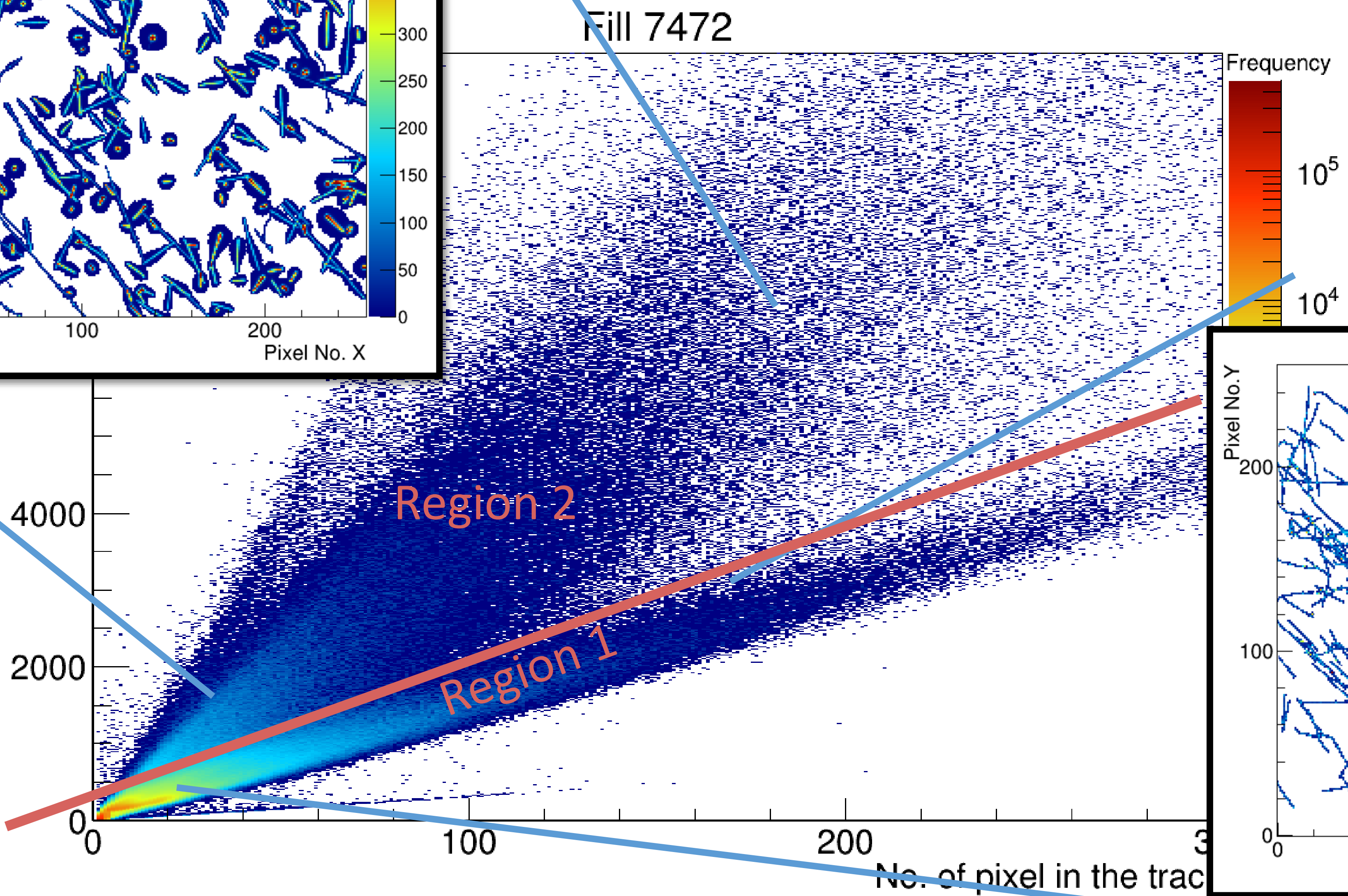

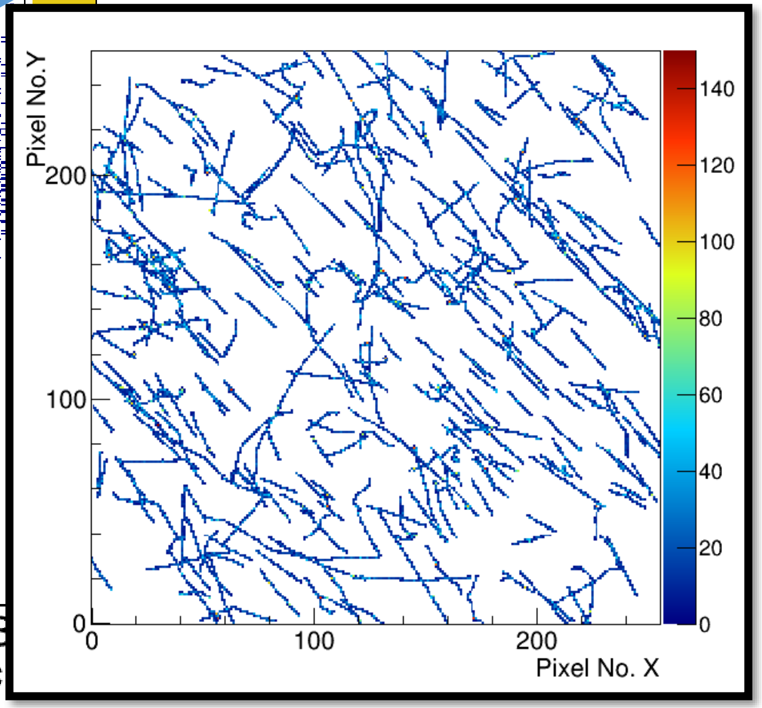

Simple splitting of the data set using the ratio of energy per track and the number of pixels

Directionality map

Directionality evaluated for penetrating particles (region 1)

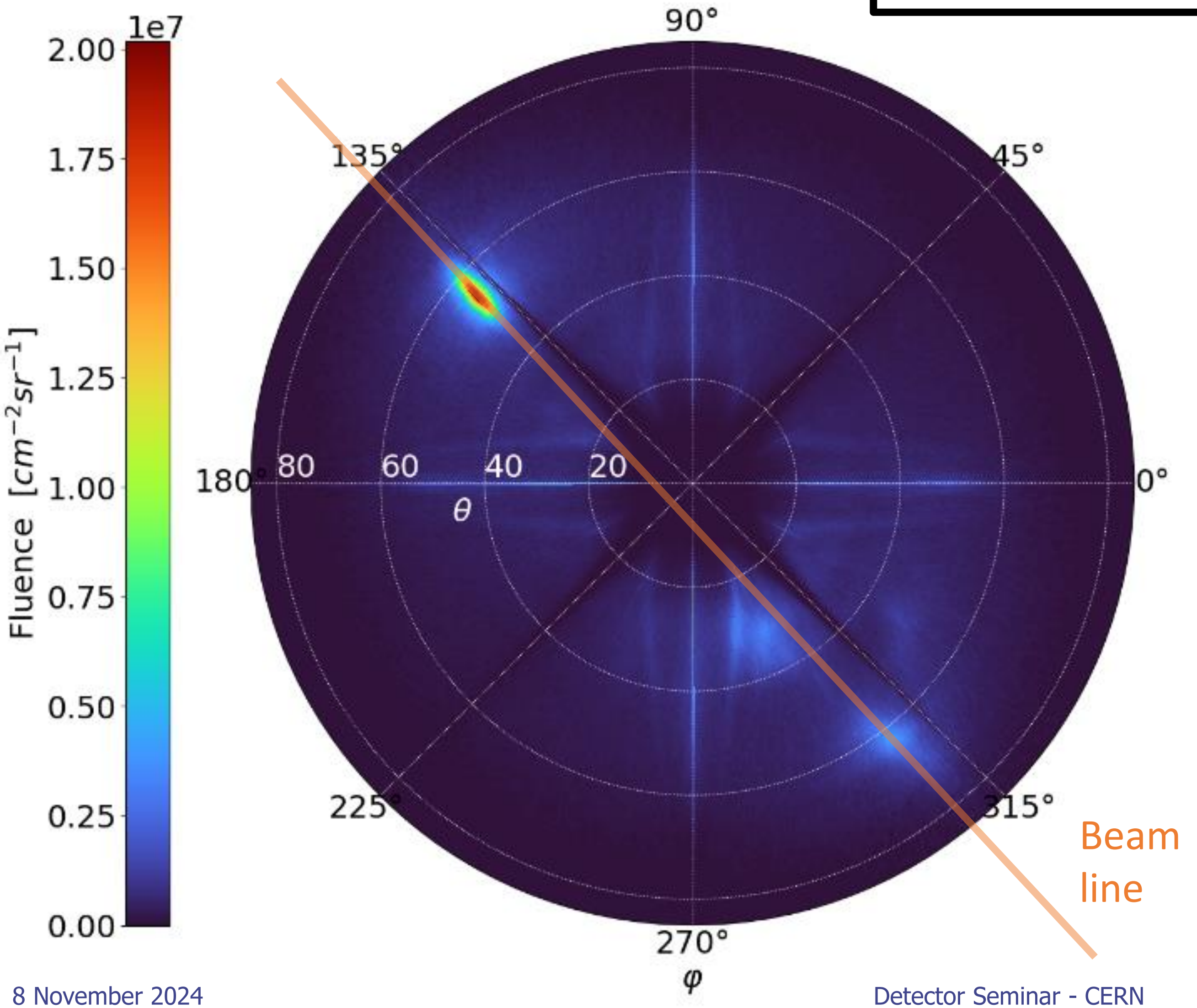

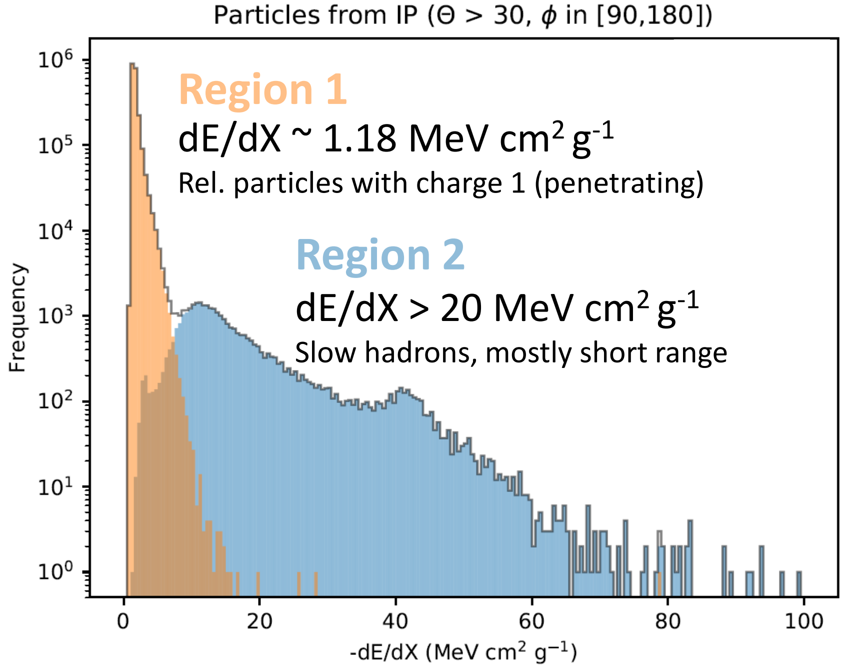

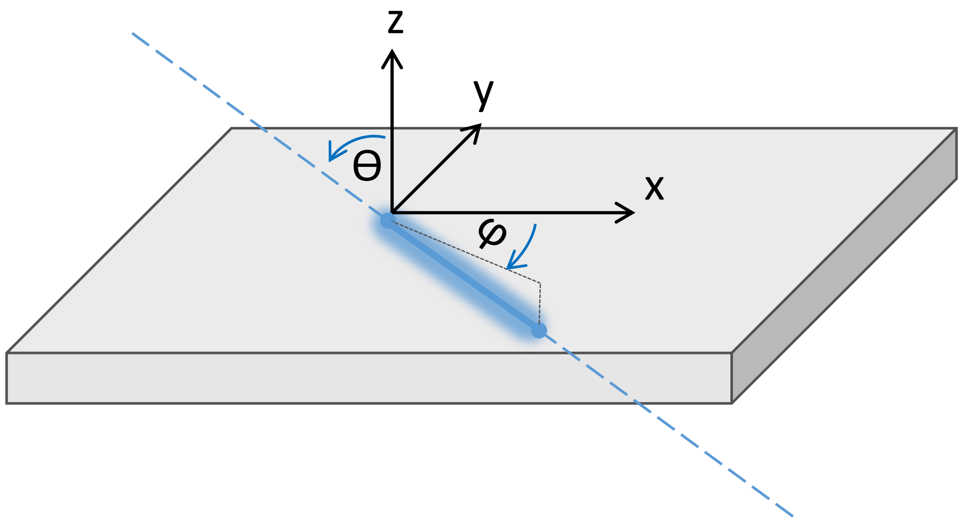

Timepix3 in MoEDAL:

Time-resolved measurement of the directionality map *Pb-Pb* collision period

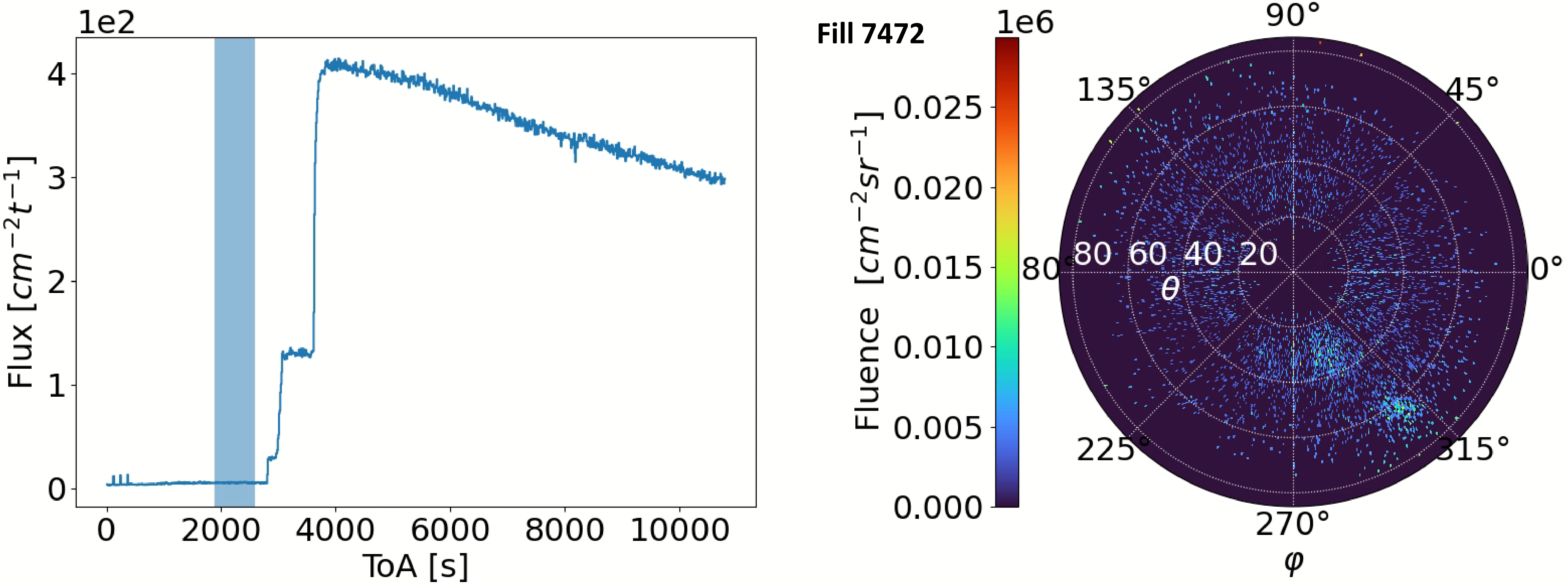

Timepix3 at MoEDAL:
The origin of the secondary peaks

- Two Fills were found where the secondary peaks were not present. These coincide with Fills where the Velo detectors were retracted from the beam pipe
- The time after beam alignment that the peaks appear corresponds approximately to the difference between beam duration and the time the Velo detectors are inserted.

→ Peaks are due to scattering in the Velo Detectors

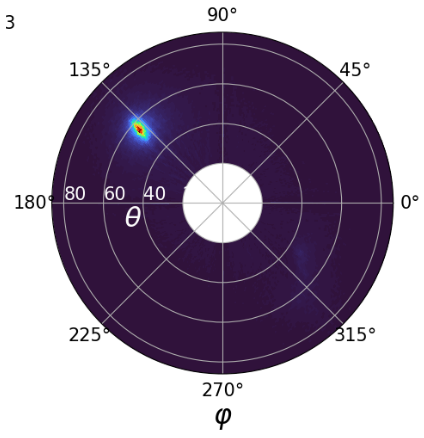

Fill id	Start Date	Duration	Time Velo IN
	Total (103 fills):	30 days 22:56:18	29 days 07:40:49
7474	2018-11-26 02:13:31	05:53:30	No duration

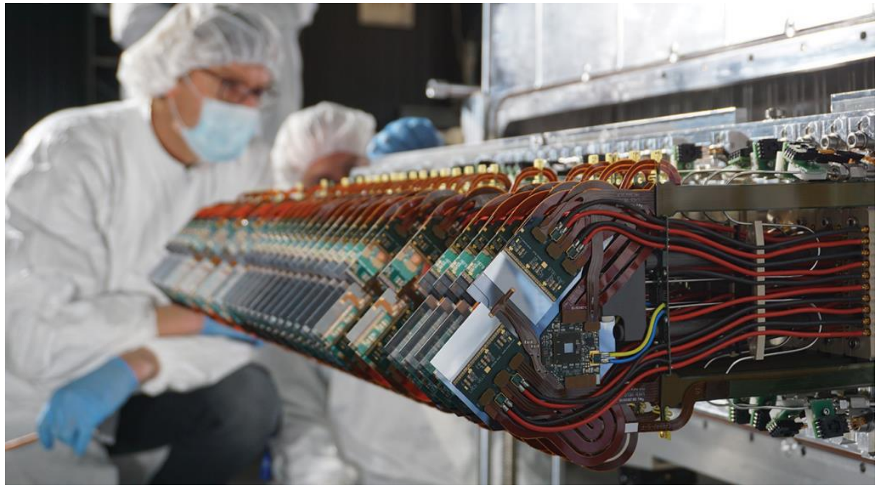

https://lhcb-outreach.web.cern.ch/detector/vertex-locator-velo/

Even with small area detector, changes of the radiation field characteristics, e.g., induced by changed material composition along the beam line are obervable.

Timepix3 at MoEDAL:

Beam spot reconstruction

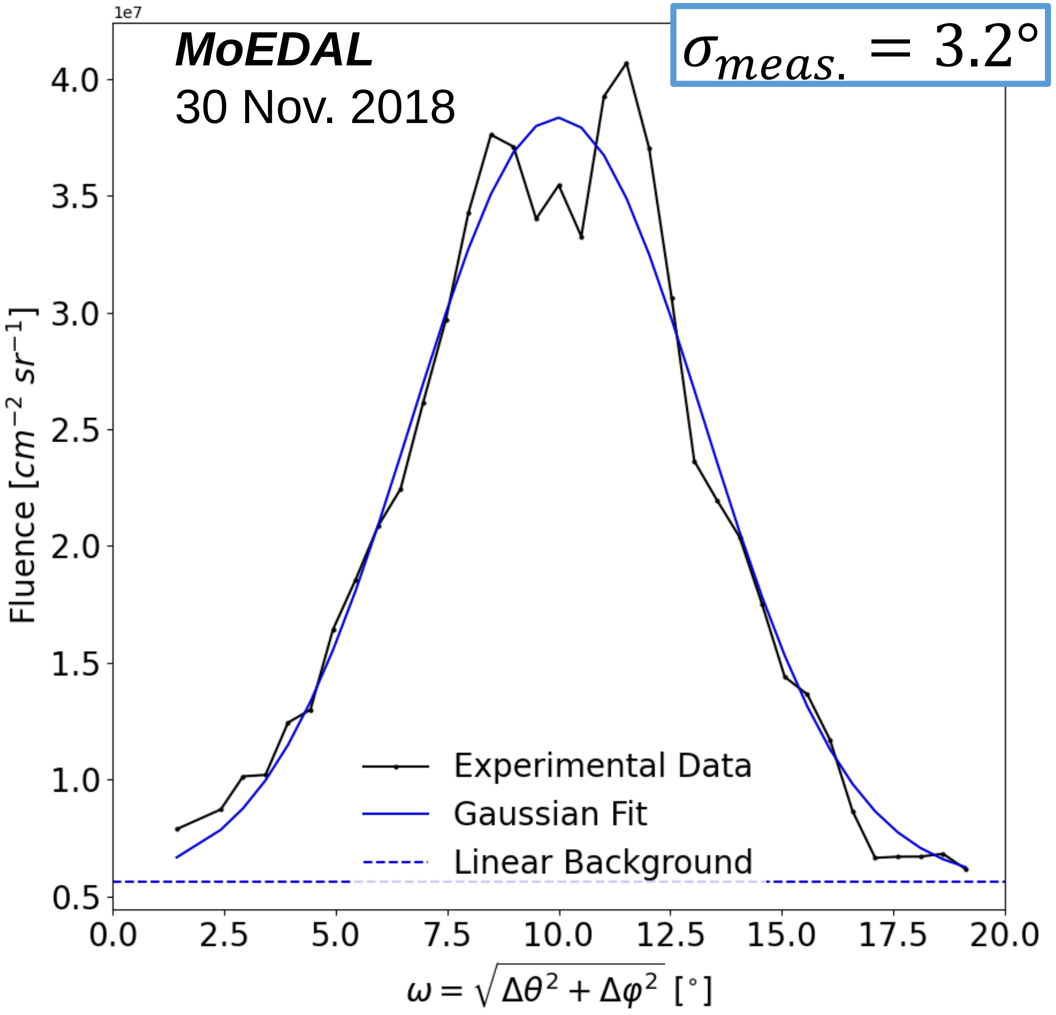

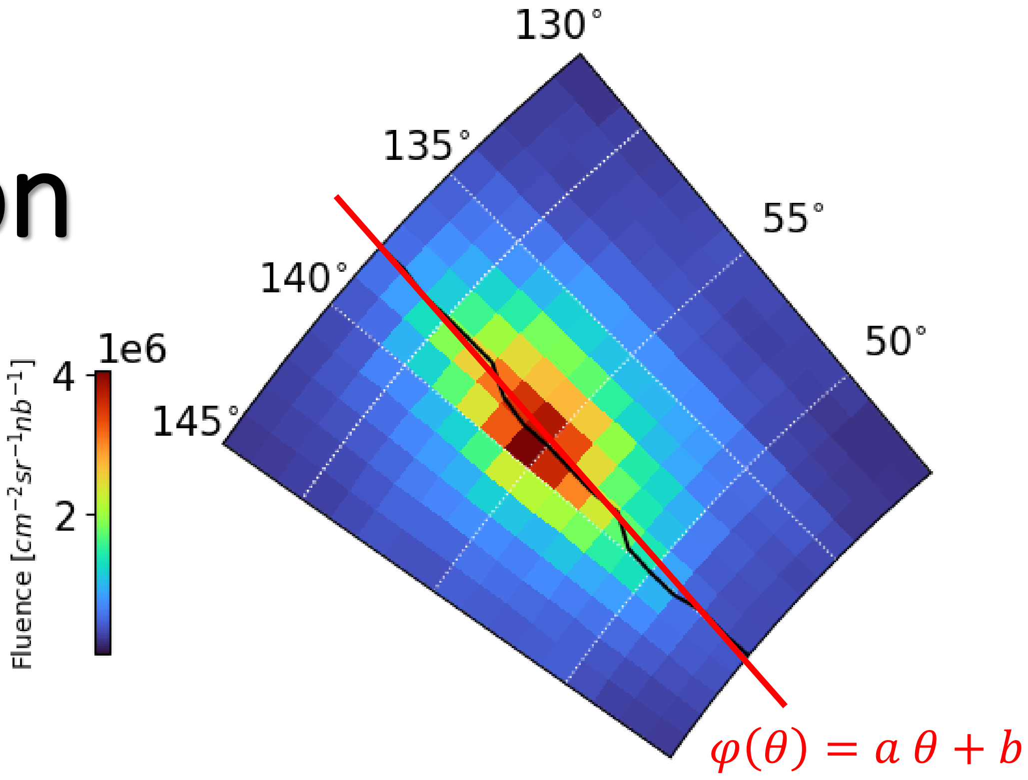

Determine the angular spread of the particles along the major axis:

- Fit slices along *Θ* with double gaussians to get *ϕ(Θ)*
- Evaluate the projection of the integral of the central gaussian along the spot axis

Timepix3 at MoEDAL:

Beam spot reconstruction

MoEDAL Preliminary

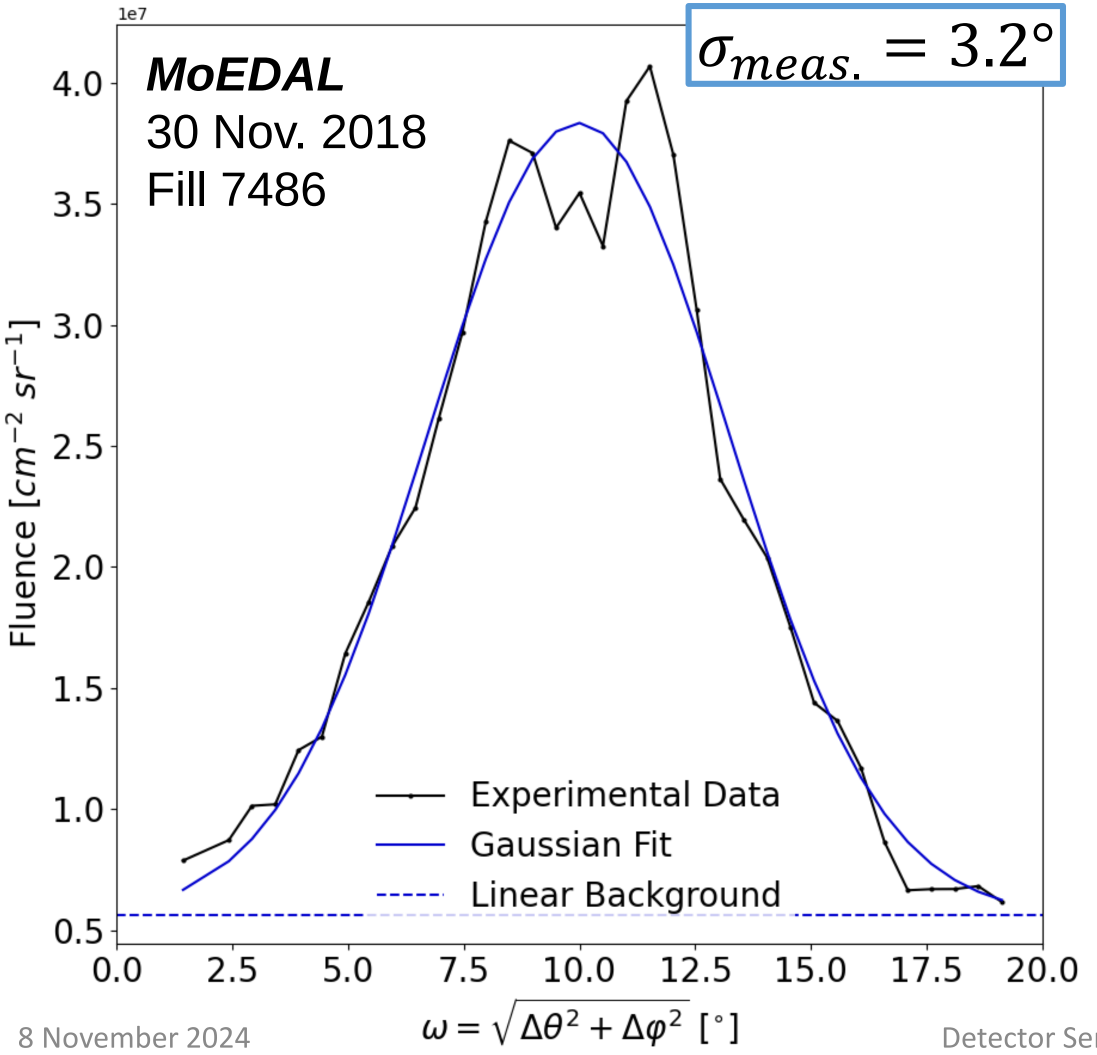

$$\sigma^2_{meas.} = \sigma^2_{det.} + \sigma^2_{scat.} + \boldsymbol{\sigma^2_{IP}}$$

$$\sigma_{scat.} = \frac{0.013\ GeV}{\beta p} \ln\left(\frac{x}{X_0}\right)\left[1 + 0.038 \ln\left(\frac{x}{X_0}\right)\right] << \sigma_{det.}$$

$$\rightarrow \sigma_{IP} = \sqrt{\sigma^2_{meas.} - \sigma^2_{det.}}$$

$\sigma_{det.} = (1.5\ \pm 0.1)$ deg.
Extracted from simulation and test beam

$$\rightarrow \sigma_z = \frac{(x^2_{det.} + y^2_{det.} + z^2) \times \sqrt{x^2_{det.} + z^2}}{y_{det.}\, z}\ \sigma_{IP}$$

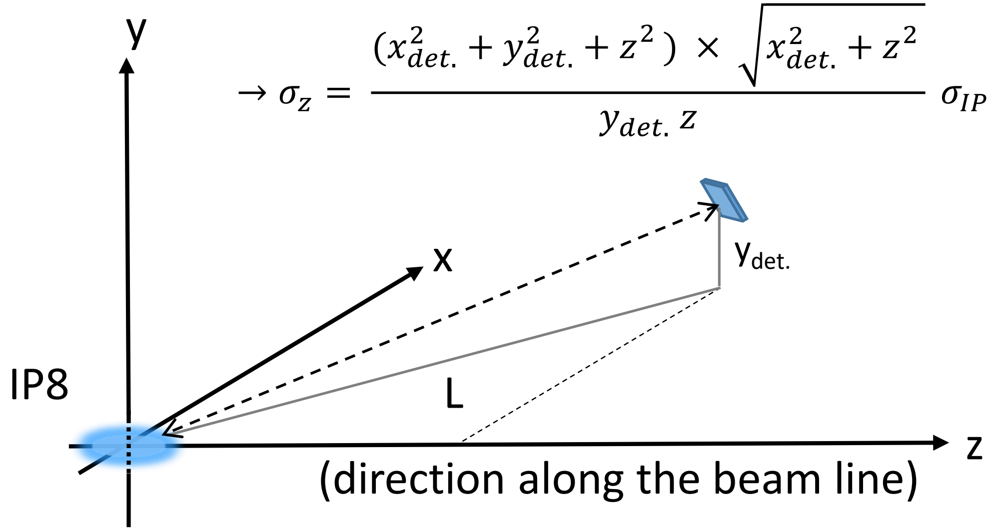

Timepix3 at MoEDAL:

Fill-by-fill variation of the interaction point size

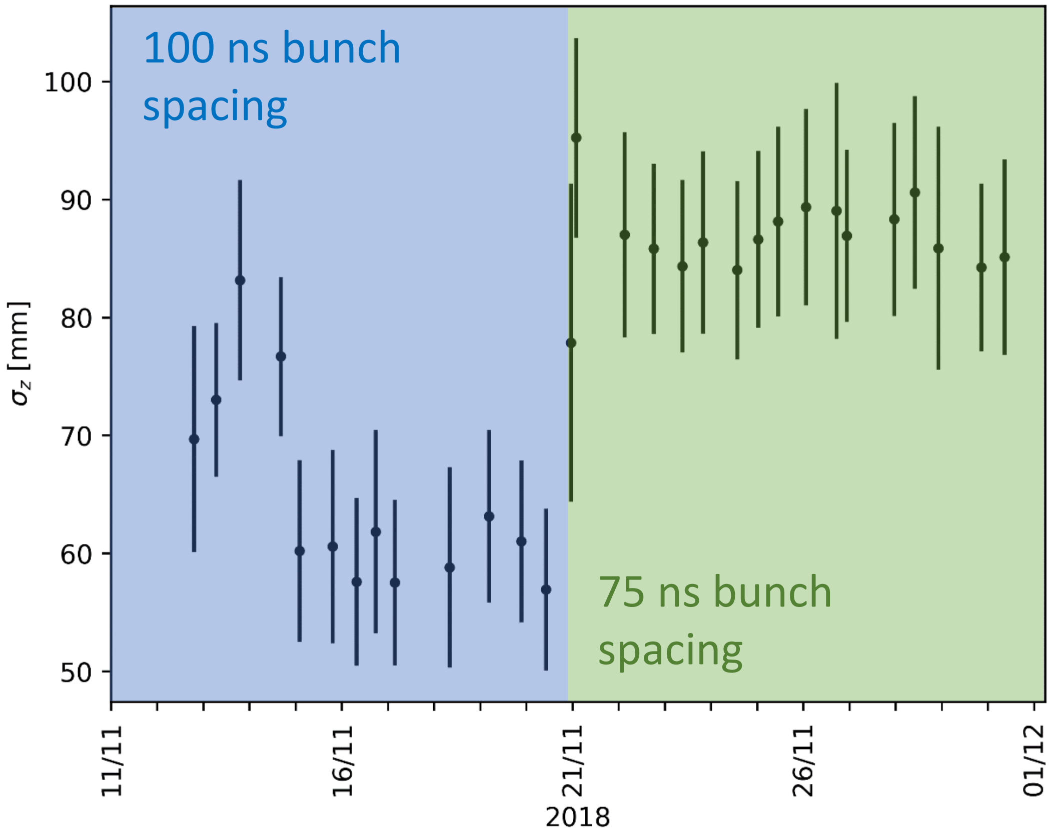

29 fills during ion physics in 2018

- The measured beam spot size per fill shows two distinct sizes
- Change of size coincides with reducing the bunch spacing

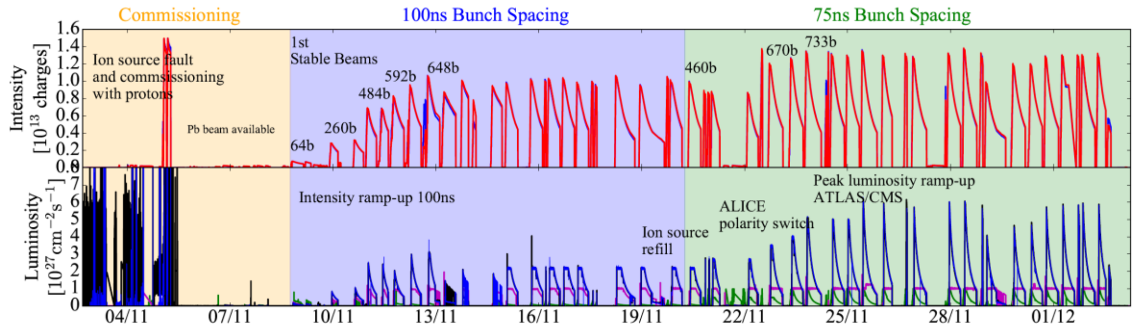

J.M. Jowett *et al.*, "The 2018 Heavy-Ion Run of the LHC", in *Proc. IPAC'19*, Melbourne, Australia, May 2019, pp. 2258-2261. doi:10.18429/JACoW-IPAC2019-WEYYPLM2

Acknowledgements

S. Pospisil, S. Gohl, J. Jelinek, D. Garvey, P. Smolyanskiy, P. Burian, L. Javora, P. Manek, M. Campbell, E. Heijne, C. Granja, A. Owens, E. Bosne, J. Pinfold, R. Soluk, M. Suk, M. Raymond, M. Ciapetti, ...

Presented results would not be possible without the Medipix collaborations.

The work has profited from funding by the Czech Science Foundation Junior Star Grant with No. GM23-04869M.

Conclusion

- In laboratory table-top experiments, half-life time measurement of Po-isotopes and the excited levels of Fe-57 were done demonstrative reliable measurement of **decay times down to 8 ns**
- **Electron and proton** separation and **proton spectrum measurement** were shown for the LEO space radiation environment.
- The power of pattern recognition was outline by the example of **gamma-neutron discrimination** and decomposition of the **single-bunch response** in the ATLAS radiation environment.
- Precise **particle tracking** was used for determination of the interaction point length within the MoEDAL experiment at IP8 during PbPb physics in 2018. Changes in the charged particle component of the radiation field were observed during insertion of Velo.

Outlook

Timepix4 @ CERN SPS heavy ion test beam

Heavy ion tracks measured with Timepix4
Courtesy of Petr Burian

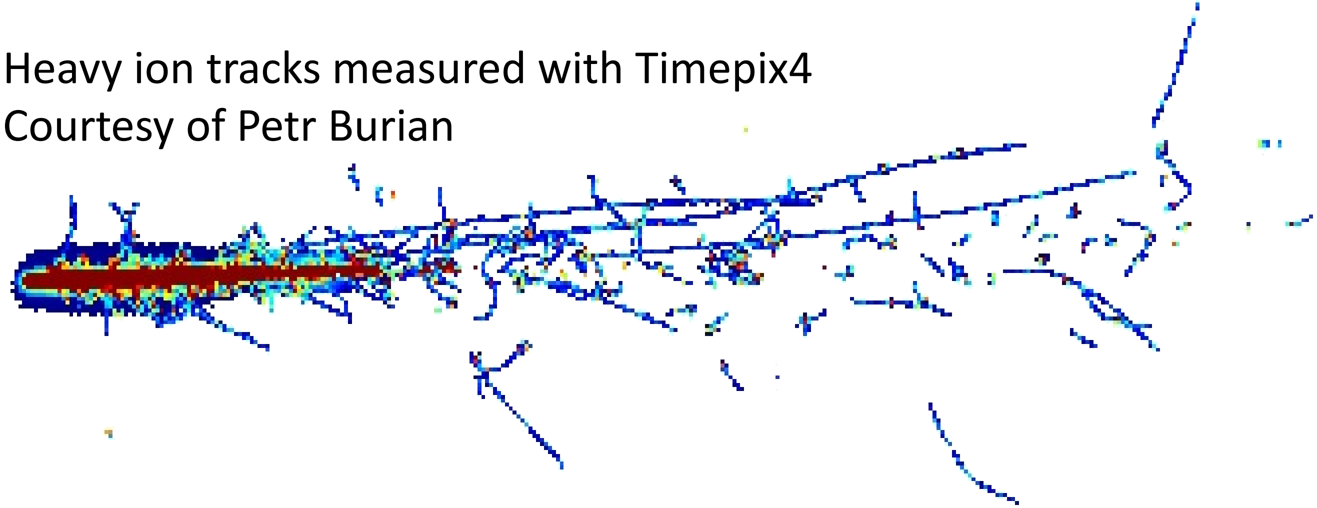

Thank you very much for your attention!

Timepix4 is available:

- 200 ps time binning
- 350 Mhits/s (8 x improvement)
- 7 cm^2 area (3.5 x improvement)

Working principle:

Modes of operation - Timepix

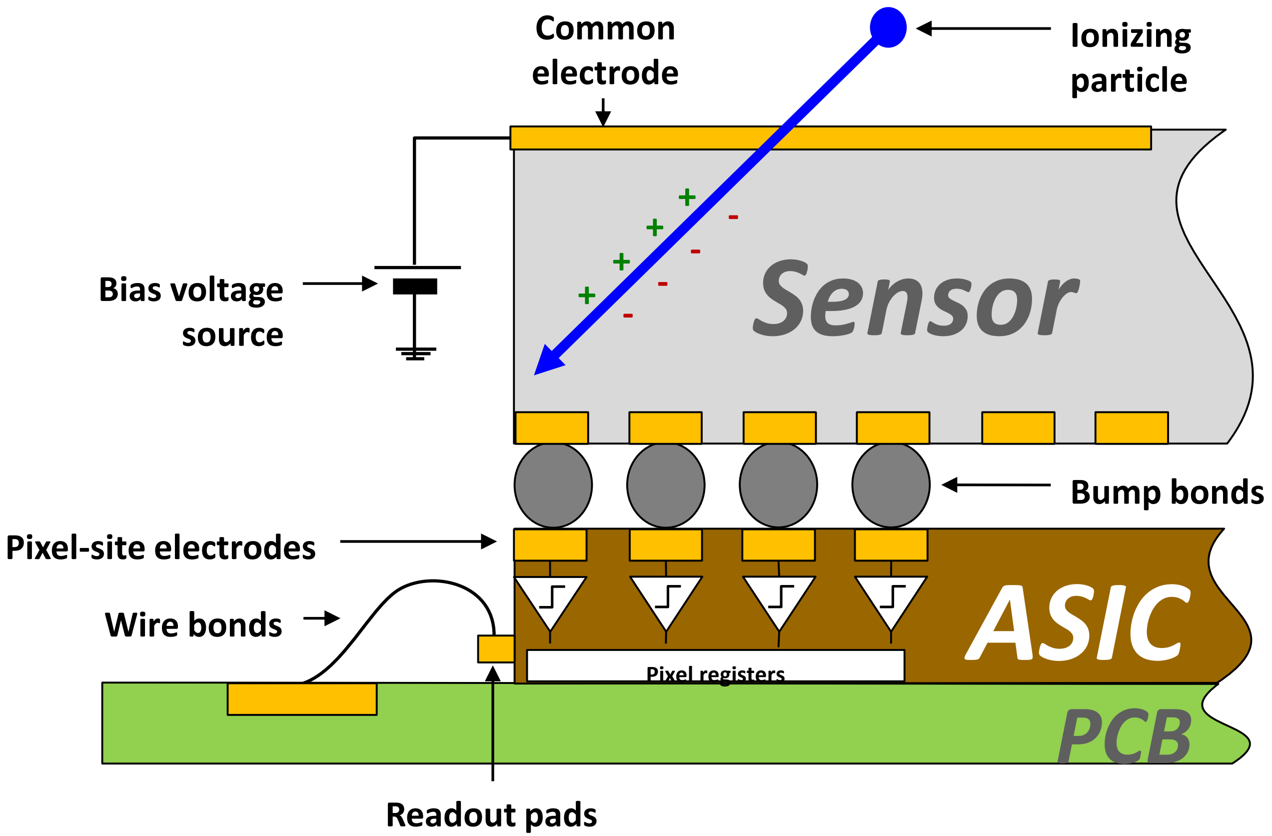

Timepix pixel processing:

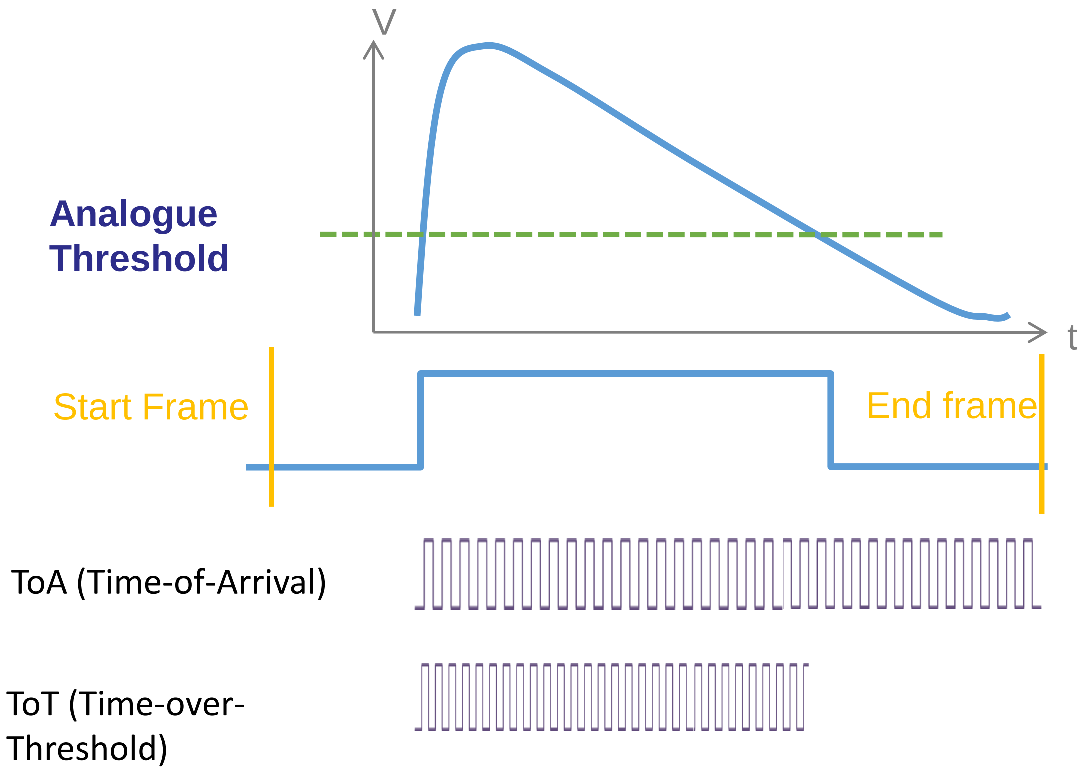

Working principle:

Timepix3

- **Data-driven** readout with continuously running 40 MHz base clock
- **Simultaneous** measurement of ToT and ToA
- Local oscillator creates **640 MHz** clock for precise time stamping

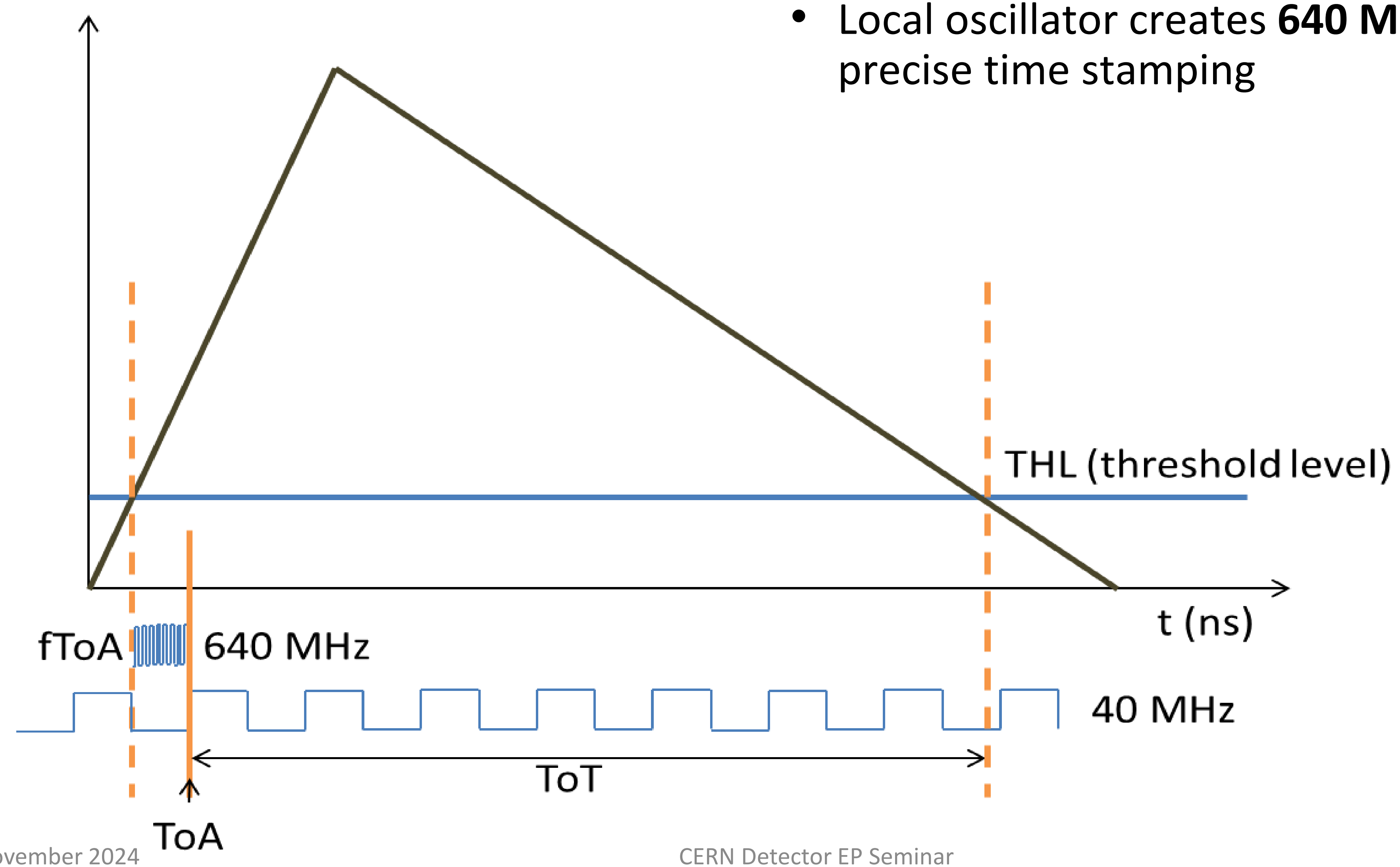

Working principle:
e⁻, photons, low energy α-particles

X- and γ-ray photons are detected through conversion to electrons
→ Difficult to separate

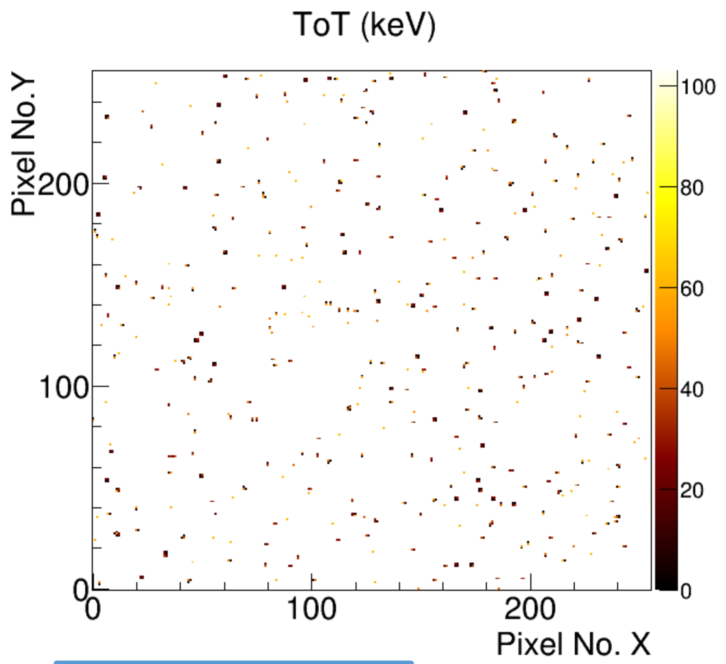

60 keV photons

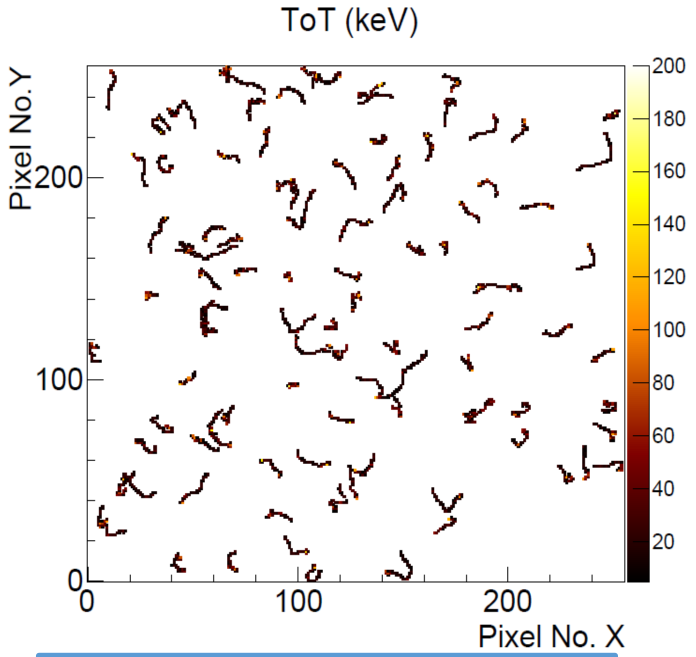

800 keV electrons/photons

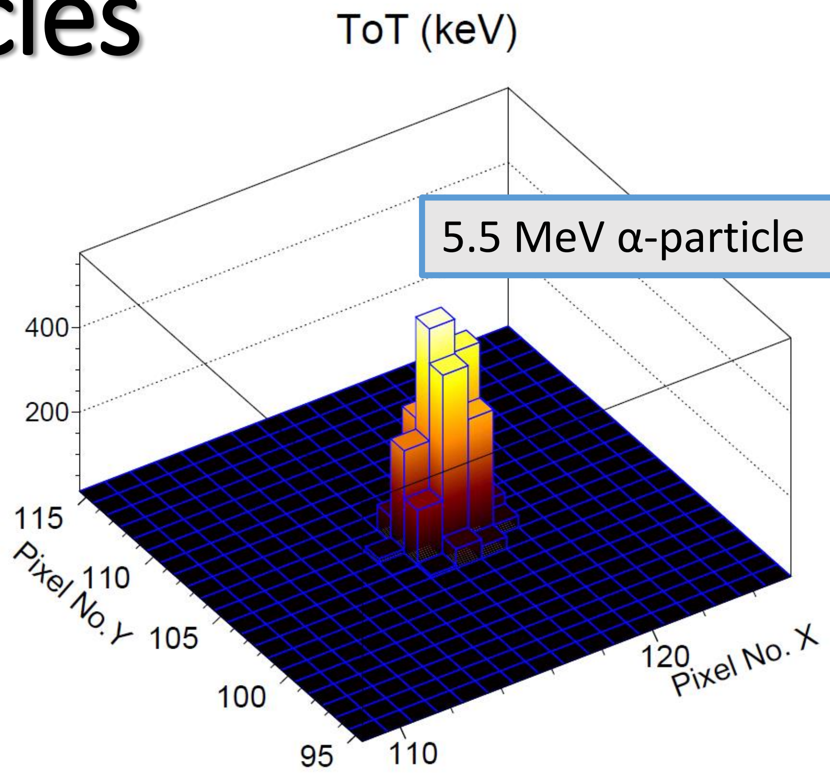

5.5 MeV α-particle

Highly localized charge deposition
→ Spread due to repulsion and diffusion during drift motion
→ **Subpixel spatial resolution** (dx ~ 400 nm)

Measurement at Van-de-Graaff:

Measurement setup

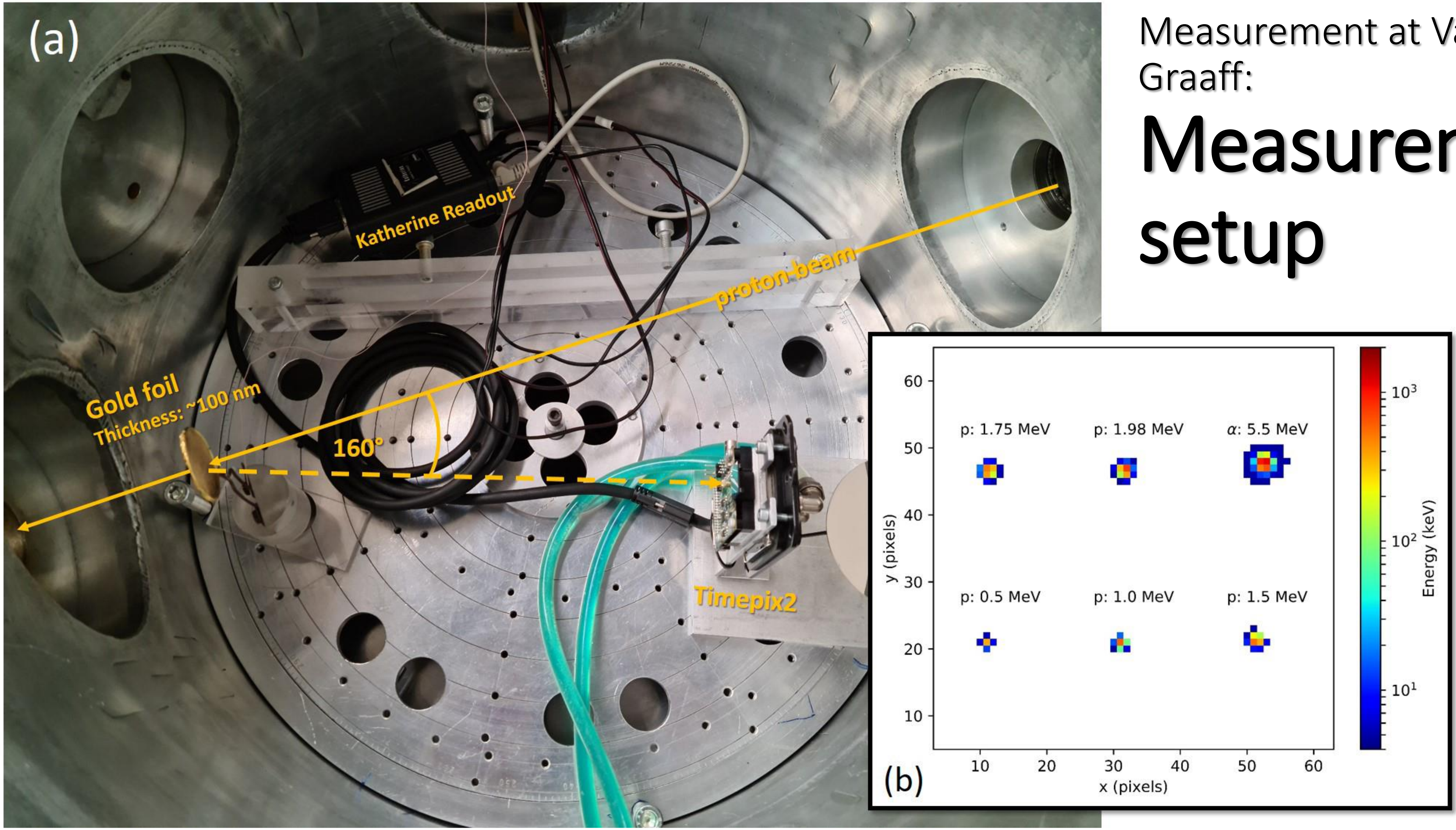

B. Bergmann *et al* 2022 *JINST* **17** C01025

Measurement at Van-de-Graaff

Proton and α spectra

Mylar foils attached to the sensor backside

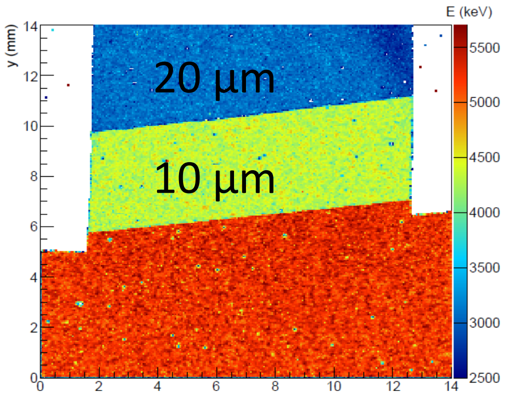

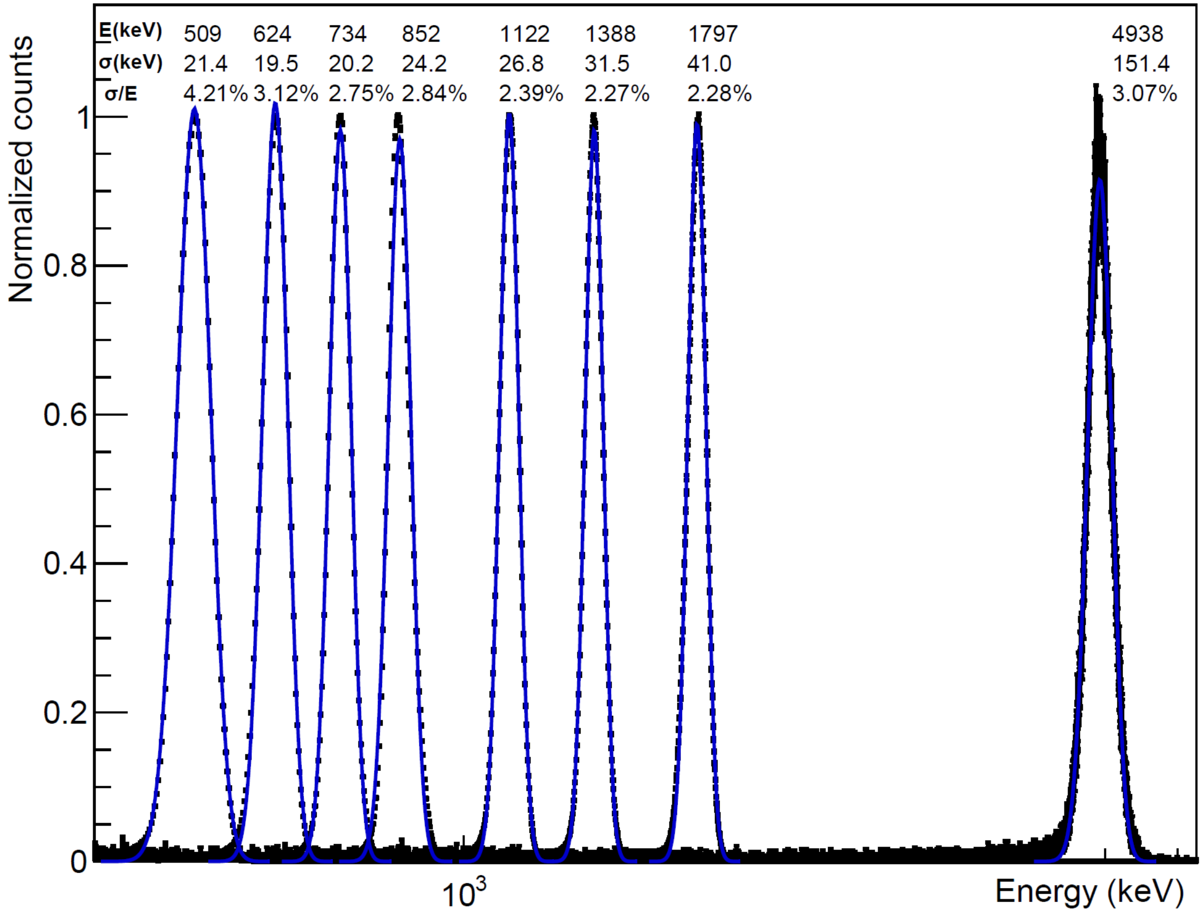

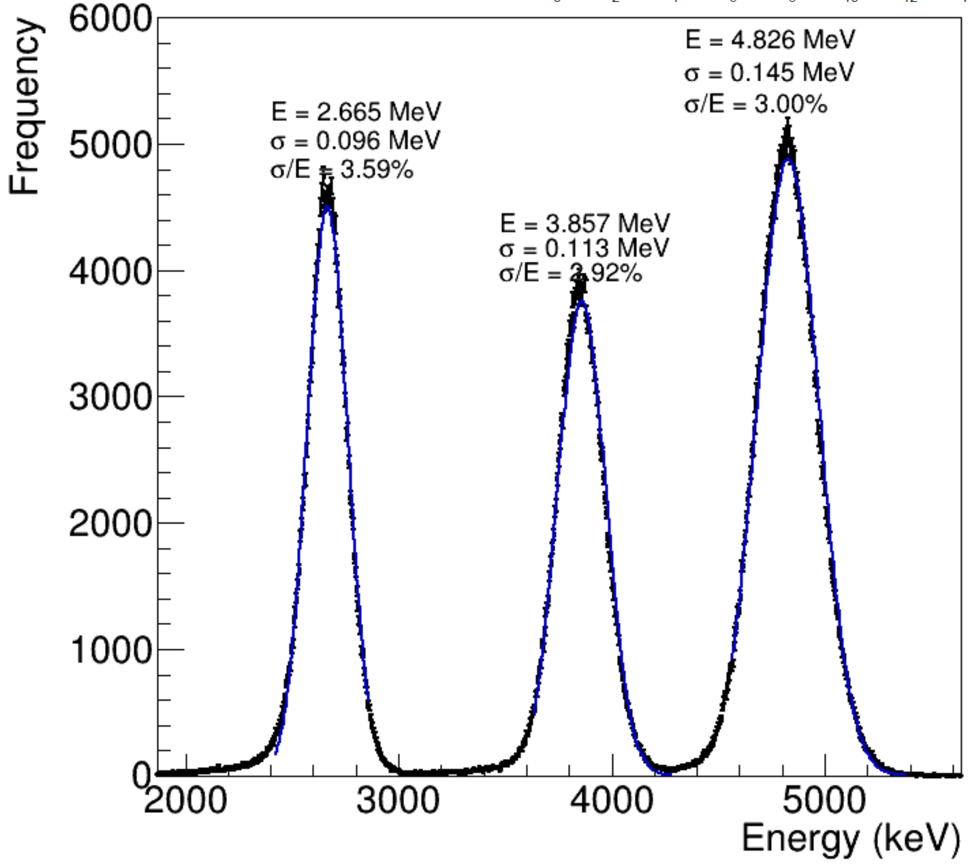

For stopped protons <3% relative resolution

For short-ranged alpha particles <4% relative resolution

Ion resolving and particle separation capability

Relativistic fragmented ion beam

$$\left\langle -\frac{dE}{dx}\right\rangle = Kz^2\frac{Z}{A}\frac{1}{\beta^2}\left[\frac{1}{2}\ln\frac{2m_ec^2\beta^2\gamma^2W_{\max}}{I^2}-\beta^2-\frac{\delta(\beta\gamma)}{2}\right]$$

Mixed field of relativistic ion fragments created by Pb beam on target.

Observed peaks relate to different ion charge:

$$\frac{dE}{dX} = \frac{dE_{Z=1}}{dX}Z^2$$

Resolving power up to Z=11

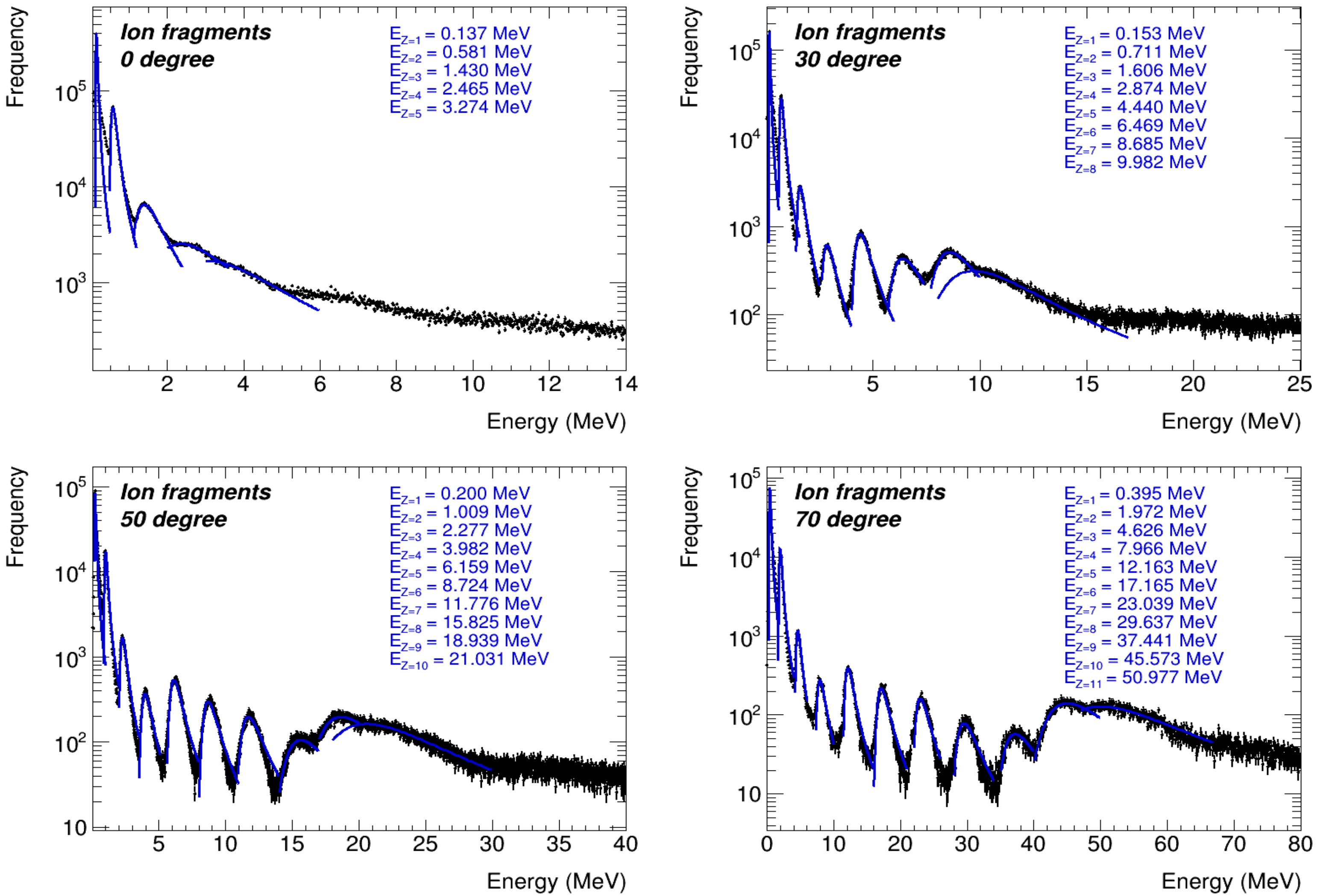

Instruments for measurements in LEO

Next Generation Radiation Monitor (NGRM)

- Mass ~ 1 kg
- Consumption ~1-2 W

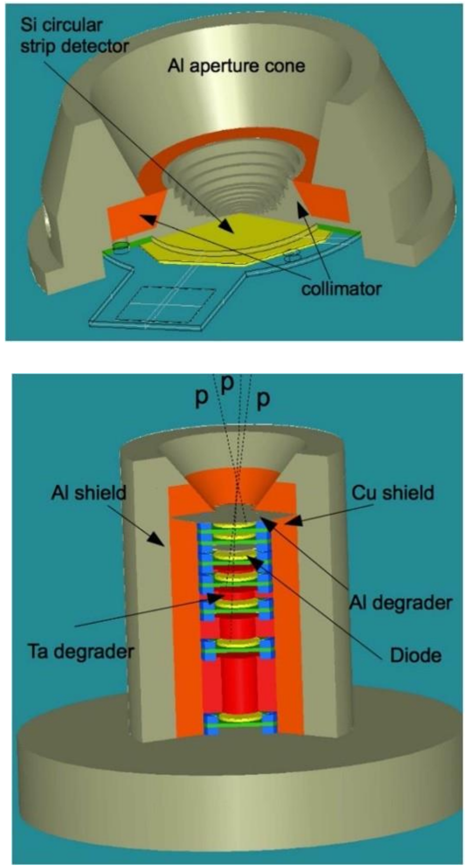

EPT (Energetic Particle Telescope)

- Mass: **4.6 kg**
- Consumption: 5.6 W

ICARE-NG:

- Mass: **2.4 kg**
- Consumption: 3 W

Timepix devices in LEO

- Single-layer particle discrimination
- Small dimensions and low mass
- Large field of view

Space flights

- REM on ISS (since 2012: different versions; MiniPIX TPX3 by Advacam deployed in 2021)
- SATRAM on Proba-V (launch in 2013, 820 km)
- LUCID-Timepix (2014-2017, 635 km)
- VZLUSAT-1 (launch in 2017, 510 km)
- RISESAT (launch in 2019, 500 km)
- VZLUSAT-2 (launch in 2022, 500 km, CdTe 2 mm)
- **HardPix** – SWIMMR* project (launched in 2023)

*Space Weather Instrumentation, Measurement, Modelling and Risk

Space radiation in LEO measured by TPX3, integrated frame, 200 s, energy display

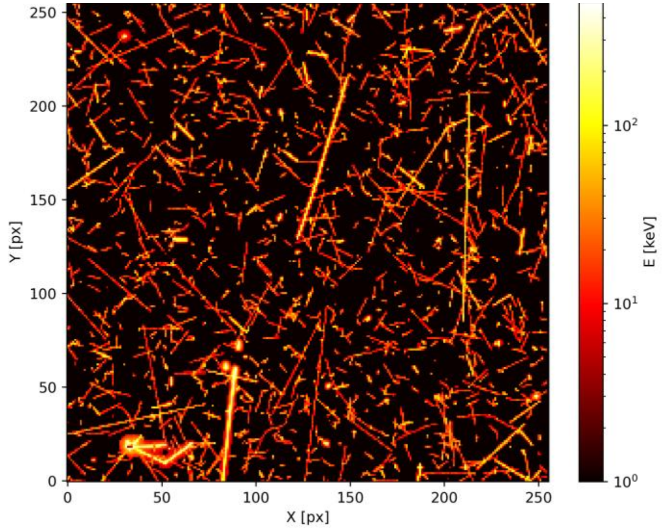

Minipix TPX3 and shielding by ADVACAM

ADVACAM *
Imaging the Unseen

Comparison with other radiation detectors in LEO

SATRAM vs. EPT (Energetic Particle Telescope)*):

Electron fluxes

S. Gohl, B. Bergmann, M. Kaplan et al., “Measurement of electron fluxes in a Low Earth Orbit with SATRAM and comparison to EPT data”, *Adv. Space Res.*, https://doi.org/10.1016/j.asr.2023.05.033

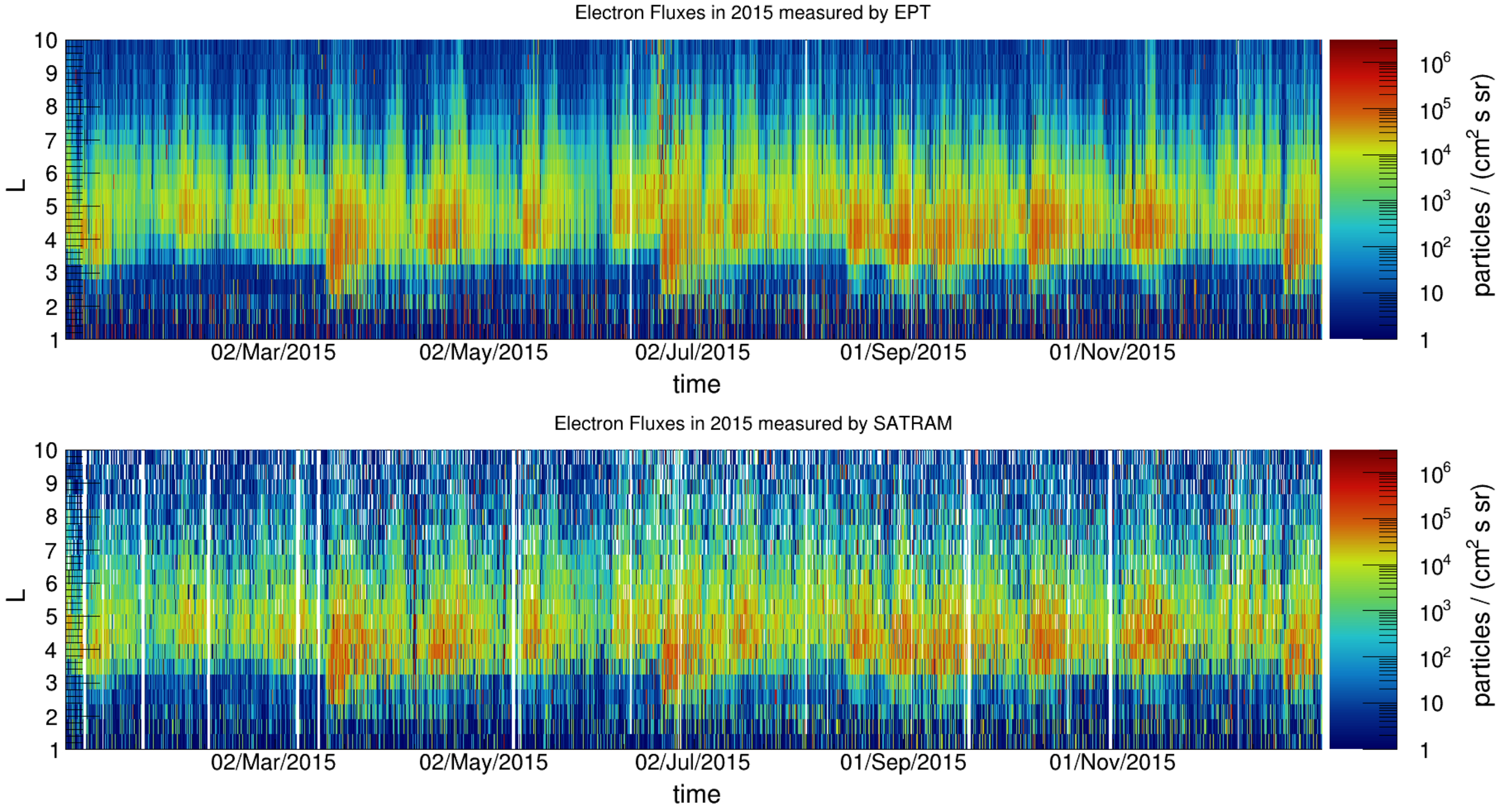

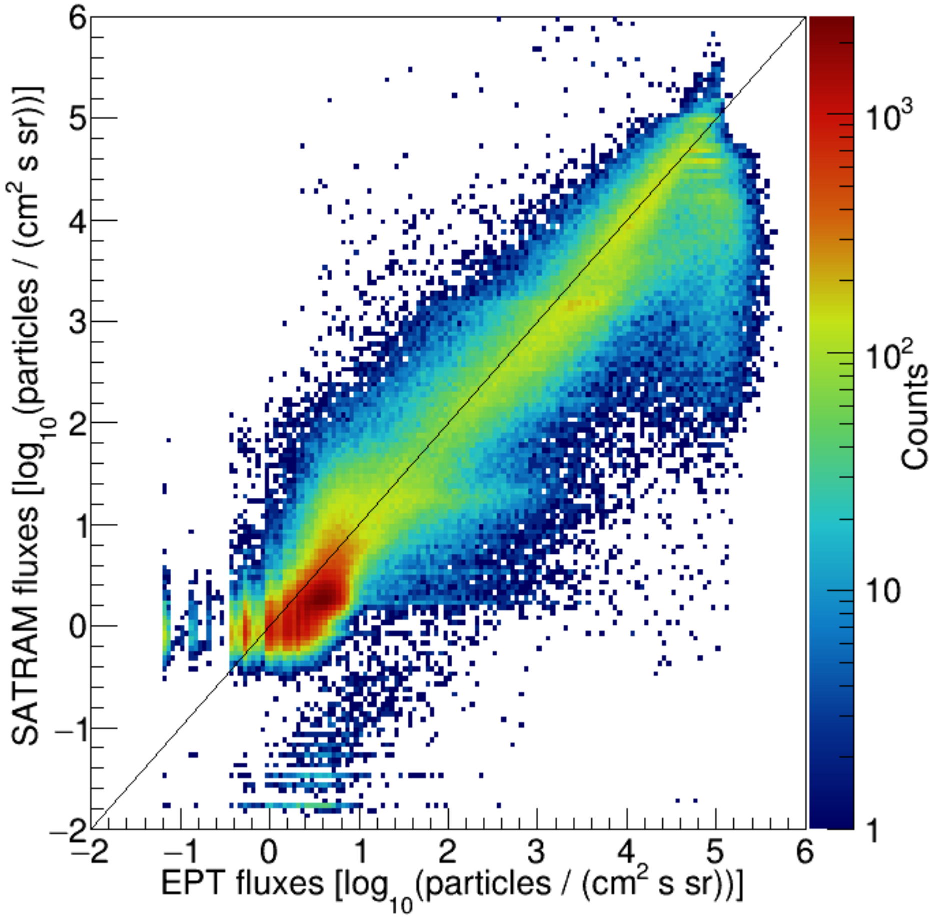

*) EPT and SATRAM are both on Proba-V.

60 seconds integration time

SATRAM vs. ICARE-NG:

Proton fluxes

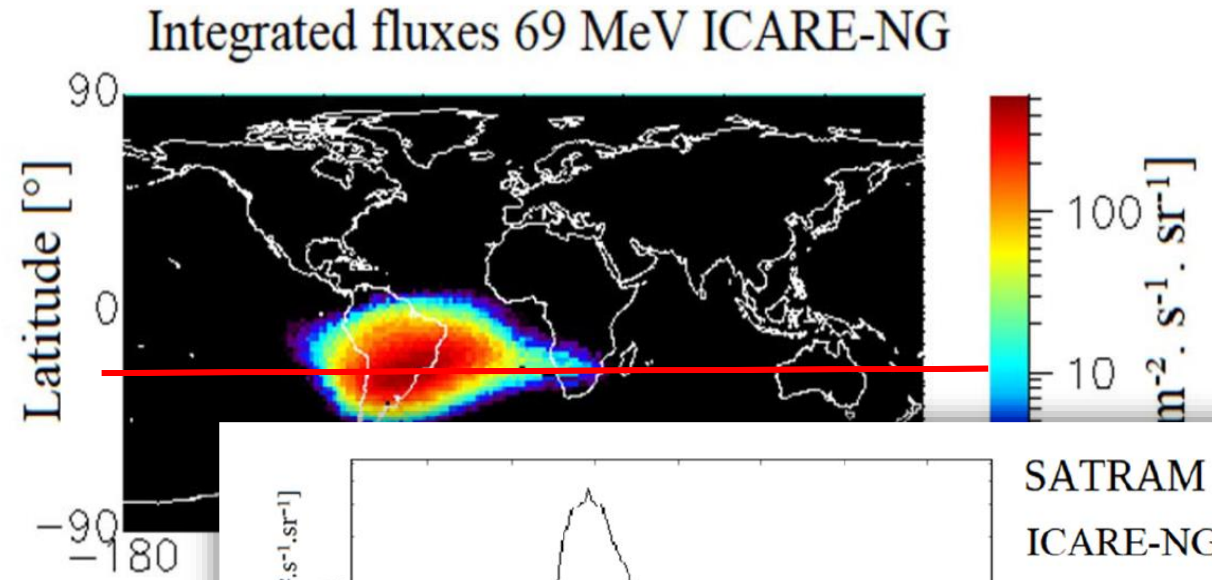

Fig. 11. Flu
ICARE-NG o

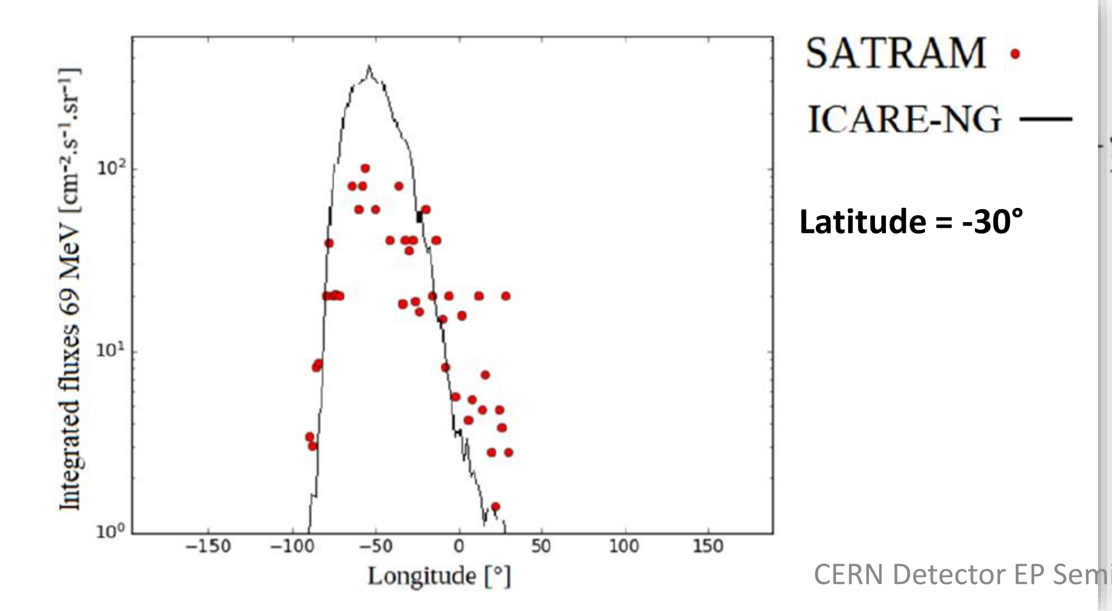

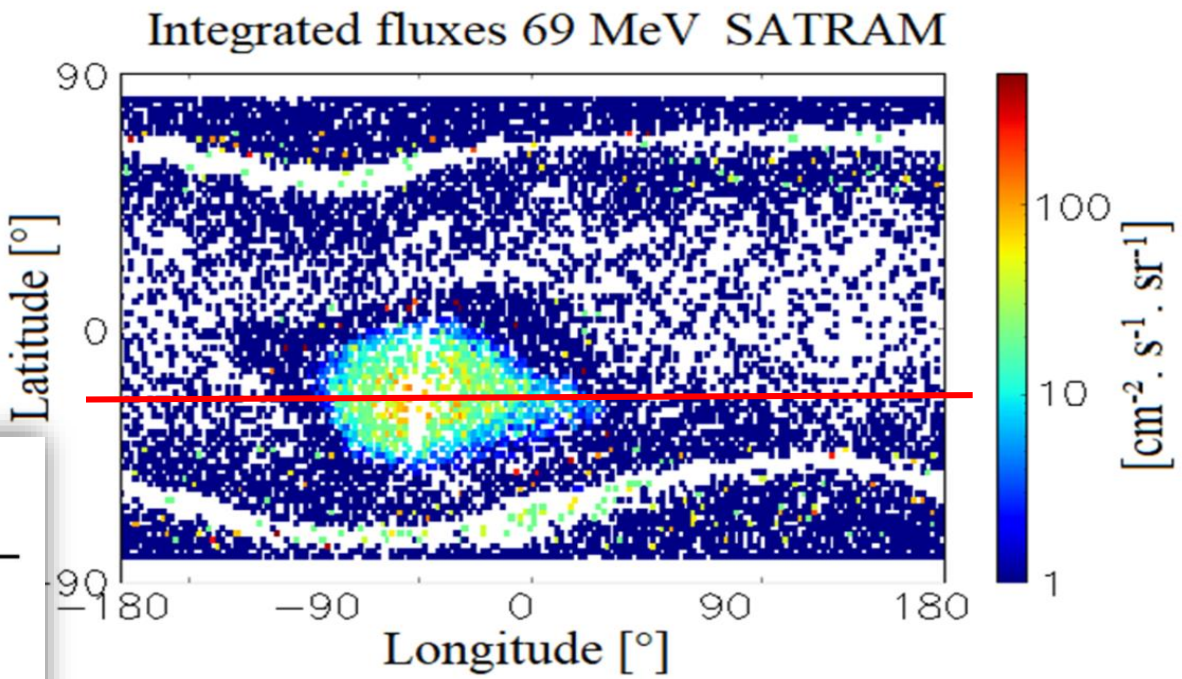

*M. Ruffenach et al., "A new technique based on convolutional neural networks to measure the energy of protons and electrons with a single Timepix detector", in IEEE TNS, **68**, 8, pp. 1746-1753, (2021). doi: 10.1109/TNS.2021.3071583*

SATRAM vs. EPT:

Proton spectrum measurement

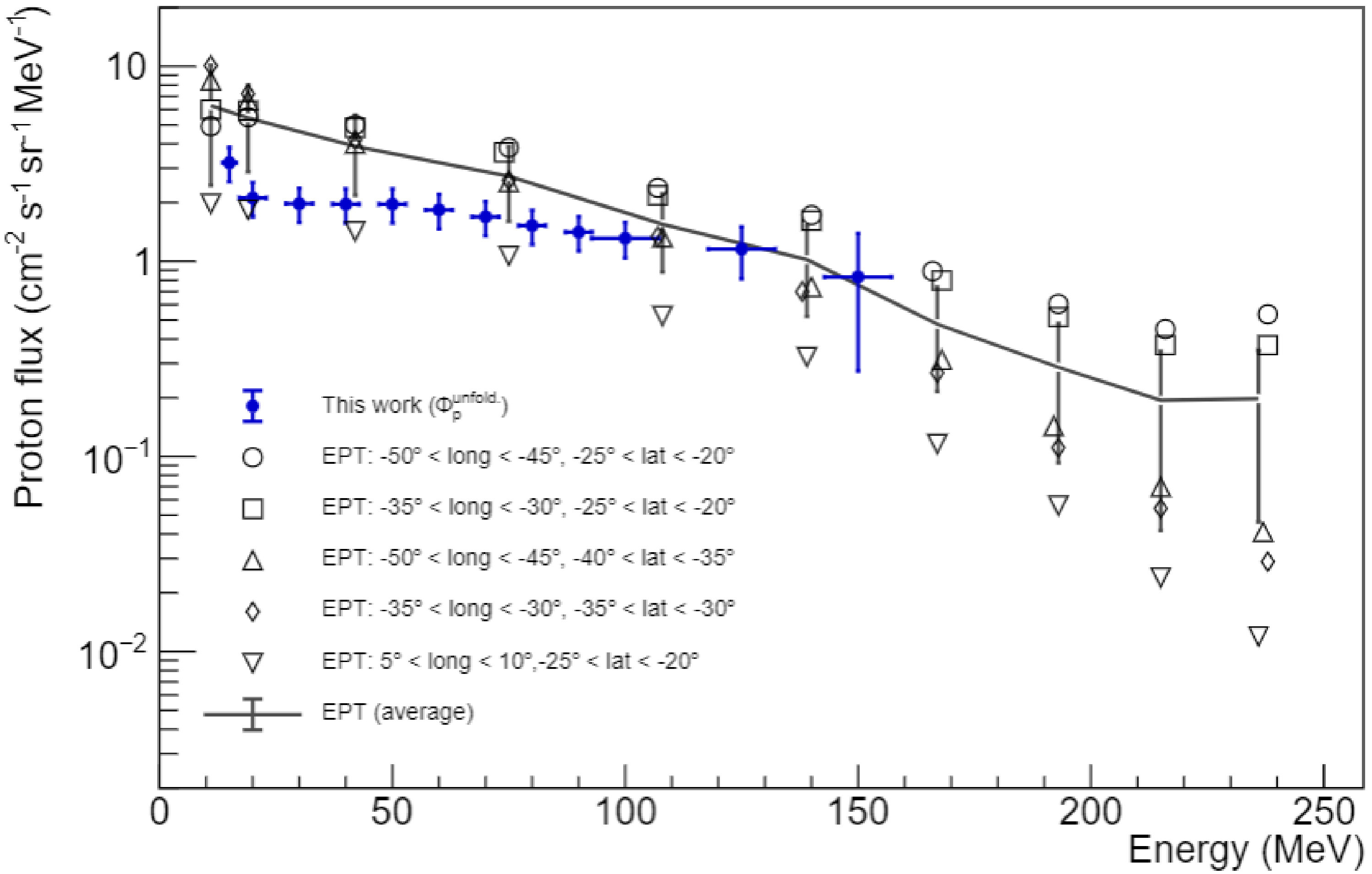

EPT data digitized from:

G. López Rosson, V. Pierrard, *"Analysis of proton and electron spectra observed by EPT/PROBA-V in the South Atlantic Anomaly",* Adv. Space Res. **60**, Issue 4, pp. 796-805 (2017). https://doi.org/10.1016/j.asr.2017.03.022

SATRAM data agree within EPT data points on a one sigma level

Near-future missions (of our Timepix radiation detectors)

- **SWIMMR2** D-Orbit satellite orbit >1000 km - launch in October 2024
- 2 modules outside of the Lunar Gateway as a part of the ESA **ERSA** (European Radiation Sensors Array) – **2024**
- **HEKI** - study radiation field influence on a superconducting magnet by Robinson-Paihau research institute in New Zealand using 2x HardPix detectors. Launch to ISS/Nanoracks in **2024**.
- **Cassini** - European Commission In-orbit demonstration mission. Managed by ESA and provided by ISISPACE 6U Cubesat - Launch **2025**
- Equipped with neutron converters selected in the MoonPool ESA call for ideas → **neutron detection for water mapping**

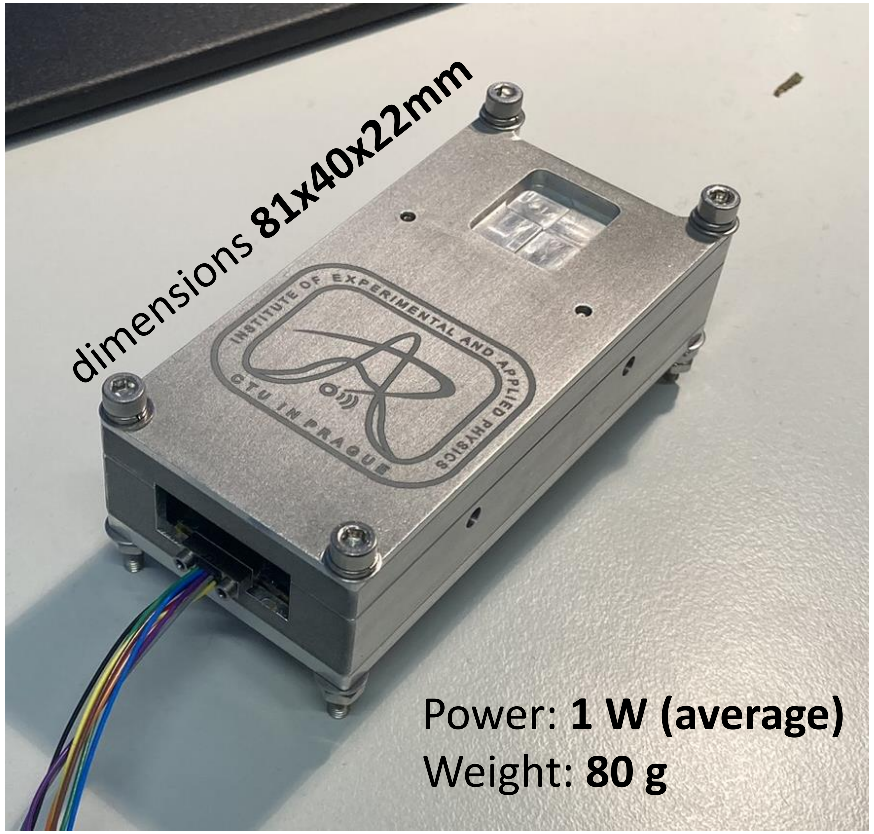

HardPix was developed with ESA projects

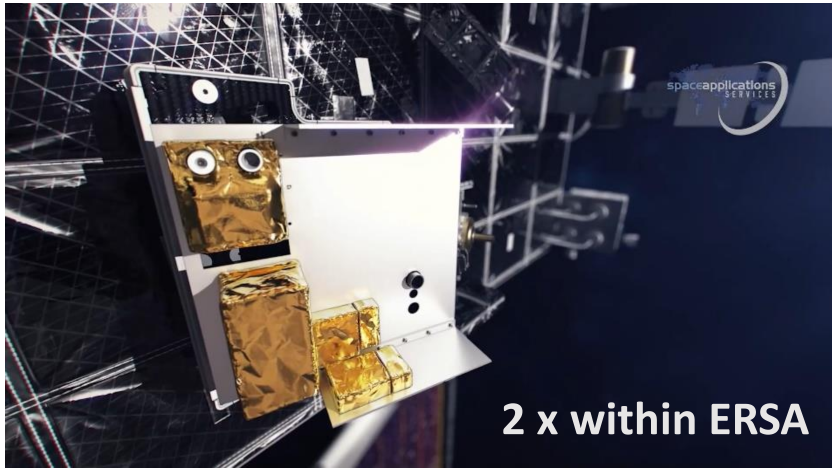

B. Bergmann, S. Pospisil, I. Caicedo, J. Kierstead, H. Takai and E. Frojdh, "Ionizing Energy Depositions After Fast Neutron Interactions in Silicon," in *IEEE Transactions on Nuclear Science*, vol. 63, no. 4, pp. 2372-2378, Aug. 2016, doi: 10.1109/TNS.2016.2574961

Interactions of fast neutrons in silicon

Time-of-Flight technique:

1-600 MeV neutrons interacting in silicon

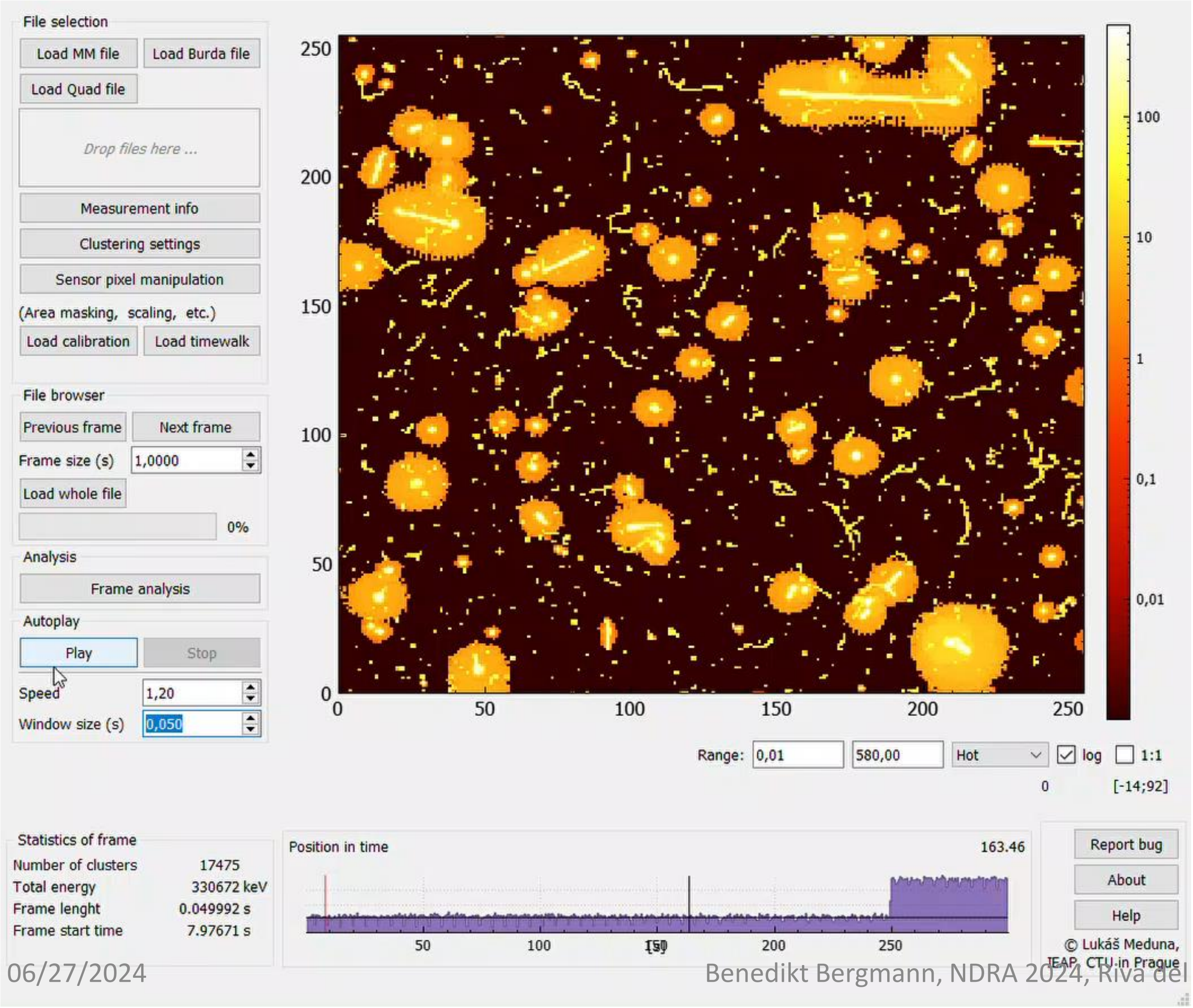

Neutron interactions in silicon show a large variety of signatures resembling the different ways neutrons interact in the sensor

- Small clusters similar to photon interactions
- Large clusters with high energy depositions like stopped charged particles
- Tracks similar to penetrating particles

→ **Can we decompose this signatures?**

Decomposing the neutron response

(1) Dot – Low energy X- and γ-rays, low energy electrons
(2) Small blob – X- and γ-rays, electrons
(3) Curly track – γ-rays and electrons (MeV)
(4) Heavy Blob – Highly ionizing particles with short range (α, protons, ...)
(5) Heavy track – Highly ionizing particles (protons, ions, ...)
(6) Straight track – Energetic light charged particles (μ, minimum ionizing light ions, ...)

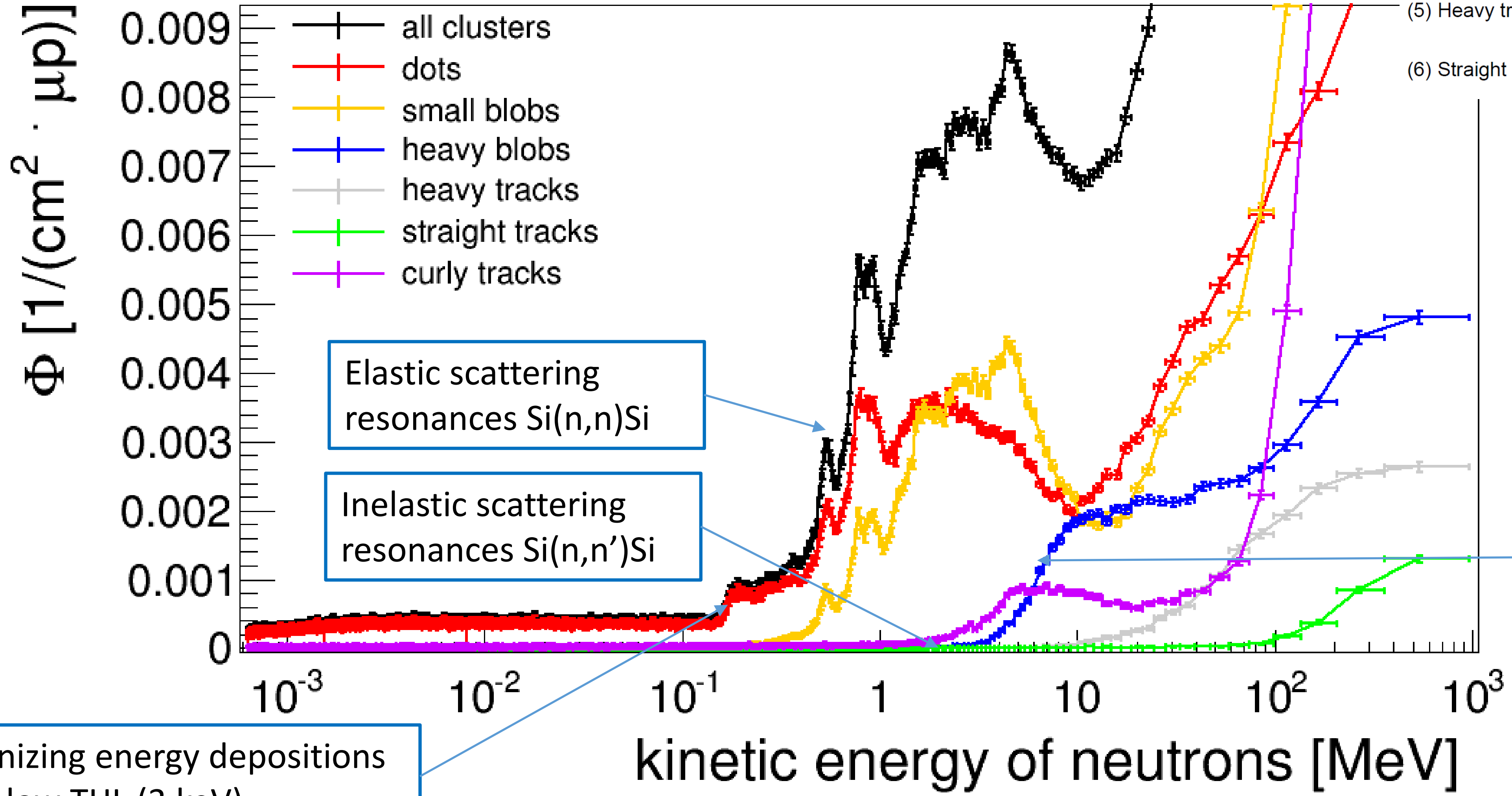

Elastic scattering resonances Si(n,n)Si

Inelastic scattering resonances Si(n,n')Si

Highly ionizing events due to nuclear interaction appear

Ionizing energy depositions below THL (3 keV)

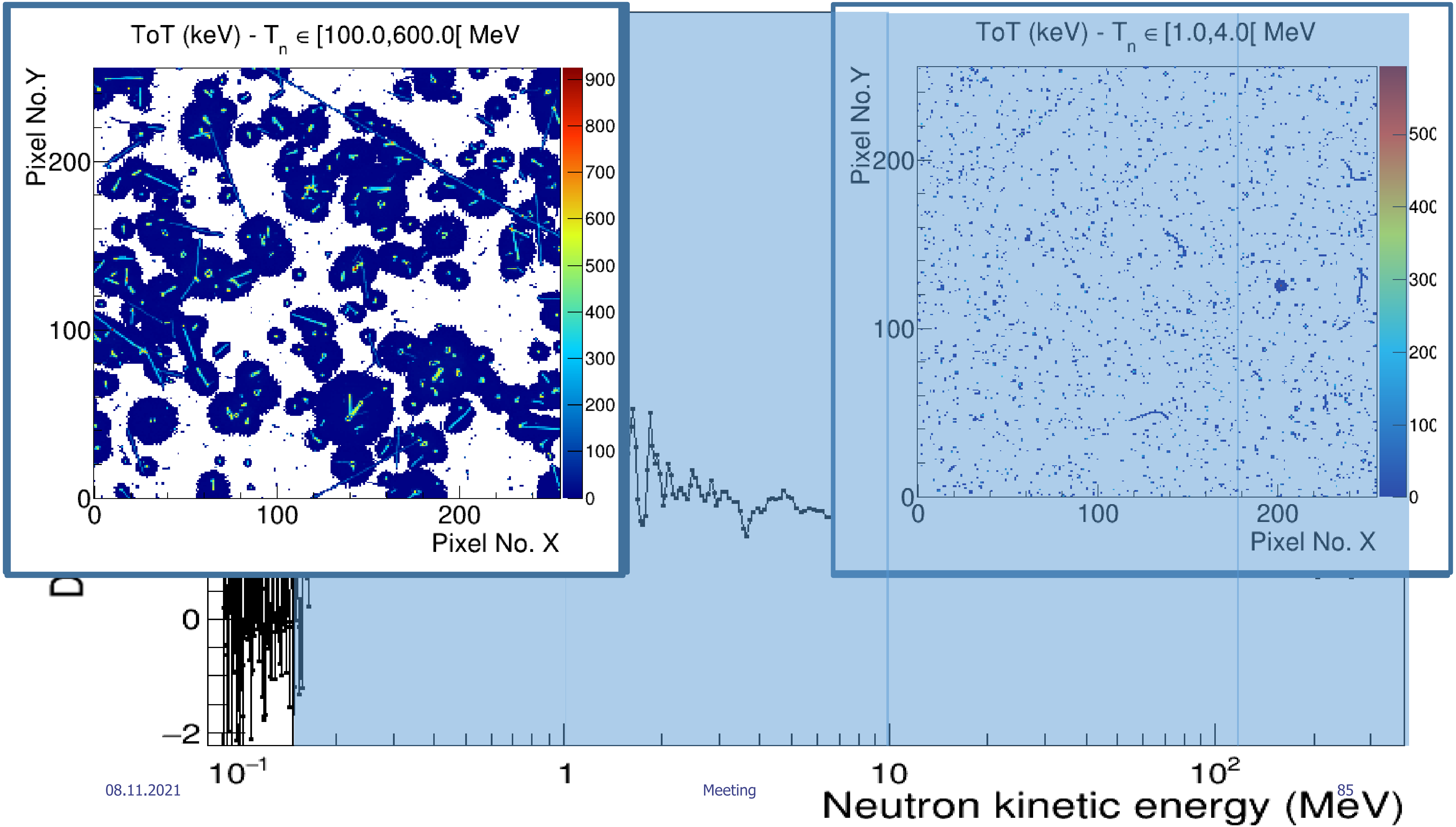
ToT (keV) - $T_n \in$ [100.0,600.0[MeV
Pixel No. Y
Pixel No. X
ToT (keV) - $T_n \in$ [1.0,4.0[MeV
Pixel No. Y
Pixel No. X
Neutron kinetic energy (MeV)

Neutron energy deposition spectra

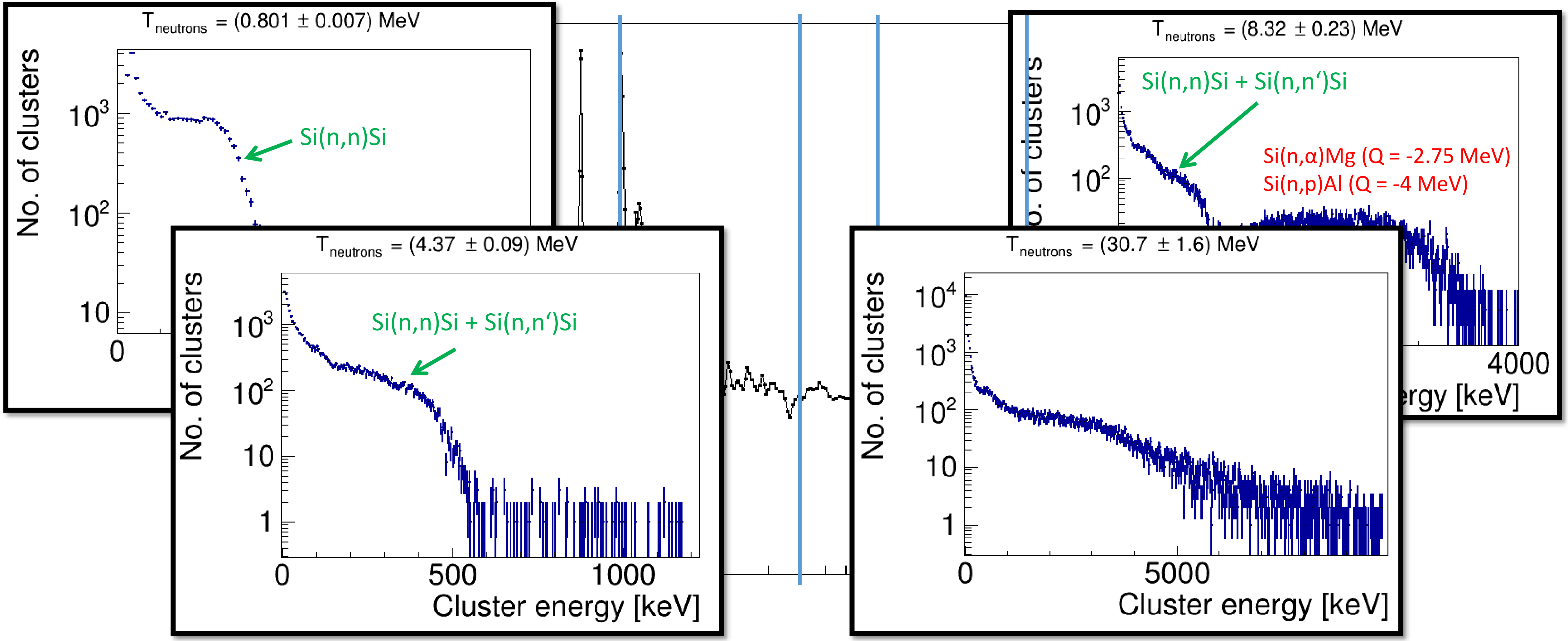

Interpretation:

Edges from backscattering

Maximal energy transfer to the recoil silicon:

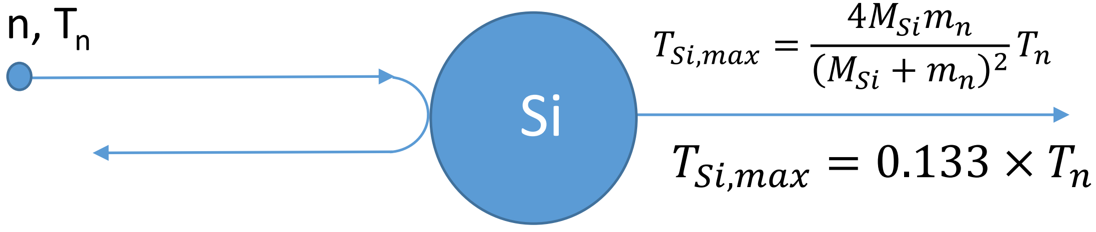

$$T_{Si,max} = \frac{4 M_{Si} m_n}{(M_{Si} + m_n)^2} T_n$$

$$T_{Si,max} = 0.133 \times T_n$$

<u>Calculation:</u>

$E_n = 3.8\ MeV$ → $T_{Si,max} = 505\ keV$

<u>Measured:</u> $T_{Si,max} = 379\ keV$

$$f_{meas,IEL} = \frac{E_{edge}}{T_{Si,\max}} = \frac{E_{edge}}{0.133 \cdot T_n}$$

$$f(E) = \frac{A}{\exp\left(\frac{E - E_{edge}}{D}\right) + 1} + B + C \cdot E$$

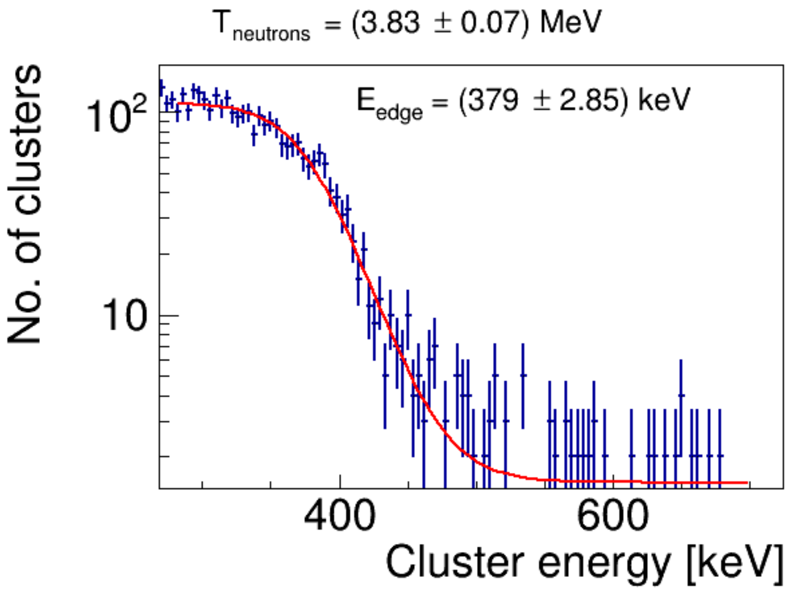

B. Bergmann, S. Pospisil, I. Caicedo, J. Kierstead, H. Takai and E. Frojdh, "Ionizing Energy Depositions After Fast Neutron Interactions in Silicon," in *IEEE Transactions on Nuclear Science*, vol. 63, no. 4, pp. 2372-2378, Aug. 2016, doi: 10.1109/TNS.2016.2574961

Partition function of IEL and NIEL

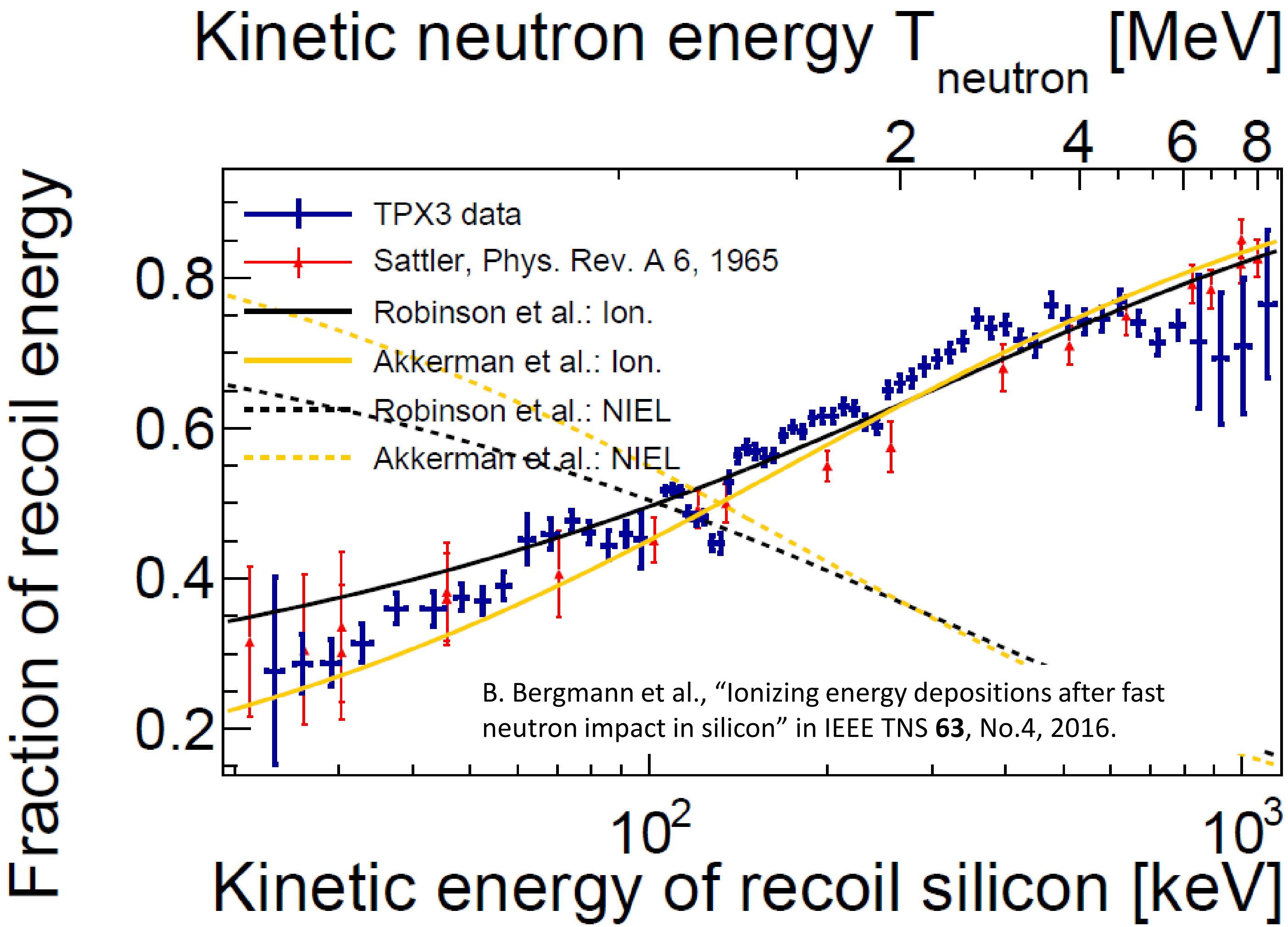

$$f_{meas,IEL} = \frac{E_{edge}}{T_{Si,\max}} = \frac{E_{edge}}{0.133 \cdot T_n}$$

Measurement: A. R. Sattler. *Phys. Rev.*, 138:A1815-1821, Jun 1965.

Theoretical predictions:

$$f_{IEL} = \frac{k \times g(\varepsilon)}{1 + k \times g(\varepsilon)}$$

M. T. Robinson and I. M. Torrens. *Phys. Rev. B*, 9: 5008-5024, Jun 1974.

$k = 0.1462, \varepsilon = 1.014 \times 10^{-2} \times Z^{-7/3} \times E,$

$g(\varepsilon) = 3.4008 \times \varepsilon^{1/6} + 0.40244 \times \varepsilon^{3/4} + \varepsilon$

A. Akkerman and J. Barak. *IEEE Transactions on Nuclear Science*, 53(6): 3667–3674, Dec 2006.

$g(\varepsilon) = 0.90656 \times \varepsilon^{1/6} + 1.6812 \times \varepsilon^{3/4} + 0.7442\ \varepsilon$